A Study of Throughput Drop Estimation Models for Concurrently Communicating Links in Wireless Local-Area Networks

March, 2022

KWENGA Ismael Munene

Graduate School of
Natural Science and Technology

(Doctor's Course)
Okayama University

Dissertation submitted to
Graduate School of Natural Science and Technology
of
Okayama University
for
partial fulfillment of the requirements
for the degree of
Doctor of Philosophy.

Written under the supervision of

Professor Nobuo Funabiki

and co-supervised by
Professor Satoshi Denno
and
Professor Yasuyuki Nogami

Okayama University, March 2022.

To Whom It May Concern

We hereby certify that this is a typical copy of the original doctor thesis of KWENGA Ismael Munene

Signature of the Supervisor	Seal of
	Graduate School of
Prof. Nobuo Funabiki	Natural Science and Technology

Abstract

Nowadays, the *IEEE 802.11 wireless local-area network (WLAN)* has been deployed world-wide for Internet access in various places, including airports, shopping malls, stations, and hotels, due to its advantages of the flexibility, the lower cost, and the high data transmission capacity. WLAN users can easily access to the Internet through wireless connections with *access points (APs)* using mobile devices like smart phones, tablets, and laptop PCs. Among the *IEEE 802.11*, currently, *IEEE 802.11n* has prevailed over WLAN due to the high-speed data transmission capability at *2.4 GHz Industrial Scientific and Medical (ISM) band* using the *channel bonding (CB)*, *frame aggregation* and *multiple input multiple output (MIMO)* technologies.

Since the limited number of frequency channels is available at 2.4 GHz ISM band, the proper channel assignment becomes a key challenge in enhancing the throughput performance of WLAN. To maximize the throughput by reducing interferences among wireless signals, previously, we studied the *orthogonal channel assignment (OC)* under *20 MHz non-channel bonding (non-CB)* for the *active AP configuration algorithm* in the *elastic WLAN system*.

However, our previous studies disclosed several limitations in the orthogonal channel (OC) assignment. Firstly, the number of OCs is very limited, where only *three* and *two* channels are available under *20MHz non-channel bonding (non-CB)* and *40MHz channel bonding (CB)* respectively. Thus, the OC assignment becomes inefficient in the dense WLAN using a number of APs. Secondly, in orthogonal channels (OCs), they are considered to be either non-interfering or interfering between the adjacent APs. The effect of the physical distance between them is not well considered. When the APs are assigned the same channel, the physical distance between them must be sufficiently large to avoid interfering. Thirdly, only the maximum transmission power is assigned to every AP as the conventional way. However, it has been reported that the minimum transmission power can improve the WLAN performance by reducing interferences while maintaining the required throughput to associated hosts.

On the other hand, in partially overlapping channels (POCs), the number of POCs is larger than that for OCs, and the interference can be changed continuously by the channel distance in addition to the physical distance and the transmission power. Thus, the proper POC assignment is important to improve the throughput performance of WLAN by estimating interference under the channel distance, the physical distance, and the AP transmission power.

In this thesis, to solve the above drawbacks, we studied the *throughput drop estimation models for concurrently communicating multiple links* where *partially overlapping channels (POCs)* are used instead of OCs. It has been observed that the use of POCs can improve the throughput performance by fully utilizing the available spectrums. However, in POCs, the frequency spectrums of adjacent channels are partially overlapped with each other, which can cause the throughput drop for concurrently communicating links using them. Thus, the POC assignment to the APs in WLAN using mathematical models is important to improve the throughput.

The proposed models estimate the *throughput drop* of the target link that is caused by the

interfered links, considering the *channel distance (chD)* and the *interfered received signal strength (RSS^i)* at the target AP from the neighbouring interfered APs on adjacent POCs. To obtain the nominal throughput of the target link under multiple interfering links, the throughput under no interference is first estimated using the model for a single link. Then, it is subtracted by the *throughput drop* estimated for each of the interfered links sequentially, in descending order of the throughput drop magnitude.

Firstly, in this thesis, we propose the *throughput drop estimation model for concurrently communicating multiple links* under *channel bonding (CB)*. The CB channels can provide high throughputs due to the wide channel width in general, where two adjacent channels are used together as one channel. It can increase the number of sub-carriers for data transmissions with *Orthogonal Frequency Division Multiplexing (OFDM)*. In addition, CB enhances the frame aggregation, which can further increase the transmission speed. We verify the accuracy of the model under CB by comparing estimated throughputs with measured ones under various conditions where both match well. Then, we confirm throughput improvements by adopting POCs from using OCs in simulations and experiments.

Secondly, in this thesis, we propose the *throughput drop estimation model* under *non-channel bonding links (non-CB)*. CB links can reduce the transmission capacity due to high interferences from other links. It has been observed that non-CB links provide higher throughputs than CB when several APs are co-located together. Therefore, we propose to extend the throughput drop estimation model under POCs for CB links to non-CB links. For evaluations, we verify the model accuracy through experiments in two network fields where measured throughput and estimated ones match well. Then, we confirm the effectiveness of the POC assignment to the APs using the model through simulations and experiments, where POC assignment outperforms OC assignment.

Thirdly, in this thesis, we propose the *throughput drop estimation model* under coexistences of *CB* and *non-CB* links. It has been observed that the simultaneous use of CB and non-CB can improve the WLAN performance. This model exploits the advantages of CB and non-CB together to increase the throughput under interferences. For evaluations, the measured throughput and estimated ones by the model match well. Besides, the performance results by the proposed joint CB and non-CB are better than *CB only* and *non-CB only*, or at least similar depending on each topology.

Lastly, in this thesis, we propose the application of the *throughput drop estimation model* under coexistences of *CB* and *non-CB* links to the joint assignment optimization of transmission power, frequency channel, and channel bonding to each AP by extending the *active AP configuration algorithm*. Either the minimum or maximum transmission power is assigned to the AP. In evaluation, it was confirmed that the proposal assigns the proper transmission power and channels for high throughputs.

In future studies, we will include further enhancements of the model to consider non-controlled APs in the WLAN, joint frequency assignment for 2.4 GHz and 5GHz, and improve its accuracy. Then, we will and evaluate it in various network topologies and fields.

To My Family and Friends

Acknowledgements

It is my great pleasure to express my heartiest thankfulness to those who gave me the valuable time and supported me in making this dissertation possible. I believe that you are the greatest blessing in my life. Thanks to all of you for making my dream successful.

I owe my deepest sense of gratitude to my supervisor, Professor Nobuo Funabiki for his excellent supervision, meaningful suggestions, persistent encouragements, and other fruitful help during each stage of my Ph.D. study. His thoughtful comments and guidance helped me to complete my research papers and present them in productive ways. Besides, he was always patient and helpful whenever his guidance and assistance were needed in both of my academic and daily life in Japan. I have really been lucky in working with a person like him. Needless to say, it would not have been possible to complete this thesis without his guidance and active support.

I am indebted to my Ph.D. co-supervisors, Professor Satoshi Denno and Professor Yasuyuki Nogami, for taking their valuable time to give me advice, guidance, insightful comments, and proofreading of this thesis.

I want to express my profound gratitude to Associate Professor Minoru Kuribayashi in Okayama University for his valuable discussions during my research. I would like to thank all my course teachers during my Ph.D. study for sharing their great ideas and knowledge with me. I would also like to give special thanks to Prof. Wen-Chung Kao of National Taiwan Normal University for his advices and supports, especially in proofing my papers before submissions.

I would like to acknowledge the Ministry of Education, Culture, Sports, Science, and Technology of Japan (MEXT) for financially supporting my Masters and Ph.D. study at Okayama University.

I would like to convey my appreciations to all the members of FUNABIKI Lab. Especially, I would like to give special thanks to Dr. Nobuya Ishihara, Ms. Keiko Kawabata, Dr. Md. Manowarul Islam, Dr. Samsul Huda, Dr. Rahardhita Widyatra Sudibyo, Dr. Hendy Briantoro, Dr. Yan Watequlis Syaifudin, Dr. Htoo Htoo Sandi Kyaw, Ms. Mousumi Saha, Mr. Md. Mahbubur Rahman, Mr. Hein Htet, Ms. Pradini Puspitaningayu, Mr. Yuanzhi Huo, Mr. Sujan Chandra Roy, Mr. Yohanes Yohanie Fridelin Panduman and all members in general. To share the time with these people in Okayama gave great experiences and unforgettable moments to me. Thank you so much for your great supports and helpfulness in this study and my daily life.

I would also like to express my special gratitude to my undergraduate teachers, especially Prof. David Gichoya and Mr. Shadrack Metto for their great support and guidance during the MEXT scholarship application process. Thank you very much for getting time to review my documents.

Last but not least, my special thanks go to my family and friends for their sincere friendships, inspirations, motivations, and supports.

KWENGA Ismael Munene
Okayama University, Japan
March, 2022

List of Publications

Journal Papers

1. **K. I. Munene**, N. Funabiki, M. Kuribayashi, R. W. Sudibyo and W. -C. Kao, "A throughput estimation model under two-link concurrent communications with partially overlapping channels and its application to channel assignment in IEEE 802.11n WLAN," Int. J. of Space-Based and Situated Computing, IJSSC, vol. 8, no. 3, pp. 123-137, 2018

2. **K. I. Munene**, N. Funabiki, M. M. Islam, M. Kuribayashi, M. S. A. Mamun, and W. -C. Kao, "An extension of throughput drop estimation model for three-link concurrent communications under partially overlapping channels and channel bonding in IEEE 802.11n WLAN," Int. Journal of Advances in Science, Technology and Engineering Systems, Vol. 4, No. 4, pp. 94-105, 2019.

3. **K. I. Munene**, N. Funabiki, H. Briantoro, M. M. Rahman, F. Akhter, M. Kuribayashi, and W. -C. Kao, "A throughput drop estimation model for concurrent communications under partially overlapping channels without channel bonding and its application to channel assignment in IEEE 802.11n WLAN," IEICE Trans. Vol. E104-D, No.05, pp.585-596, May. 2021.

4. **K. I. Munene**, N. Funabiki, M. M. Rahman, H. Briantoro, S. C. Roy, and M. Kuribayashi, "A throughput drop estimation model and its application to joint optimization of transmission power, frequency channel, and channel bonding in IEEE 802.11n WLAN for large-scale IoT environments," (conditionally accepted, Internet of Things Journal).

International Conference Papers

5. **K. I. Munene**, N. Funabiki, R. W. Sudibyo and W. -C. Kao, "A throughput drop estimation model for two-link concurrent communications with partially overlapping channels in IEEE 802.11n WLAN," IEEE global conf. on consumer electr., (GCCE 2018), pp 809-810, Japan, 2018.

6. **K. I. Munene**, N. Funabiki, R. W. Sudibyo, H. Briantoro, M. M. Rahman, and W. -C. Kao "A study of throughput drop estimation model for concurrently communicating two links without channel bonding in IEEE 802.11n wireless local-area network," IEEE Int. Conf. on Cons. Elect. (ICCE-TW), pp. 1-2, Sept. 2020.

7. **K. I. Munene**, N. Funabiki, H. Briantoro, M. M. Rahman, F. Akhter, and M. Kuribayashi, "Application of throughput drop estimation model under partially overlapping channels to channel assignment in IEEE 802.11n WLAN," Int. Conf. on Emerg. Techn. for Commun. (ICETC 2020), B3-2, Dec. 2020.

8. **K. I. Munene**, N. Funabiki, H. Briantoro, M. M. Rahman, S. C. Roy, and M. Kuribayashi, "A study of throughput drop estimation model for concurrently communicating links Under coexistence of channel bonding and non-bonding in IEEE 802.11n WLAN," Int. Work. on Virt. Environ. and Net.-Orien. Appl. (VENOA-2021), pp. 700-714, July 2021.

Other Papers

9. **K. I. Munene**, M. S. A. Mamun, K. S. Lwin, and N. Funabiki, "Throughput measurements under partially overlapping channels in IEEE 802.11n wireless local-area networks," 2017 (68th) Chugoku branch Joint Conv. Inst. Elec. Info. Eng., Oct. 2017.

10. **K. I. Munene**, N. Funabiki, M. S. A Mamun, K. S. Lwin, and S. K. Debnath , "A study of throughput estimation model and channel assignment algorithm for partially overlapping channels in IEEE 802.11n wireless local-area networks," IEICE Technical Report, vol. 117, no. 303, pp. 23-28, 2017.

11. **K. I. Munene**, K. S. Lwin, N. Funabiki, and M. Kuribayashi, "A throughput estimation model for two concurrently communicating links under partially overlapping channels and channel bonding in IEEE 802.11n WLAN," IEICE Tech. Report on Short Range Wireless Comm. (SRW), pp 13-18, August 20, 2018.

12. **K. I. Munene**, N. Funabiki, R. W. Sudibyo, M. M. Islam, M. Kuribayashi, and W. -C. Kao, "An extension of throughput drop estimation model for three-link concurrent communications under partially overlapping channels and channel bonding in IEEE 802.11n WLAN," IEICE Technical Report, pp. 89-94, Dec. 2018.

13. **K. I. Munene**, N. Funabiki, R. W. Sudibyo, H. Briantoro, and M. M. Rahman, "A throughput drop estimation model for two-link concurrent communications with non-bonded partially overlapping channels in IEEE 802.11n WLAN," IEICE General Conference, pp. S8-S9, March 2020.

14. **K. I. Munene**, N. Funabiki, H. Briantoro, M. M. Rahman, and M. Kuribayashi, "An extension of throughput estimation model for three-link concurrent communications under partially overlapping channels without channel bonding in IEEE 802.11n WLAN," IEICE Technical Report, NS2020-29, pp. 13-18, June. 2020.

15. **K. I. Munene**, N. Funabiki, H. Briantoro, M. M. Rahman, S. C. Roy, and M. Kuribayashi, "Application of throughput drop estimation model to frequency channel and channel bonding assignment in IEEE 802.11n WLAN," IEICE Society Conf., BS-6-11, pp. S-42-43, Sept. 14-17, 2021.

List of Figures

List of Tables

List of Abbreviations

WLAN wireless local area network

AP access point

ISM Industrial Scientific and Medica

MAC media access control

RF radio frequency

NIC network interface card

BSS basic service set

IBSS independent basic service set

ESS extended service set

MIMO multiple input multiple output

non-CB non channel bonding

CB channel bonding

OC orthogonal channel

POC partially overlapping channel

RSS^i interfered received signal strength

PC personal computer

chD channel distance

phD physical distance

lkD link distance

tpD throughput drop

DAP dedicated access point

VAP virtual access point

MAP mobile access point

List of Notations

E_1 number of active APs

E_2 minimum average host throughput

E_3 total interfered communication time

tp_{ij} link speed between AP_i and $host_j$

tpD_{nec} throughput drop for *NEC AP*

tpD_{pi} throughput drop for *Raspberry Pi AP*

tpM^{nec} maximum throughput for *NEC AP*

tpM^{pi} maximum throughput for *Raspberry Pi AP*

$Srf(m)$ contention factor at AP_i among the associated hosts to send data by the CSMA/CA

Contents

Chapter 1

Introduction

1.1 Background

Nowadays, the *IEEE 802.11 wireless local-area network (WLAN)* has been deployed world-wide for Internet access in various places, including airports, shopping malls, stations, and hotels, due to its advantages of the flexibility, the lower cost, and the high data transmission capacity [1–3]. WLAN users can easily access to the Internet through wireless connections with *access points (APs)* using mobile devices like smart phones, tablets, and laptop PCs.

The IEEE 802.11 WLAN can operate in two unlicensed frequency bands of *2.4 GHz Industrial, Scientific, and Medical (ISM)* band and *5 GHz Unlicensed National Information Infrastructure (U-NII)* band [4,5]. Currently, the *IEEE 802.11n* at *2.4 GHz ISM* band has prevailed over WLAN due to the wide coverage range with the stronger penetration capability for indoor environments [6]. Besides, it provides the high-speed data transmission capability using the *channel bonding (CB)*, *frame aggregation* and *multiple input multiple output (MIMO)* technologies. The *channel bonding (CB)* increases the data transmission rate by allowing the wireless NIC device to operate on *40 MHz* width channels by combining two adjacent *20 MHz* channels into one [7, 8]. On the other hand, *MIMO* allows a single radio channel to support multiple data streams by using multiple antennas at the transmitter and the receiver [9]. The *frame aggregation* increases the data transmission rate by concatenating several data frames into one to reduce the overhead.

At *2.4 GHz ISM* band, the IEEE 802.11 standards define the limited number of channels for use, where only *three* channels under *non-channel bonding (non-CB)* are orthogonal. One channel basically has the $20MHz$ width, and the frequency gap between two adjacent channels is merely *5 MHz*. Thus, the spectrums of adjacent channels are partially overlapped with each other, which names the *partially overlapping channels (POCs)* [10, 11]. For example, *channel* 1 partially overlaps with three channels 2, 3, and 4. Therefore, the proper channel assignment becomes a key challenge in enhancing the throughput performance of WLAN.

To maximize the throughput performance by reducing interferences among wireless signals, previously, we studied the *orthogonal channel assignment (OC)* assignment under *20 MHz non-CB* in the *active AP configuration algorithm* for the *elastic WLAN system* [12,13]. Figure 1.1 shows a simple topology of the elastic WLAN system. The system applies the active AP configuration algorithm to dynamically control the number of active APs according to throughput demands and device conditions, while providing the necessary minimum throughput to every host. The elastic WLAN system controls the number of active APs by deactivating the unnecessary APs. Hence, it can reduce the interference and power consumption. Each active AP is assigned an orthogonal non-CB channel in a way to minimize the overall interference in the network.

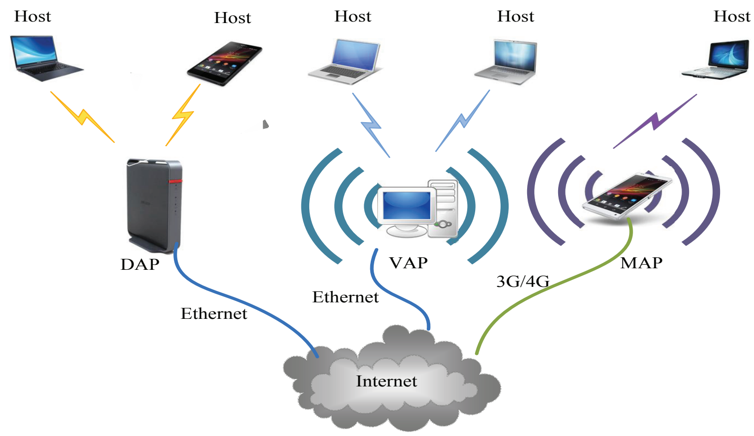

Figure 1.1: Overview of Elastic WLAN.

However, it has been found that the following limitations need to be solved to enhance throughput performance:

- Firstly, the number of orthogonal channels (OCs) is very limited, where only *three* and *two* channels are available under *20MHz non-channel bonding (non-CB)* and *40MHz channel bonding (CB)* respectively. Thus, the OC assignment becomes inefficient in the dense WLAN using a number of APs due to the high interference.

- Secondly, in orthogonal channels (OCs), they are considered to be either non-interfering or interfering between the adjacent APs. The effect of the physical distance between them is not well considered. When the APs are assigned the same channel, the physical distance between them must be sufficiently large to avoid interfering.

- Thirdly, it has been observed that the simultaneous use of CB and non-CB in the network can improve the WLAN performance. Thus, both CB and non-CB should be considered together to enhance the throughput performance under interferences in WLAN by exploiting the advantages of CB and non-CB together.

- Fourthly, it has been reported that the minimum transmission power can improve the WLAN performance by reducing interferences while maintaining the required throughput to associated hosts. Thus, both the maximum and minimum transmission powers should be considered together.

On the other hand, in partially overlapping channels (POCs), the number of POCs is larger than that for OCs, and the interference can be changed continuously by the channel distance in addition to the physical distance and the transmission power. Thus, the proper POC assignment is important to improve the throughput performance of WLAN by estimating interference under the channel distance, the physical distance, and the AP transmission power.

1.2 Contributions

In this thesis, we have carried out the following research contributions.

We studied the *throughput drop estimation models for concurrently communicating multiple links* where *partially overlapping channels (POCs)* are used [14–16] instead of *orthogonal channels (OCs)* used in our previous study. We observed that the proper use of POCs can give better performance than OCs. Similarly, in literature, it has been reported that the use of POCs can improve the throughput performance by fully utilizing the available spectrums [10, 11, 17–20]. However, in POCs, the frequency spectrums of adjacent channels are partially overlapped with each other, which can cause the throughput drop for concurrently communicating links using them. Thus, the POC assignment to the APs in WLAN using mathematical models is important to improve the throughput.

Our models adopting POCs estimate the *throughput drop* of the target link that is caused by the interfered links, considering the *channel distance (chD)* and the *interfered received signal strength (RSS^i)* at the target AP from the neighbouring interfered APs on adjacent POCs. To obtain the nominal throughput of the target link under multiple interfering links, the throughput under no interference is first estimated using the model for a single link in [21]. Then, it is subtracted by the *throughput drop* estimated for each of the interfered links sequentially, in descending order of the throughput drop magnitude.

As the first contribution, we propose the *throughput drop estimation model* for concurrently communicating multiple links under CB channels [14, 22, 23]. The CB channels can provide high throughputs due to the wide channel width in general, where two adjacent channels are used together as one channel [7, 8, 24]. It can increase the number of sub-carriers for data transmissions with *Orthogonal Frequency Division Multiplexing (OFDM)* to 108 from 52 in the conventional non-CB 20 MHz channel, [25]. In addition, CB enhances the frame aggregation, which can further increase the transmission speed. We verify the accuracy of the model under CB by comparing estimated throughputs with measured ones under various conditions where both match well. Then, we confirm throughput improvements by adopting POCs from using OCs in simulations by the WIMNET simulator [26] and experiments using the testbed system.

As the second contribution, we propose the *throughput drop estimation model* under *non-CB* links [15, 27, 28]. The CB reduces the number of non-interfered channels, thus reducing the transmission capacity of links due to high interferences from other links. Besides, as shown in [29], the wider bandwidth of the *CB* link can cause the reduction of *signal to interference plus noise ratio (SINR)* at the distant host from the AP. Then, the lower $SINR$ can cause the adoption of the slower *modulation and coding scheme (MCS)* and the *hidden terminal problem*, which can further lower the throughput. Thus, it has been observed that the conventional non-CB links are still common in numerous WLANs, because they provide higher throughputs than CB when several APs are co-located together. Especially, the non-CB links are used in a dense WLAN to reduce interferences.

Therefore, we extend the throughput drop estimation model under POCs for CB links to the conventional non-CB links. For evaluations, we verify the model accuracy through experiments in two network fields where measured throughput and estimated ones match well. Then, we confirm the effectiveness of the POC assignment to the APs using the model through simulations by the WIMNET simulator [26] and experiments, where the POC assignment outperforms the OC assignment.

As the third contribution, we propose the *throughput drop estimation model* under coexistences of *CB* and *non-CB* links [16]. It has been observed that the simultaneous use of CB and non-CB can improve the WLAN performance. This model exploits the advantages of CB and non-CB together to increase the throughput under interferences. For evaluations, the measured throughput and estimated ones by the model match well. Besides, the performance results by the proposed joint CB and non-CB are better than *CB only* and *non-CB only*, or at least similar depending on the topology.

Lastly, we study the application of the *throughput drop estimation model* under coexistences of *CB* and *non-CB* links to the joint assignment optimization of transmission power, frequency channel, and channel bonding by extending the *active AP configuration algorithm* [30]. Either the minimum or maximum transmission power is assigned to the AP. It is noted that the minimum transmission power at the AP can provide throughput similar to that of maximum transmission power when the host is located near the AP due to the non-linear relationship between RSS and the throughput. At the same time, the minimum transmission power can reduce interferences among the co-located APs. When the host is located far from the AP, the maximum transmission power at the AP is necessary to provide the sufficient RSS for better throughput [31, 32]. Through evaluations, it was confirmed that the proposal assigns the proper transmission power and channels for high throughputs.

1.3 Thesis Outline

The remaining part of this thesis is organized as follows.

In Chapter 2, we review IEEE 802.11 wireless network technologies related to this thesis, including the IEEE 802.11n protocols, features of IEEE 802.11n protocols, and software tools in the Linux operating system.

In Chapter 3, we review our previous studies related to this thesis.

In Chapter 4, we describe the throughput measurement method in general for concurrently communicating links adopted in this thesis.

In Chapter 5, we describe the proposed throughput drop estimation model under channel bonding and its evaluations.

In Chapter 6, we describe the proposed throughput drop estimation model under non-channel bonding and its evaluations.

In Chapter 7, we describe the proposed throughput drop estimation model under coexistence of channel bonding and non-channel bonding with transmission power tuning and its evaluation.

In Chapter 8, we describe the proposed application of throughput drop estimation model under coexistence of channel bonding and non-channel bonding to joint optimizations of transmission power, frequency channel, and channel bonding assignment in WLAN.

In Chapter 9, we review relevant works in literature.

Finally, in Chapter 10, we conclude this thesis with some future works.

Chapter 2

Background Technologies

This chapter introduces background technologies for this thesis. First, we give an overview of *IEEE 802.11 WLAN* including advantages, components, types and standards. Then, we discuss the *IEEE 802.11n protocol* and its key features. Finally, we outline some Linux tools and commands for WLANs that are used for measurements, and the implementation of elastic WLAN system.

2.1 802.11 WLAN Overview

IEEE 802.11 standards define *physical (PHY)* and *media access control (MAC)* layer specifications for implementing high-speed *wireless local area network (WLAN)* technologies. WLAN is an extension to a wired LAN that enables the user mobility by the wireless connectivity and supports the flexibility in data communications [1]. It can reduce the cabling costs in the home or office environments by sending and receiving data over the air using *radio frequency (RF)* technology. Therefore, WLANs are adopted in many places such as home, school, campus, and offices.

2.1.1 Advantages of WLAN

WLAN provides several benefits over the traditional wired networks in the following [1]:

- *User mobility:*
  Wireless networking allows mobility than wired networking. In wired networking, users need to use wired lines to stay connected to the network. WLAN gives users the ability to move around within a local coverage area and still be connected to the network.

- *Easy and rapid deployment:*
  WLAN can eliminate the requirement of network cables between hosts and connection hubs or APs. Thus, the installation of WLAN can be much easier and quicker than the wired LAN.

- *Cost:*
  The cost of installing and maintaining a traditional wired LAN is normally higher than installing and maintaining WLAN. WLAN reduces the cost of cabling and the works related to installation and reparation. Because WLAN simplifies moving, adding, and changing, the indirect cost of user downtime and administration are decreased.

- *Increased flexibility:*
  WLAN installation eliminates the need to pull cable through walls and ceilings. The network coverage area of WLAN can be easily expanded because the network medium is everywhere.

- *Scalability:*
  WLAN can be configured for a variety of topologies suitable to applications. WLAN can support both peer-to-peer networks suitable for a small number of users and full infrastructure networks of thousands of users. New access points can be added easily to expand the coverage area.

2.1.2 IEEE 802.11 WLAN Components

IEEE 802.11 WLAN consists of four primary components as shown in Figure 2.1 [1]:

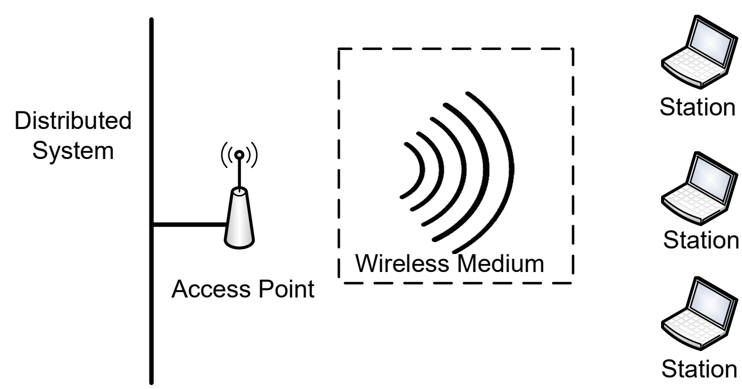

Figure 2.1: Components of IEEE 802.11 WLANs.

- *Stations or hosts:*
  WLAN transfers the data between *stations or hosts*. A *station* in WLAN indicates an electronic device such as a desktop/laptop PC, a smartphone, or a tablet that has the capability of accessing the network over the wireless *network interface card (NIC)*.

- *Access points (APs):*
  An AP acts as the generic base station for WLAN that performs the similar role as a hub/switch in a wired Ethernet LAN. It also provides the bridging function between the wireless and the wired networks with some other tasks.

- *Wireless medium:*
  The IEEE 802.11 standard uses the wireless medium to convey the information/ data from one host to another host in a network.

- *Distribution system:*
  When several APs are connected together to make the large coverage area, they must communicate with each other to trace the movements of the hosts. The distribution system is the logical component of WLAN which serves as the backbone connections among APs. It is often referred to as the *backbone network* used to relay data frames between APs. In most cases, *Ethernet* is commonly used as the backbone network technology.

2.1.3 Types of WLANs

The basic unit of *IEEE 802.11* WLAN is simply a set of hosts that can communicate with each other known as the *basic service set (BSS)*. Based on the types of BSS, the IEEE 802.11 standards support two types of WLAN as illustrated in Figure 2.2.

- *Independent or ad hoc type:*
  In this type, a collection of stations or hosts can send frames directly to each other without an AP. It is also called as an *independent BSS (IBSS)* as shown in Figure 2.2(a). This *ad hoc network* is rarely used for practical networks due to the lack of required performances and security issues.

- *Infrastructure type:*
  In this type, the stations exchange the data through an AP as shown in Figure 2.2(b). A single AP acts as the main controller to all the hosts within its BSS, known as *infrastructure BSS*. In this type, a host must be associated with an AP to obtain network services [33].

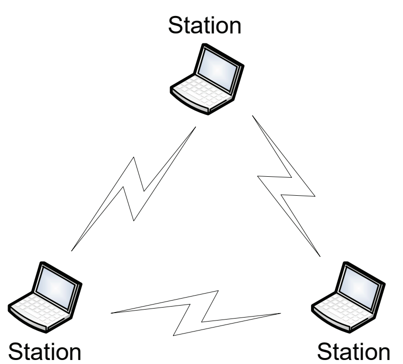

(a) Adhoc network.

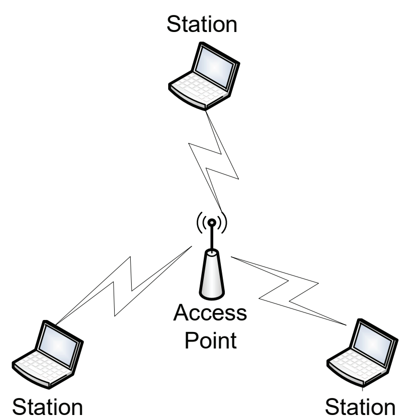

(b) Infrastructure network.

Figure 2.2: Types of IEEE 802.11 WLAN networks.

To extend WLAN further, multiple BSSes can be connected together with a backbone network to form *extended service set (ESS)* as shown in Figure 2.3.

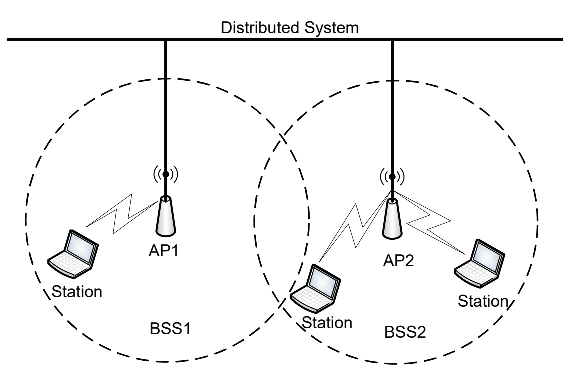

Figure 2.3: Extended service set (ESS).

ESS can form a large size WLAN. Each AP in ESS is given an ID called the *service set identifier (SSID)*, which serves as the "network name" for the users. All the hosts within the same ESS can mutually communicate with each other, even if they are in different basic service areas.

2.1.4 IEEE 802.11 Standards for WLAN

The IEEE 802.11 working group has improved the existing PHY and MAC layer specifications to realize WLAN at the 2.4-2.5 GHz, 3.6 GHz and 5.725-5.825 GHz unlicensed ISM *(Industrial, Scientific and Medical)* frequency bands defined by the ITU-R. In this working group, several types of IEEE Standard Association Standards are available, where each of them comes with a letter suffix, covers from wireless standards, to standards for security aspects, Quality of Service (QoS) and others, shown in Table 2.1 [33–38].

Table 2.1: IEEE 802.11 Standards.

Standard	Purpose
802.11a	Wireless network bearer operating in the 5 GHz ISM band, data rate up to $54 Mbps$
802.11b	Operate in the 2.4 GHz ISM band, data rates up to $11 Mbps$
802.11c	Covers bridge operation that links to LANs with a similar or identical MAC protocol
802.11d	Support for additional regulatory differences in various countries
802.11e	QoS and prioritization, an enhancement to the 802.11a and 802.11b WLAN specifications
802.11f	Inter-Access Point Protocol for handover, this standard was withdrawn
802.11g	Operate in 2.4 GHz ISM band, data rates up to $54 Mbps$
802.11h	Dynamic Frequency Selection (DFS) and Transmit Power Control (TPC)
802.11i	Authentication and encryption
802.11j	Standard of WLAN operation in the 4.9 to 5 GHz band to conform to the Japan's rules
802.11k	Measurement reporting and management of the air interface between several APs
802.11l	Reserved standard, to avoid confusion
802.11m	Provides a unified view of the 802.11 base standard through continuous monitoring, management and maintenance
802.11n	Operate in the 2.4 and 5 GHz ISM bands, data rates up to $600 Mbps$
802.11o	Reserved standard, to avoid confusion
802.11p	To provide for wireless access in vehicular environments (WAVE)
802.11r	Fast BSS Transition, supports VoWiFi handoff between access points to enable VoIP roaming on a WiFi network with 802.1X authentication
802.11s	Wireless mesh networking
802.11t	Wireless Performance Prediction (WPP), this standard was cancelled
802.11u	Improvements related to "hotspots" and 3rd party authorization of clients
802.11v	To enable configuring clients while they are connected to the network

Table 2.1: IEEE 802.11 Standards.

Standard	Purpose
802.11w	Protected Management Frames
802.11x	Reserved standard, to avoid confusion
802.11y	Introduction of the new frequency band, 3.65-3.7GHz in US besides 2.4 and 5 GHz
802.11z	Extensions for Direct Link Setup (DLS)
802.11aa	Specifies enhancements to the IEEE 802.11 MAC for robust audio video (AV) streaming
802.11ac	Wireless network bearer operating below 6 GHz to provide data rates of at least $1Gbps$ for multi-station operation and $500Mbps$ on a single link
802.11ad	Wireless Gigabit Alliance (WiGig), providing very high throughput at frequencies up to 60GHz
802.11ae	Prioritization of management frames
802.11af	WiFi in TV spectrum white spaces (often called White-Fi)
802.11ah	WiFi uses unlicensed spectrum below 1GHz, smart metering
802.11ai	Fast initial link setup (FILS)
802.11aj	Operation in the Chinese Milli-Meter Wave (CMMW) frequency bands
802.11ak	General links
802.11aq	Pre-association discovery
802.11ax	High efficiency WLAN, providing 4x the throughput of 802.11ac
802.11ay	Enhancements for Ultra High Throughput in and around the 60GHz Band
802.11az	Next generation positioning
802.11mc	Maintenance of the IEEE 802.11m standard

Figure 2.4 demonstrates the current and future WiFi standards. Among them, the common and popular ones are IEEE 802.11a, 11b, 11g, 11n, 11ac, and the latest is 11ax. For the physical layer, the 11a/n/ac use *Orthogonal Frequency Division Multiplexing (OFDM)* modulation scheme while the 11b uses the *Direct Sequence Spread Spectrum (DSSS)* technology. 11g supports both technologies. The latest 11ax uses *Orthogonal Frequency Division Multiple Access (OFDMA)* that is a multi-user version of OFDM. Table 2.2 summarizes the features of these common WiFi standards [1, 39–41].

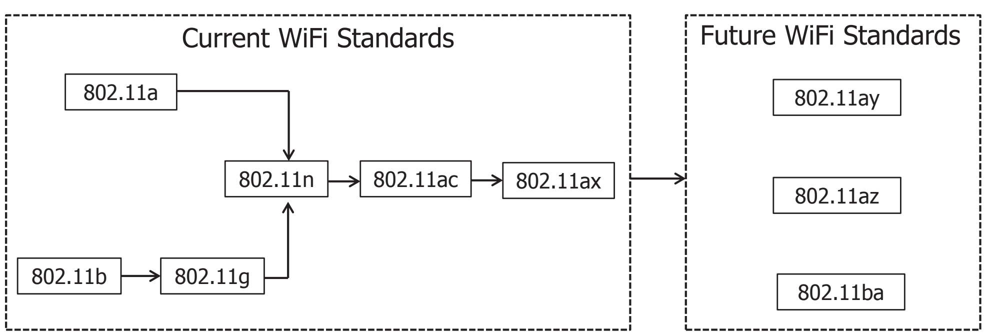

Figure 2.4: Current and future WiFi Standards.

Table 2.2: Characteristics of common IEEE802.11 standards.

	IEEE 802.11b	IEEE 802.11a	IEEE 802.11g	IEEE 802.11n	IEEE 802.11ac	IEEE 802.11ax
Release	Sep 1999	Sep 1999	Jun 2003	Oct 2009	Dec 2013	Feb 2021
Frequency Band	2.4 GHz	5 GHz	2.4 GHz	2.4/5 GHz	5 GHz	2.4/5/6 GHz
Max. Data Rate	11 Mbps	54 Mbps	54 Mbps	600 Mbps	1300 Mbps	9608 Mbps
Modulation	CCK[1] modulated with PSK	OFDM	DSSS[2], CCK, OFDM	OFDM	OFDM	OFDMA
Channel Width	20 MHz	20 MHz	20 MHz	20/40 MHz	20/40/80/160 MHz	20/40/80/160 MHz
# of Antennas	1	1	1	4	8	8
security	Medium	Medium	Medium	High	High	High

[1] CCK: Complementary Code Keying
[2] DSSS: Direct Sequence Spread Spectrum

The IEEE 802.11a, b, and g are considered to have medium security because they use the *wired equivalent privacy (WEP)* security mechanism. The WEP encryption uses the RC4 symmetric stream cipher with 40-bit and 104-bit encryption keys. The WEP has the following weaknesses; *1) short initializer vectors (IVs) and keys, 2) authentication messages can be easily forged, 3) IV reuse problem which makes stream ciphers vulnerable to analysis, 4) use of cryptographically insecure cyclic redundancy check (CRC) for integrity check, and 5) lack of key-management protocol* [42].

On the other hand, the IEEE 802.11n, ac and ax are considered to have high security because they use the more advanced WPA encryption technology called *temporal key integrity protocol (TKIP)* with message integrity check (MIC). WPA also provides a scheme of mutual authentication using either IEEE 802.1X/extensible authentication protocol (EAP) or pre-shared key (PSK) technology.

- *IEEE 802.11b:* IEEE 802.11b operates at 2.4 GHz band with the maximum data rate up to 11 Mbps. 11b is considered to be robust and has a capacity to compensate the same IEEE 802.11 protocols. Because of the interoperability feature between the products from different vendors, this standard has not only boosted the manufacturing of the products but also motivated the competitions between WLAN vendors. The limitation of this standard is the interference among the products using *industrial, scientific and medical* (ISM) band that uses the same 2.4 GHz band of frequency [43, 44].

- *IEEE 802.11a:* IEEE 802.11a operates at 5 GHz ISM band. It adopts on orthogonal frequency division multiplexing (OFDM) coding scheme that offers a high data rates up to 6, 12, 24, 54 Mbps, and sometimes beyond this speed in comparison to 11b. Two main limitations of 11a are the compatibility issue of the 11a products with the 11b products and the unavailability of 5 GHz band with free of costs in some countries in the world [43, 44].

- *IEEE 802.11g:* IEEE suggested 11g standard over 11a to improve the 2.4 GHz 11b technology. 11g introduces two different modulation techniques including the *packet binary convolution code (PBCC)* that supports the data rate up to 33 Mbps and the *orthogonal frequency division multiplexing (OFDM)* that supports up to 54 Mbps data rate. Compatibility issues are also resolved in 11g products with 11b products [43,44].

- *IEEE 802.11n:* The primary purpose of initiating the 11n standard to improve the usable range and the data rate up to 600 Mbps. 11n supports both of the 2.4 GHz and 5 GHz ISM band *unlicensed national information infrastructure* (UNII) band, and is backward compatible with earlier standards. It introduces new technology features including the use of *channel bonding* and *multiple antennas* to get the better reception of the RF signals to enhance the throughput and coverage range [5,43].

- *IEEE 802.11ac:* The aim of the 11ac standard to improve the individual link performance and the total network throughput to more than $1Gbps$. Many of the specifications like static and dynamic channel bonding and simultaneous data streams of 11n have been kept and further enhanced for 11ac to reach the gigabit transmission rate. It supports static and dynamic channel bonding up to $160MHz$ and *Multi-User Multiple-Input-Multiple-Output (MU-MIMO)*. 11ac operates only on the $5GHz$ band [45–47].

- *IEEE 802.11ax: IEEE 802.11ax* standard was approved on February 2021, which operates in the frequency bands between $1GHz$ and $7.125GHz$. This standard focuses on enhancing the throughput-per-area or the ratio between the total network throughput and the network area size. The maximum data rate of this standard is $9.6Gbps$. It also adopts channel bonding up $160MHz$. *IEEE 802.11ax* supports *orthogonal frequency division multiple access (OFDMA)* approach that is commonly applied in cellular networks [48–52]. However, only few devices are compatible with this standard now.

2.2 IEEE 802.11n Protocol

In this section, we describe the IEEE 802.11n protocol that has been used for our throughput measurements, proposed models and implementations in this thesis. IEEE 802.11n is an amendment to the IEEE 802.11 2007 wireless networking standard. It adopts several performance enhancement features such *channel bonding (CB)*, *Multiple Input Multiple Output (MIMO)*, frame aggregation, and security improvements over the previous 11a, 11b, and 11g standards. Table 2.3 summarizes the key features of *IEEE 802.11n* standard.

Table 2.3: IEEE 802.11n specification.

Specification	**IEEE 802.11n**	
Frequency Band	2.4 GHz	5 GHz
Simultaneous Uninterrupted Channel	2 ch	9 ch
Available Channel	13 ch	19 ch
Max. Speed	$600Mbps$	
Max. Bandwidth	40 MHz	
Max. Spatial Streams	4	
Subcarrier Modulation Scheme	64 QAM	
Release Date	Sept 2009	

The IEEE 802.11n supports both on 2.4GHz and 5GHz bands. Currently, 2.4GHz is most popular. This frequency band has become crowded with lots of WiFi signals using the same channel or partially overlapping channels. As a result, these WiFi signals with adjacent channels will suffer from interferences between them, and end up with throughput performance drops [14, 15, 37, 39]. For 2.4GHz band, there is a limited number of non-interfered channels, which are Channel 3 and Channel 11 in the 40MHz bandwidth. While for the 20MHz bandwidth, Channel 1, Channel 6, and Channel 11 are basically free from interferences among them. In overall, the wider bandwidth will reduce the number of orthogonal channels. Figure 2.5 [38] shows the WiFi channels for IEEE 802.11n 2.4 GHz band.

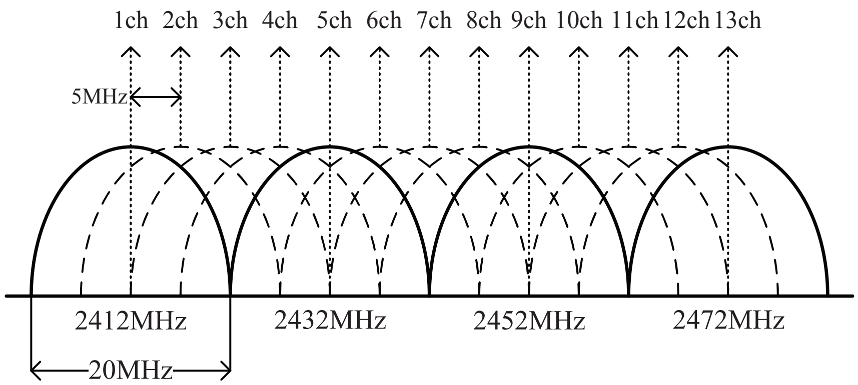

Figure 2.5: WiFi channels in 2.4 GHz band.

In the 5 GHz band of IEEE 802.11n protocol, it has 19 uninterrupted channels available with the 20 MHz bandwidth. In the 40 MHz bandwidth, which doubles the channel width from the 20 MHz, there are nine channels. For the 80 MHz bandwidth, there are four of them. Figure 2.6 shows the channels for the 5GHz band [53].

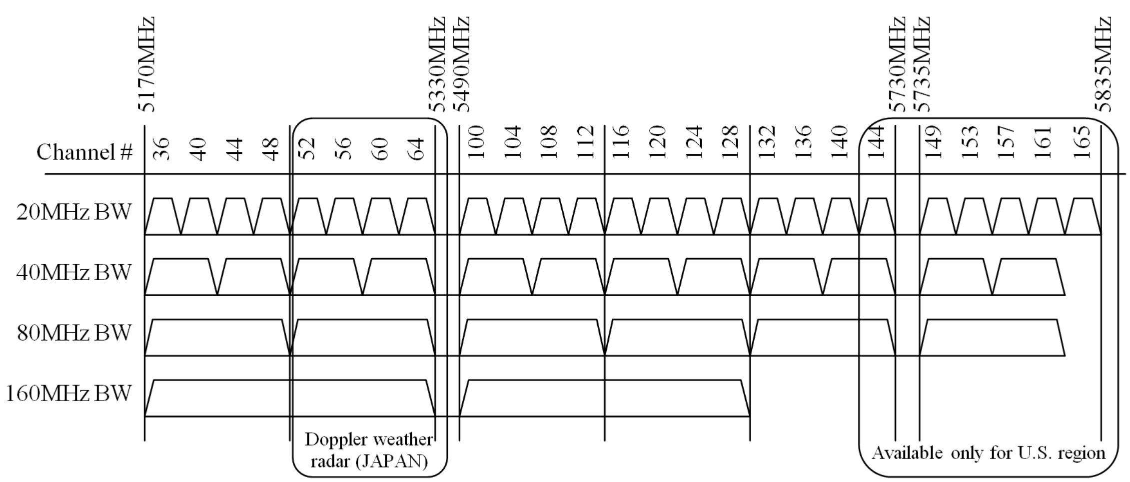

Figure 2.6: WiFi channels in 5 GHz band.

2.3 Features of IEEE 802.11n Protocol

IEEE 802.11n protocol incorporates several new technologies to boost up its performance. The standard uses the multiple antennas technology, channel bonding, frame aggregation, and security improvements mechanism to improve the throughput. In this section, we describe these features of the protocol.

2.3.1 Channel Bonding

The *IEEE 802.11n* protocol supports channel bonding where each channel can operate with the 40 MHz bandwidth by using two adjacent 20 MHz channels together to double its physical data rate [54] as shown in Figure 2.7. However, the usage of the channel bonding will reduce the available non-interfered channels for other devices as there are only two non-interfered bonded channels available at 2.4 GHz band. Table 2.4 summarizes the channel bonding for the 13 *20 MHz* channels at *2.4 GHz* band [55].

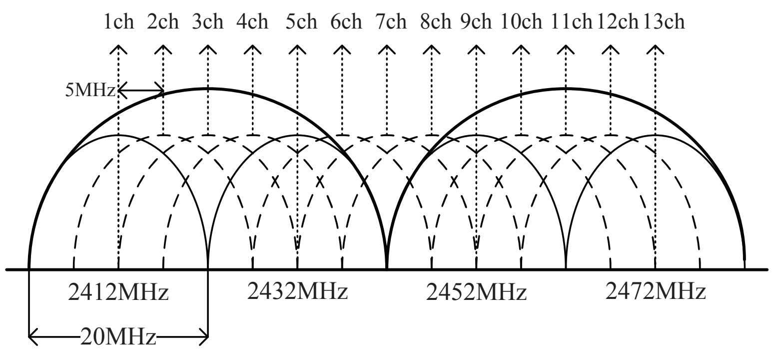

Figure 2.7: IEEE 802.11n channel bonding concept.

Table 2.4: Channel bonding in IEEE 802.1n.

20MHz		40MHz	
center frequency of primary channel	center frequency of secondary channel	bonded channel	center frequency of bonded channel
1	5	1+5	3
2	6	2+6	4
3	7	3+7	5
4	8	4+8	6
5	9	5+9	7
6	10	6+10	8
7	11	7+11	9
8	12	8+12	10
9	13	9+13	11

Table 2.5 shows the usage of different channel bandwidths and spatial streams towards the throughput of *IEEE 802.11n*.

Table 2.5: Effects of channel bandwidth and spatial stream's selection towards IEEE 802.11n's throughput.

Stream number	Bandwidth	
	20 MHz	40 MHz
1 Stream	$72.2Mbps$	$150Mbps$
2 Streams	$144.4Mbps$	$300Mbps$
3 Streams	$216.7Mbps$	$450Mbps$
4 Streams	$288.9Mbps$	$600Mbps$

2.3.2 Partially Overlapping Channels

In *IEEE 802.11*, at 2.4 GHz band, each channel has 20 MHz width, and two adjacent channel bands are 5 MHz apart. Thus, all the adjacent channels are partially overlapped with each other. That is to say, each channel is partially overlapped with at least three neighbour channels.

2.3.3 MIMO (Multiple Input Multiple Output)

In MIMO, the throughput can be linearly increased to the number of transmitting (T_X) and receiving (R_X) antennas up to four times, without the additional bandwidth or transmission power. The coverage area can be enhanced over the single antenna technology in *Single-Input Single-Output* (SISO). The multiple antenna configurations in *MIMO* can overcome the detrimental effects of multi-path and fading, trying to achieve high data throughput in limited bandwidth channels. For example, in the 4×4 MIMO, four independent data streams can be multiplexed and transmitted simultaneously with the *spatial division multiplexing* (*SDM*), to speed up the transmission capacity by quadruple as shown in Figure 2.8.

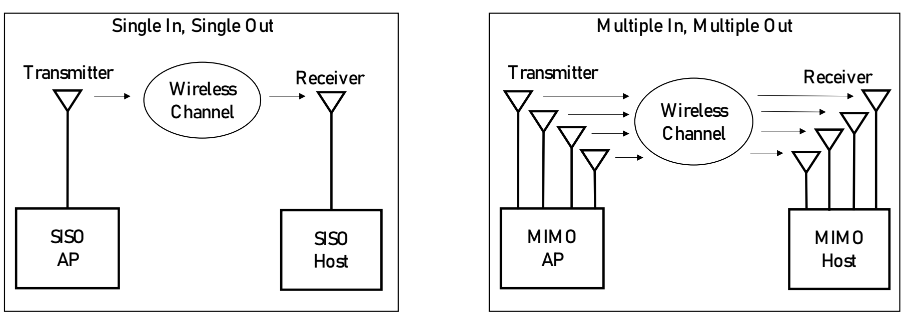

Figure 2.8: Comparison between SISO and 4×4 MIMO technology.

When the *space-time block coding* (*STBC*) is adopted in the 4×4 MIMO link, the sender can transmit four copies of the data stream over four antennas to improve the reliability and the effective range of data transmissions.

2.3.4 MAC Layer Enhancements

Besides the introduction of channel bonding and MIMO, IEEE 802.11n also provides performance improvements through the *frame aggregation* and the proper selection of the *modulation and coding scheme (MCS)*.

- *Frame Aggregation:*
  The *IEEE 802.11n* provides extra performance improvement through the frame aggregation in the MAC layer, besides MIMO. The frame aggregation can transmit multiple frames by one big frame with a single pre-ample and header information to reduce the overhead by them. IEEE 802.11n introduces the *Aggregation of MAC Service Data Units (A-MSDUs)* and *Aggregation of MAC Protocol Data Units (A-MPDUs)*. Frame aggregation is a process of packing multiple A-MSDUs and A-MPDUs together to reduce the overheads and average them over multiple frames, thereby increasing the user level data rate [56].

- *Modulation and Coding Scheme:*
  Various modulation, error-correcting codes are used in the IEEE 802.11n, represented by a Modulation and Coding Scheme (MCS) index value, or *mode*. IEEE 802.11n defines 31 different modes and provides the greater immunity against selective fading by using the Orthogonal Frequency Division Multiplexing (OFDM). This standard increases the number of OFDM sub-carriers of 56 (52 usable) in *High Throughput (HT)* with $20MHz$ channel width and 114 (108 usable) in HT with $40MHz$. Each of these sub-carriers is modulated with BPSK, QPSK, 16-QAM or 64-QAM, and Forward Error Correction (FEC) coding rate of 1/2, 2/3, 3/4 or 5/6 [57].

2.4 Linux Tools for Wireless Networking

As an open-source operating system, *Linux* has been used as a platform to implement new algorithms, protocols, methods, and devices for advancements of wireless networks [58]. In this section, we give the overview of the Linux tools and software used for the measurement performed throughout the thesis and the implementation of the *elastic WLAN system*.

2.4.1 'hostapd' - to Make AP-mode Linux-PC

hostapd is a Linux tool to realize the AP and the authentication server. It implements IEEE 802.11 AP managements, along with other IEEE 802.1X protocols and security applications. In *Linux*, *hostapd* can be installed by downloading the source code from [59] or using the following command:

```
$ sudo apt-get install hostapd
```

After installing this tool in a Linux PC that contains WLAN driver that supports the AP mode, it can be configured to create a command-line based AP in the Linux-PC. The *hostapd* can be started or stopped by the following commands:

```
$ sudo /etc/init.d/hostapd start
$ sudo /etc/init.d/hostapd stop
```

2.4.2 'ssh' - to Remotely Execute Command

ssh is an abbreviation of *Secure Shell* that is a cryptographic network protocol to securely initiate a shell session on a remote machine [60, 61]. It is operated in two parts: *SSH client* and *SSH server*, and establishes a secure channel between them over an insecure network. The open source version of *ssh* is *OpenSSH* [62] that can be installed using the following command [63]:

```
$ sudo apt-get install openssh-server openssh-client
```

The following list shows an example to remotely execute *nm-tool* on a remote host through the network using *ssh* [60, 61, 64]:

```
$ ssh username@192.168.1.31 'nm-tool'
username@192.168.1.31's password:
```

Here, 192.168.1.31 represents the IP address of the remote host.

2.4.3 'iperf' - to Measure Link Speed

iperf [65] is a software to measure the available throughput or bandwidth on IP networks. It supports both TCP and UDP protocols along with tuning various parameters related to timing and buffers, and reports the bandwidth, the loss, and other parameters. *iperf* is usually installed by default in the Ubuntu distribution. It can also be installed manually using the following command:

```
$ sudo apt-get install iperf
```

To measure the TCP throughput between two devices using *iperf*, one of them uses the server-mode and the other one uses the client-mode, where packets are transmitted from the client to the server. The *iperf* output contains the time-stamped report of the transmitted data amount and the measured throughput. The following list shows the typical use of *iperf* on the server and client side for throughput measurement:

```
$ iperf -s //server side
$ iperf -c 172.24.4.1 //client side
```

Here, 172.24.4.1 represents the IP address of the server. In this thesis, we use *iperf* to measure the throughput between an AP and a host through the *IEEE802.11n* protocol.

2.5 Summary

In this chapter, we presented various wireless network technologies, the key features of IEEE 802.11n protocols, and Linux tools which are adopted in this thesis for our implementations in this study. In the next chapter, we will review our previous studies related to this thesis.

Chapter 3

Review of Previous Studies

In this chapter, we overview our previous studies related to this thesis. Firstly, we review the *elastic WLAN system*. Secondly, we review the study of throughput estimation model for single link communication under no interference. Thirdly, we review the study of the active AP configuration algorithm with orthogonal channel assignment for the elastic WLAN system. Finally, we review the implementation details of the elastic WLAN system testbed using *Raspberry Pi* APs.

3.1 Elastic WLAN System

In this section, we review the elastic WLAN system. It dynamically optimizes the network configuration by activating/deactivating APs, according to traffic demands and network conditions. Thus, it can reduce energy consumptions and interferences while improving the throughput.

3.1.1 Overview

Nowadays, WLANs have been deployed in several areas including educational institutions and public places like buses, airplanes, or trains. Unplanned or independently controlled APs can lead to causing problems of throughput drops and/or wastages of energy. In one hand, WLANs can suffer from over-allocation problems with redundant APs that have overlapped coverage areas. On another hand, WLANs can be overloaded with hosts suffering from low performances. Therefore, WLANs should be adaptive according to the network traffic demands and conditions by changing the number of active APs and the hosts associated to them. To realize this feature, previously, we have studied the elastic WLAN system.

The motivations behind the elastic WLAN system study are summarized as follows:

1. Operational cost and energy consumption reduction:

    - Companies, educational institutions, and offices may allocate a high number of APs to provide high WLAN performances at peak times and may activate these APs for the entire days. However, only a small number of APs are used during off-peak hours or holidays. The elastic WLAN system can resolve this problem by minimizing the number of APs by traffic demands and can reduce energy consumptions.
    - Most developing countries can suffer from volatile Internet connections due to electricity supply discontinuities. The elastic WLAN system can improve the network performance by optimizing the power usage.

2. WLAN performance improvement:

    - When the current active APs cannot cover the users, new APs should be added to ensure the WLAN performance according to the required traffic demands.
    - When the WLAN performance becomes low due to shortages of *internet service provider (ISP)* connections or the supplied power, it activates the cellular networks using *mobile APs* to maintain the required WLAN performance.
    - In a dense WLAN, as the number of APs increases, interferences due to the frequency signal overlaps can increase causing throughput drop. The elastic WLAN system can dynamically change the assigned orthogonal channels of APs, so it can reduce the interferences among them and enhance the WLAN performance.

3.1.2 Design and Operational Flow

Figure 3.1 demonstrates an example topology of the elastic WLAN system. It dynamically controls the number of active APs in the network by activating or deactivating the allocated APs according to traffic demands and network conditions.

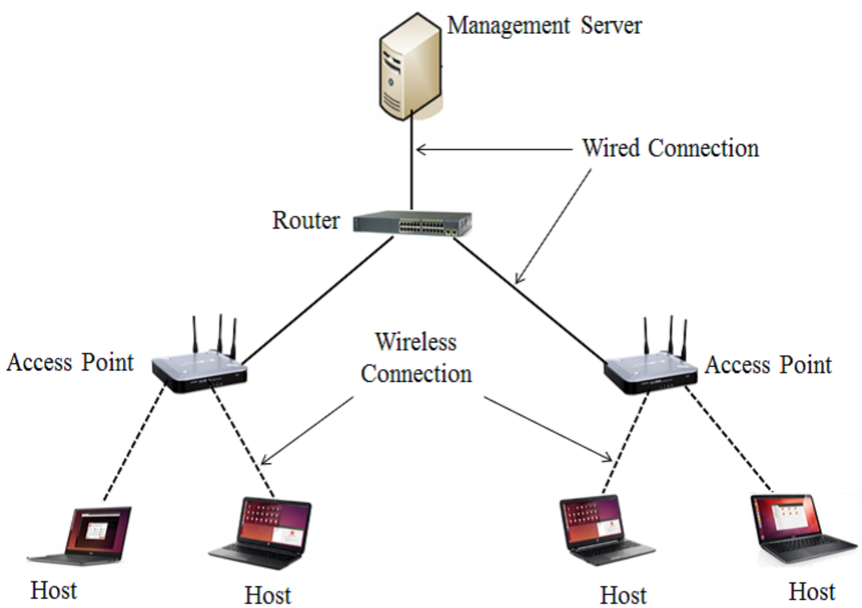

Figure 3.1: Design of Elastic WLAN system.

The implementation of the elastic WLAN system adopts the *management server* to manage the necessary information for the system and control the APs and the hosts by running the *active AP configuration algorithm*. This server not only has the administrative access rights to all the devices in the network, but also controls the whole system through the following three steps:

1. The server explores all the devices in the network and collects the requisite information for the active AP configuration algorithm.

2. The server executes the active AP configuration algorithm using the inputs derived in the previous step. The output of the algorithm contains the list of the active APs, the host associations, and the assigned channels.

3. The server applies this output to the network by activating or deactivating the specified APs, changing the specified host associations, and assigning the channels.

3.2 Throughput Estimation Model for Single Link Communication

The throughput between an AP and a host can be changed by several factors such as the modulation and coding scheme, the transmission power, the transmission distance, and transmission obstacles. Therefore, the theoretical computation of the accurate link speed can be challenging [8,66]. In this section, we review the *throughput estimation model* for IEEE 802.11n link in WLAN.

3.2.1 Overview

The *throughput estimation model* estimates the link speed or throughput of an IEEE 802.11 link in WLAN. It has two main steps to estimate the throughput between a source node (AP) and a destination node (host).

In the first step, it estimates the *receiving signal strength* (*RSS*) at the host by using the *log distance path loss model* [66]. In the second step, it converts the estimated *RSS* into the corresponding throughput by the *sigmoid function* [21]. Both functions have several configuration parameters that can affect the estimation accuracy, which depends on link specifications and network field environments.

3.2.2 Receiving Signal Strength Estimation

The signal strength is estimated by the log-distance path loss model in [66]. First, the Euclidean distance *d (m)* is calculated for each link (AP/host pair) by:

$$d = \sqrt{(AP_x - H_x)^2 + (AP_y - H_y)^2} \tag{3.1}$$

where AP_x, AP_y and H_x, H_y does the x and y coordinates for the AP and the host respectively.

Then, the *RSS*, RSS_d (dBm) at the host is estimated using the *log distance path loss model* by considering the distance and the obstacles loss between end nodes [66]:

$$RSS_d = P_1 - 10\alpha \log_{10} d - \sum_k n_k W_k \tag{3.2}$$

where P_1 represents the signal strength at $1m$ from the AP (source) for no obstacles, α is the path loss exponent, d (m) does the link distance from the AP, n_k does the number of the type-k walls along the path between the AP and the host, and W_k does the signal attenuation factor (dBm) for the type-k wall in the environment. The estimation accuracy of *RSS* relies on the parameter values, which depend on the propagation environment [66].

3.2.3 Throughput Estimation by Sigmoid Function

From the estimated *RSS* RSS_d, the throughput tp_{ij} ($Mbps$) of the link is estimated using the *sigmoid function* as follows:

$$tp_{ij} = \frac{a}{1 + e^{-(\frac{(RSS_d + 120) - b}{c})}} \tag{3.3}$$

where a, b, and c are the constant parameters of the sigmoid function that should be optimized by parameter optimization tool [67]. The assumption of the sigmoid function for the throughput estimation is based on our real-world measurement results which clearly reflects the relationship between the RSSs and the estimated throughput. Figure 3.2 demonstrates the sigmoid function curve using $a = 140$, $b = 54$ and $c = 8$.

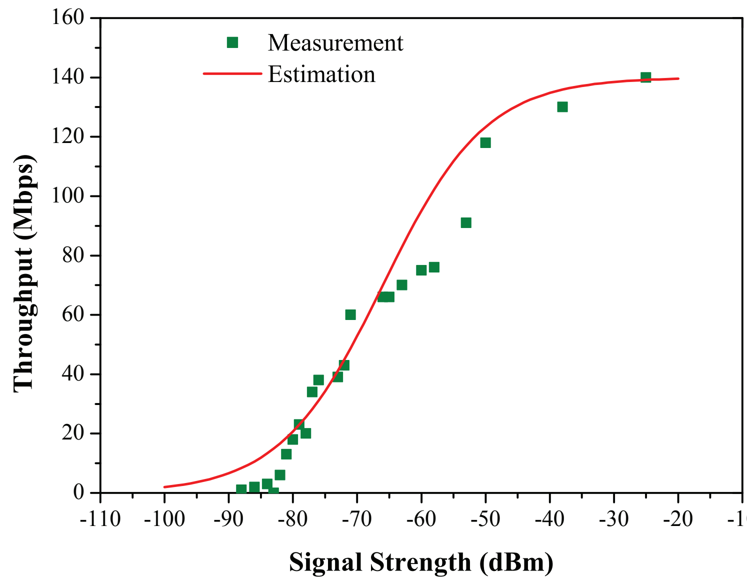

Figure 3.2: Sigmoid function for throughput estimation from signal strength.

3.3 Active AP Configuration Algorithm

In this section, we review the *active AP configuration algorithm* for the elastic WLAN system that optimizes the number of active APs and the host associations [12, 13].

3.3.1 Problem Formulation

The active AP configuration problem for this algorithm is formulated as follows:

1. Inputs:

    - Number of hosts: H
    - Number of APs: $N = N^D + N^V + N^M$ where N^D, N^V, and N^M represent the number of DAPs, VAPs, and MAPs respectively.
    - Link speed between AP_i and $host_j$ for $i = 1$ to N, $j = 1$ to H: tp_{ij}, where the link speed can be estimated by the model in [21].
    - Minimum link speed for association: tp

- Number of non-interfered channels: C

2. Outputs:

- Set of active APs
- Set of hosts associated with each active AP
- Channel assigned to each active AP

3. Objectives:

- To minimize E_1.
- Holding the first objective, to maximize E_2.
- Holding the two objectives, to minimize E_3 for channel assignments.

Let, E_1 represents the number of active APs (DAPs, VAPs, and MAPs) in the network:

$$E_1 = E_1^D + E_1^V + E_1^M \tag{3.4}$$

where E_1^D represents the number of active DAPs, E_1^V does the number of active VAPs, and E_1^M does the number of active MAPs respectively.
The transmission delay of the jth AP can be defined by:

$$T_j = \sum_{k \in \mathcal{P}_j} \frac{D_k}{tp_{jk}} \tag{3.5}$$

where D_k represents the traffic of the kth host, tp_{jk} does the link speed between the jth AP to the kth host, and $\mathcal{P}_j$ does the set of the hosts associated with the jth AP. Then, the average throughput TH_{ij} of the ith host associated with the jth AP can be estimated by:

$$TH_{ij} = \frac{D_i}{T_j} = \frac{D_i}{\sum_{k \in \mathcal{P}_j} \frac{D_k}{tp_{jk}}} \tag{3.6}$$

Since the real traffic of each host is unpredictable, we assume the identical traffic for every host, which can be represented by the unit traffic for the sake of simplicity. Then, the average host throughput for AP_j is given by:

$$TH_j = \frac{1}{\sum_{k \in \mathcal{P}_j} \frac{1}{tp_{jk}}} \tag{3.7}$$

If $TH_j \geq G$, the minimum host throughput constraint is satisfied, where G represents the threshold for this constraint. Then, the second objective function E_2 is defined to maximize the *minimum average host throughput* for the bottleneck AP, which is given by:

$$E_2 = \min_j \left[TH_j \right] \tag{3.8}$$

E_3 signifies the total interfered communication time:

$$E_3 = \sum_{i=1}^{N} [IT_i] = \sum_{i=1}^{N} \left[\sum_{\substack{k \in I_i \\ c_k = c_i}} T_k \right] \tag{3.9}$$

where IT_i represents the *interfered communication time* for AP_i, T_i does the *total communication time* for AP_i, I_i does the *set of the interfered APs* with AP_i, and c_i does the *assigned channel* to AP_i. They are given by follows:

- T_k is given by the sum of the time that is required to transmit one bit data between AP_k and its each associated host.
- I_i represents the set of the indices of the APs that are interfered with AP_i if they are assigned the same channel.
- c_k signifies the channel assigned to AP_k by the active AP configuration algorithm.
- IT_i is given by the sum of the total communication time for the APs that are interfered with AP_i.

4. Constraints:

   - Minimum host throughput constraint: each host in the network must enjoy the given threshold G on average when all the hosts are communicating simultaneously.
   - Bandwidth limit constraint: the bandwidth of the wired network to the Internet must be less than or equal to the total available bandwidth of the network B^a.
   - Channel assignment constraint: each AP must be assigned one channel between 1 and C.

3.3.2 Algorithm Procedure

The active AP configuration algorithm consists of three phases: the *active AP and associated host selection* phase, the *channel assignment* phase, and the *channel load averaging* phase.

3.3.2.1 Active AP and Associated Host Selection Phase

In this phase, the set of the active APs and their associated hosts are selected. This phase comprises following eight steps:

1. **Preprocessing**
   The link speed for each possible pair of an AP and a host is estimated with the measurement or the throughput estimation model [21]. Then, this step initializes the variables for the following steps:

   (a) For each AP, make a list of hosts that can be associated with this AP, where the throughput of the link between a host and an AP is S or larger, it can be associated. This list is called the *associable host list for APs*.

   (b) Initialize each AP as the *non-active* AP. Initially, only the DAPs are selected as *candidate APs*.

2. **Initial Solution Generation**
   An initial solution to the cost function E_1 is derived using a greedy algorithm [68], which repeats the following procedures:

(a) Select the AP that can be associated with the maximum number of non-associated hosts.

(b) Activate this AP and increment E_1 by one.

(c) Update the number of non-associated hosts in the host list for APs.

3. **Host Association Improvement**
The cost function E_2 is calculated for the greedy solution using Eq. (3.8). Then, this solution is improved by repeating the following procedure:

   (a) Find the AP that gives the lowest host throughput in Eq. (3.8).

   (b) Select one host randomly from the associated hosts with this AP, and associate it with another active AP that is selected randomly. Then, calculate E_2.

   (c) Keep the new association only if this new E_2 is higher than the previous E_2. Otherwise, return to the previous association.

4. **AP Selection Optimization**
The cost functions E_1 and E_2 are further jointly improved in this step under the constraints mentioned before by the *local search* [69]. This local search repeats the following three procedures:

   (a) If the current solution satisfies the *minimum host throughput constraint*, it seeks to reduce the number of active APs E_1 by deactivating an active AP. In the implementation, it repeats to 1) randomly select an active AP and deactivate it, 2) apply *Host Association Improvement*, and 3) check the feasibility of this deactivation.

   (b) Otherwise, it seeks to improve the *minimum average host throughput* E_2 with the same number of active APs by changing the active AP. In the implementation, it repeats to 1) randomly select a non-active AP and activate it, 2) apply *Host Association Improvement*, and 3) check the possibility of deactivating another active AP.

   (c) If (b). is not achieved, it seeks to satisfy the *minimum host throughput constraint* by increasing the number of active APs while improving the *minimum average host throughput*. In the implementation, it 1) randomly selects a non-active AP and 2) applies *Host Association Improvement*.

5. **Link Speed Normalization**
The fairness criterion will be applied when the total expected bandwidth exceeds B^a. Generally, the link speed is normalized as:

   (a) Calculate the expected total bandwidth B^e by the summation of the throughputs of all the APs.

   (b) If $B^e > B^a$, adjust each AP-host link speed as:

$$\hat{tp}_{ij} = tp_{ij} \times \frac{B^a}{B^e} \tag{3.10}$$

   where $\hat{tp}_{ij}$ is the normalized link speed.

6. **Termination Check**
   The algorithm is terminated when either of the following conditions is satisfied:

   (a) The *minimum host throughput constraint* is satisfied.

   (b) All the APs in the network have been activated.

7. **Additional VAP Activation**
   If all the DAPs become active but the *minimum host throughput constraint* is still not satisfied, VAPs are newly selected as candidate APs. A VAP is slower than a DAP, but faster than a MAP. The locations of hosts are considered as the locations of the candidate VAPs, because user hosts may be used for VAPs. Then, it returns to *AP Selection Optimization* step.

8. **Additional MAP Activation**
   If all the DAPs and VAPs become active but the *minimum host throughput constraint* is still not satisfied, MAPs are newly selected as candidate APs. A MAP is the slowest among the three AP types. The locations of hosts are considered as the locations of the candidate MAPs, because users may have MAPs. Then, it returns to *AP Selection Optimization* step.

3.3.2.2 Orthogonal Channel Assignment Phase

In this phase, the channels to assign to the active APs are selected and it has the following four steps:

1. **Preprocessing**
   The interference and delay conditions of the network are represented by a graph.

   (a) Construct the *interference graph*, $G = (V, E)$, from the APs and the hosts, where the vertex V represents the set of APs and the edge E presents the existence of the interference between two APs. $e(i, j) \in E$ if AP_i is interfered with AP_j in the network.

   (b) Calculate the *communication time* for each AP. The communication time T_i for AP_i is defined as the total time when the AP transmits 1-bit to all the associated hosts. It is given by:
   $$T_i = \sum_j \frac{1}{tp_{ij}} \tag{3.11}$$
   where tp_{ij} represents the link speed between AP_i and $host_j$.

   (c) Calculate the *neighbor interfered communication time* for each AP. The neighbor interfered communication time NT_i for AP_i is given by:
   $$NT_i = \sum_{e(i,k)=1} T_k \tag{3.12}$$

2. **Interfered AP Set Generation**
   The set of APs that are interfering with each other is found for each AP.

   (a) Sort the APs in descending order of NT_i, where the tie-break is resolved by T_i.

   (b) Find the interfered AP set for each AP by repeating the following steps:

i. Initialize the interfered AP set by $I_i = \{i\}$ for AP_i.

ii. Expand I_i by examining the APs in sorted order in a) whether the AP is interfered with each AP in I_i. If so, include this AP, AP_j, into I_i, i.e. $I_i = I_i \cup \{j\}$.

(c) Calculate the total interfered communication time AT_i for AP_i, which is given by:

$$AT_i = \sum_{k \in I_i} T_k \tag{3.13}$$

3. **Initial Solution Construction**
Then, an initial solution is derived with a greedy algorithm.

(a) Sort the APs in descending order of the total interfered communication time AT_i, where the tie-break is resolved by NT_i.

(b) Assign a channel c to AP_i such that the interfered communication time IT_i is minimized if it is assigned. IT_i is given by:

$$IT_i = \sum_{\substack{k \in I_i \\ c_k = c_i}} T_k \tag{3.14}$$

where c_k represents the assigned channel to AP_k.

(c) Repeat 2) until each active AP is assigned to one channel.

(d) Calculate the cost function E_3 using Eq. (3.9) and save this initial solution as the best solution E_3^{best}.

4. **Solution Improvement by Simulated Annealing**
Finally, the initial solution is improved by repeating the following *simulated annealing (SA)* procedure with the constant *SA temperature* T^{SA} at the *SA repeating times* R^{SA}, where T^{SA} and R^{SA} are given algorithm parameters:

(a) Randomly select one AP and one new channel for the channel change trial.

(b) Calculate the interfered communication time IT_i after assigning this new channel by:

(c) Calculate E_3^{new} using Eq. (3.9) for the new channel assignment, and $\Delta E_3 = E_3^{new} - E_3$.

(d) If $\Delta E_3 \leq 0$, accept the new channel assignment, and address this new solution as the best one.

(e) Otherwise, generate a 0-1 random number, *rand*, and if $rand \leq \frac{-\Delta E_3}{T^{SA}}$, then accept the new channel assignment.

3.3.2.3 Channel Load Averaging Phase

After the channel assignment using the limited number of channels, the total loads may be imbalanced depending on different channels that are assigned to the APs. In this phase, the channel load is averaged by changing associated APs for hosts. It has four steps as follows:

1. **Preprocessing**
The *AP flag* for each AP is initialized with OFF to avoid processing the same AP.

2. **AP Selection**
   One AP is selected to move its associated host to a different AP that is assigned a different channel.

   (a) Terminate the procedure if each AP has ON AP flag.

   (b) Initialize the host flag by OFF for each host.

   (c) Select one AP, say AP_i, that satisfies the two conditions:

      i. The AP flag is OFF.

      ii. The interfered communication time IT_i is largest among the OFF APs.

   (d) Set the AP flag ON.

3. **Host Selection**
   Then, one host associated with AP_i is selected for the associated AP movement.

   (a) Select one host, say H_j, that satisfies the four conditions:

      i. The host flag is OFF.

      ii. The host is associated with AP_i.

      iii. The host can be associated with another AP assigned a different channel from AP_i, or is located out of the interference range of AP_i.

      iv. The link speed with AP_i is the smallest among the hosts satisfying (a)–(c).

   (b) If one host is selected, set the host flag ON.

   (c) Otherwise, return to *AP Selection* for the new AP selection.

4. **Association Change Application**
   Finally, the new associated AP is selected for H_j.

   (a) Select the AP that has the largest link speed among the APs that are assigned to a different channel from AP_i and can be associated with H_j.

   (b) Calculate the new cost function E_3^{new} with Eq. (3.9) if H_j is associated with this AP.

   (c) If E_3^{new} is equal to or smaller than the previous E_3, accept the new association, and return to *Host Selection*.

   (d) Otherwise, select another AP that has the next largest link speed, and return to 3).

   (e) If no such AP exists, return to *Host Selection* for the new host selection.

3.4 Implementation of WLAN Testbed System Using Raspberry Pi

In this section, we describe the testbed implementation of the elastic WLAN system using *Raspberry Pi* and Linux PCs. *Raspberry Pi* is a small-size low-cost computer, and has become popular in academics and industries around the world. Therefore, the use of *Raspberry Pi* in the elastic WLAN system is significant for its disseminations in developing countries.

3.4.1 Implementation Environment/Platform

As the initial implementation platform of our elastic wireless LAN system, we choose the Linux environment that has been used as a platform to implement new algorithms, protocols, methods, and devices for advancements of wireless networks, because of being an open-source operating system. Linux environment has a lot of open source tools to use. Most of them are easily configurable and have flexibility to use and integrate with other tools [58]. On the other hand, while searching for the network configuration and management tools in Windows operating system, we found most of them are less flexible and less configurable, and not open source. Currently, we are using *Ubuntu* for our implementation platform as the popular distribution of Linux environment for general-purpose users. The Ubuntu LTS 14.04 version of the operating system was adopted in *elastic WLAN system testbed* for compatibility and similarity of throughput performance in measurements. Implementations of the elastic WLAN system on various platforms and latest version of Ubuntu OS will be in our future studies.

The device environments and software in Table 3.1 are used for the testbed implementation of the system. The IEEE 802.11n protocol is used for any communication link with the channel bonding.

Table 3.1: Device environment and software in testbed.

devices and software		
server PC	OS	Ubuntu LTS 14.04
	model	Lesance W255HU
	Processor	Intel(R), Core(TM)-i3
client PC	OS	Ubuntu LTS 14.04
	Model	Fujitsu Lifebook S761/C/SSD
	Processor	Intel(R), Core-i5
access point	OS	Raspbian
	Model	Raspberry Pi 3
	Processor	1.2 GHz
software/tools	openssh	to access remote PC and AP
	hostapd	to prepare and configure AP
	nmcli	for association change
	nm-tool	to measure signal strength
	arp-scan	to discover active network devices

3.4.2 System Topology

Figure 3.3 shows the simple network topology of the elastic WLAN system. *Raspberry Pi* is used for the AP and a *Linux laptop PC* is for the server and the host. The server can manage and control all the APs and the hosts by using the administrative access to them. The APs are connected to the server through wired connections. The hosts and the APs are connected through wireless connections.

3.4.3 AP Configuration of Raspberry Pi

This section explains how to configure *Raspberry Pi* for AP using *hostapd* daemon [70, 71].

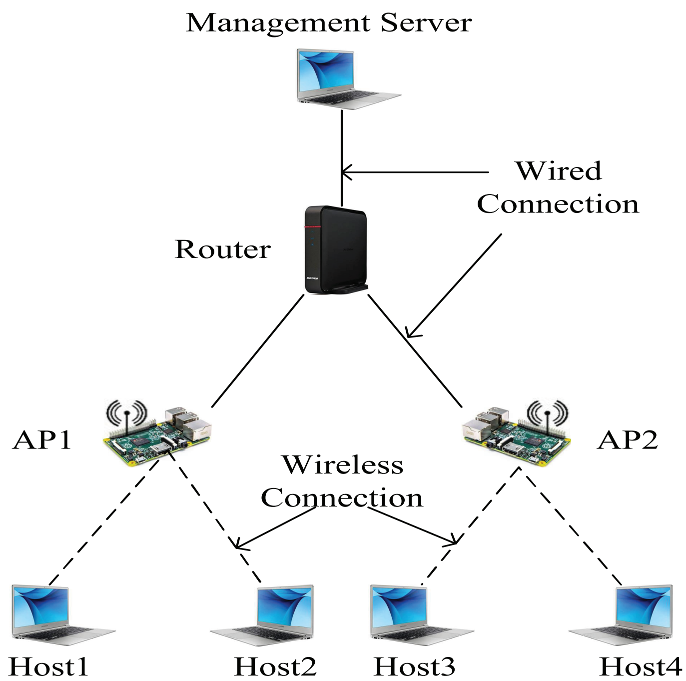

Figure 3.3: Elastic WLAN system topology.

1. Install the *hostapd* using the following command:

   ```
   $ sudo apt-get install hostapd
   ```

2. Modify the configuration file */etc/hostapd/hostapd.conf* with the desired SSID and PASSWORD. A simple example of the configuration file is given below:

   ```
   interface=wlan0
   ssid=SSID
   channel=1
   wpa_passphrase=PASSWORD
   ```

3. Uncomment and set *DAEMON_CONF* to the absolute path of a hostapd configuration file to start hostapd during system boot:

   ```
   DAEMON_CONF="/etc/hostapd/hostapd.conf"
   ```

4. Setup the *wlan0* interface to have a static IP address in the network interface configuration file */etc/network/interfaces*. An example of the interface file is given below:

   ```
   auto wlan0
   iface wlan0 inet static
   address 192.168.1.11
   netmask 255.255.255.0
   network 192.168.1.0
   ```

5. Finally, install the DHCP server for assigning the dynamic IP addresses to the hosts.

3.4.4 Execution Flow of Elastic WLAN

Figure 3.4 shows the execution flow of the elastic WLAN system testbed implementation.

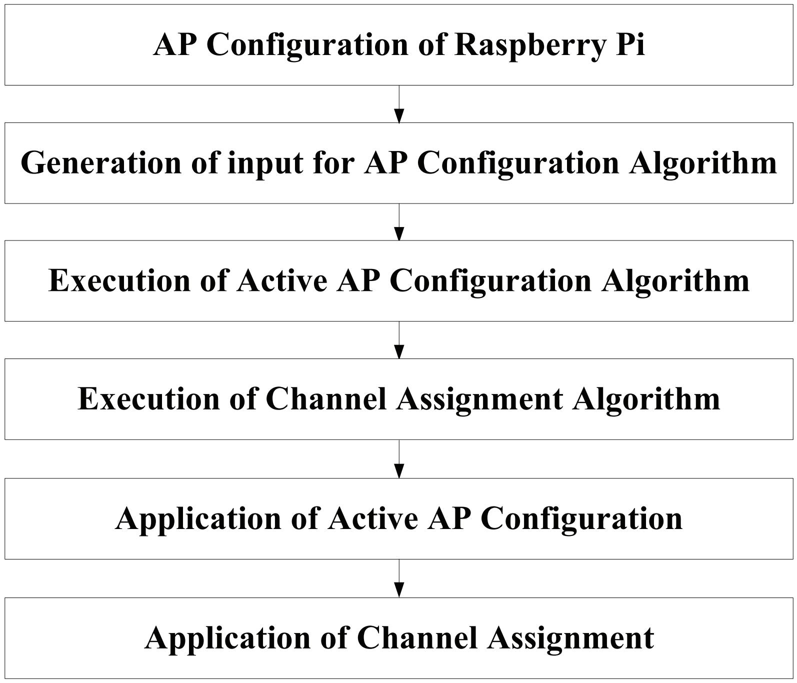

Figure 3.4: Execution Flow of Elastic WLAN system.

3.4.4.1 Generation of input for Active AP Configuration Algorithm

In this step, the server explores all the connected device to the network and generates the input for the active AP configuration algorithm using the following procedure:

1. The server explores all the connected device to the network using *arp-scan* [72]. The command is given below:

   ```
   $ sudoarp-scan --interface=eth0 192.168.11.0/24
   ```

   Here, *–interface=eth0* represents the interface and 192.168.11.0/24 is the network IP range to scan. The output consists of the IP and MAC addresses of the hosts and the APs that are available in the network. A simple C program is developed to identify the hosts and APs in this system using the MAC addresses of the devices. After this, the server generates the list of permitted APs and the list of permitted hosts.

2. The following command finds the receiving signal strength of each host from each AP using *nm-tool* [73, 74]. *ssh* protocol is used to execute the command remotely in each host [60, 61, 64].

   ```
   $ sudo nm-tool
   ```

3. After this, the server converts the receiving signal strength to the estimated link speed using the sigmoid function in [75], and generates the input for the active AP configuration algorithm.

3.4.4.2 Execution of Active AP Configuration Algorithm

The active AP configuration algorithm is executed in this step. The following commands compile the program for the active AP configuration algorithm and execute it respectively. The *minimum host throughput constraint* and the *bandwidth limitation constraint* are specified by the user.

```
$ g++ -o apc APConfigurationAlgorithm.cpp
$ ./apc input.txt min_host_throughput bw_limit
```

Here, *input.txt* presents the input file generated in the previous step, *min_host_throughput* does the minimum host throughput constraint, and *bw_limit* does the bandwidth limitation constraint. After this, the list of active APs and their associations with the hosts are obtained.

3.4.4.3 Execution of Channel Assignment Algorithm

The following commands compile the program for the channel assignment extension and execute it respectively.

```
$ g++ -o ca ChannelAssignment.cpp
$ ./ca HostAPassociation.txt num_of_channels
```

HostAPassociation.txt presents the input file to the channel assignment extension that contains the list of active APs and their associations with the hosts, and *num_of_channels* does the number of available channels.

3.4.4.4 Application of Active AP Configuration

The management server applies the output of the two algorithm.

1. The server adjusts the number of active APs according to the algorithm output by activating or deactivating APs in the network. The two commands given below is used to activate and deactivate the Raspberry Pi AP respectively.

   ```
   $ sudo /etc/init.d/hostapd start
   $ sudo /etc/init.d/hostapd stop
   ```

2. The following command connects a host to a new AP using *nmcli* [76, 77]. *NewSSID* represents the new AP for the host and *PASSWORD* does the security key of the AP. The server modifies the AP-host association according to the algorithm output using this command.

   ```
   $ sudo -s nmcli dev wifi connect NewSSID password PASSWORD
   ```

3.4.4.5 Application of Channel Assignment

The server uses the following commands to assign the new channel to the Raspberry Pi AP using *sed* [78]. For this, the server modifies the configuration file */etc/hostapd/hostapd.conf* with the channel number.

```
$ sed -i -e ‘s/.*channel.*/channel=’$NewChannel‘/’
/etc/hostapd/ hostapd.conf
$ sudo /etc/init.d/hostapd restart
```

Here, *‘s’* represents the substitution command and *NewChannel* does the channel to be assigned in the *hostapd.conf* file of the AP. After the assignment of the new channel, the server restarts it to make the change take effect.

3.5 Summary

In this chapter, firstly, we reviewed the elastic WLAN system. Secondly, we review the study of throughput estimation model for single link communication under no interference. Thirdly, we review the study of the active AP configuration algorithm with orthogonal channel assignment for the elastic WLAN system. Finally, we review the implementation details of the elastic WLAN system testbed. In the next chapter, we will present the throughput measurement method for concurrently communicating links.

Chapter 4

Throughput Measurement Method for Concurrently Communicating Links

In this chapter, we present the throughput measurement method for concurrently communicating links that is adopted in this thesis. Firstly, we describe the three distances used in the models. Secondly, we describe the details of throughput measurement methods. Thirdly, we explain the TCP verses UDP protocols. Finally, we explain our motivation of using empirical models.

4.1 Definitions of Three Distances

Firstly, three distances, namely, the *channel distance (chD)*, the *physical distance (phD)*, and the *link distance (lkD)*, are defined to describe our contributions of throughput drop estimation models in the subsequent chapters.

4.1.1 Channel Distance

The *channel distance (chD)* of two links, namely $link_1$ and $link_2$, is defined as the minimum channel difference between the assigned channels to these links. For example, when both links are assigned the same channel, *chD* is 0, and they are fully overlapped. When $link_1$ is assigned *channel 3* and $link_2$ is *channel 5*, *chD* is 2. In this case, these channels are overlapped by 50% for 20MHz, and by 75% for 40MHz. The largest *chD* is 12 for 20MHz and 8 for 40MHz, where any frequency overlapping does not exist theoretically.

The open source software *Homedale* [79] is adopted to monitor multiple WLAN APs in the network field. This software shows the signal strength of detected AP, encryption security (such as WEP, WPA, WPA2, WPA3) network SSID, AP MAC address, and assigned channel. Using *Homedale*, Figure 4.1 shows the frequency overlapping for the different *chD* with *phD = 5m* under 40MHz CB. Also, Figures 2.5 and 2.7 demonstrate frequency overlapping for 20MHz and 40MHz respectively.

In Figure 4.1 (a), the two links are assigned *same CB channel 1+5 (chD = 0)*. Thus, their frequencies are fully overlapped as demonstrated by the horizontal line in red color. In (b), the two links are assigned *CB channel 1+5 and 5+9 (chD = 4)*. Their frequencies are less overlapped compared to (a). In (c), the two links are assigned *CB channel 1+5 and 7+11 (chD = 6)*, where the overlap is smaller. In (d), the two links are assigned *CB channel 1+5 and 9+13 (chD = 8)*, where they are least overlapped.

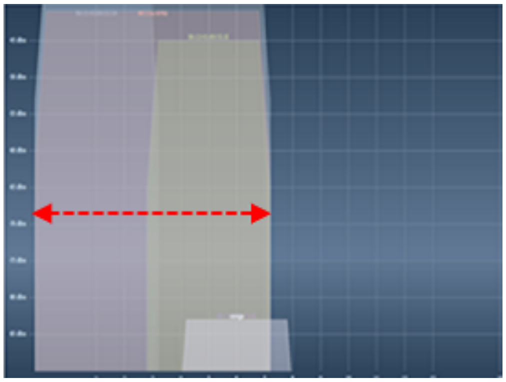

(a) *chD* = 0

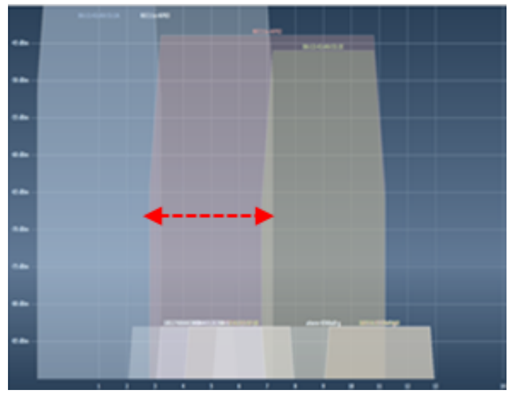

(b) *chD* = 4

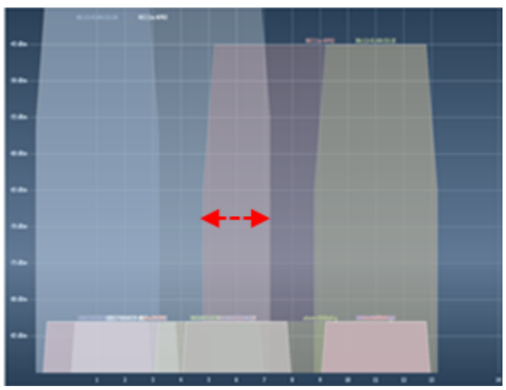

(c) *chD* = 6

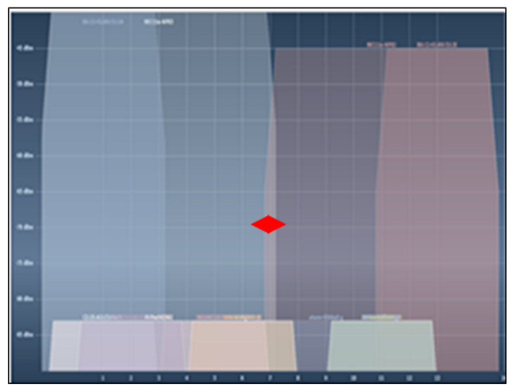

(d) *chD* = 8

Figure 4.1: Frequency overlapping between two links.

4.1.2 Physical Distance

The *physical distance (phD)* is defined as the Euclidean distance between the two APs of the links, $link_1$ and $link_2$. Since it represents the separation distance between the interfering links, the farther apart the two links are placed, the higher the physical distance is. Accordingly, the interference between them becomes lower. By increasing the physical distance between the interfering links, the interfering signal between them fades due to the path loss and the absorption by obstacles on the path of the signal [80].

4.1.3 Link Distance

The *link distance (lkD)* is defined as the Euclidean distance between the sender (AP) and the receiver of the link (host). Since the signal is propagated from the sender to the receiver, the link distance will affect the *received signal strength (RSS)* at the receiver as well as the signal power [80], and the throughput will degrade while the link distance increases.

Table 4.1: Devices and software for measurements.

Access Point	
model	NEC WG2600HP or Raspberry Pi 3 Model B
operating mode	IEEE 802.11n
operating band	2.4 GHz
channel width	20 MHz or 40 MHz
wireless NIC	Atheros XSPAN (NEC) [81] or Broadcom BCM2837 (Raspberry Pi) [82]
host PC	
model	Toshiba dynabook R731/B
OS	Ubuntu 14.04 LTS (kernel 3.13.0-57)
processor	Intel Core i5-2520M 2.54 Ghz
chipset	Intel HM65 Express
wireless NIC	Atheros AR938x [83]
server PC	
model	Fujitsu lifebook S761/C
OS	Ubuntu 14.04 LTS (kernel 4.2.0-27)
processor	Intel Core i5-2520M 2.5GHz
chipset	Mobile Intel QM67 Express
wireless NIC	Atheros XSPAN [84]

4.2 Throughput Measurement Methods

The models presented in this thesis are derived empirically through extensive experiments. Thus, we conducted a lot of throughput and RSS measurement experiments for concurrently communicating links under various interferences and channel conditions. In this section, we discuss the approaches that were adopted to conduct those measurements.

4.2.1 Measurement Setup

Table 4.1 shows the adopted devices and software in our measurements. For the AP, the device by NEC WG2600HP or Raspberry Pi 3 model B is used. The Raspberry Pi uses Raspbian OS, Broadcom BCM2837, 1.2Ghz 64-bit quad-core ARM Cortex-A53 CPU, LPDDR2-900MHz 1GB SDRAM, 10/100Mbps Ethernet, IEEE802.11b/g/n wireless NIC, Blue-tooth 4.1 classics/low energy [82]. For the server and client host PCs, the ones by Fujitsu and Toshiba respectively are used with the Linux OS. If different devices are used, the results can be different, because each device may use a different network adapter and software.

Figure 4.2 illustrates the two links between the server PCs and the host PCs via APs, namely $link_1$ and $link_2$, in our measurements. The server PC is connected to the AP through the Gigabit Ethernet cable, and the host PC is connected with the AP by the wireless link. The AP setup optimization approach in [21] is applied to maximize the throughput for each link.

For the throughput measurements, Iperf is adopted as a popular tool for measuring the TCP throughput by generating TCP packets [65]. This software automatically saturates the TCP traffics of the WLAN link.

The *frame aggregation* in the IEEE 802.11n is used in the measurements. It allows multiple frames to be transmitted in the single block and be acknowledged together over a single channel access. By reducing the overhead induced by the *carrier sense multiple access with collision avoidance (CSMA/CA)* protocol, it can increase the throughput performance of the IEEE 802.11n over the IEEE 802.11a/b/g without the frame aggregation.

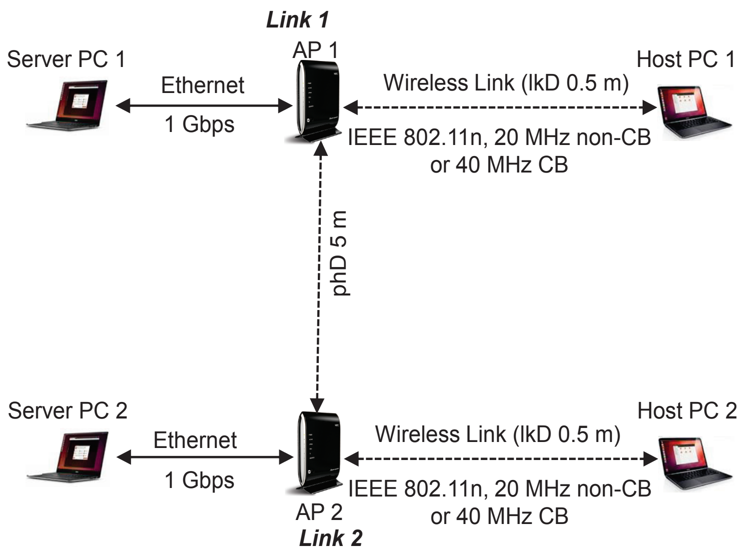

Figure 4.2: Measurement setup.

4.2.2 Measurement Field in Outdoor

The outdoor environment of *Asahi riverbed* was adopted for the measurement field in outdoor. Figure 4.3 illustrates the photo of the outdoor field and experiment setup there. By using *Homedale* software [79], it is confirmed that the outdoor environment is free of interfering signals. The physical distance *phD* and the link distance *lkD* can be changed there to measure throughput drops from the normal ones under various conditions of *interfered received signal strength* (RSS^i) at the AP.

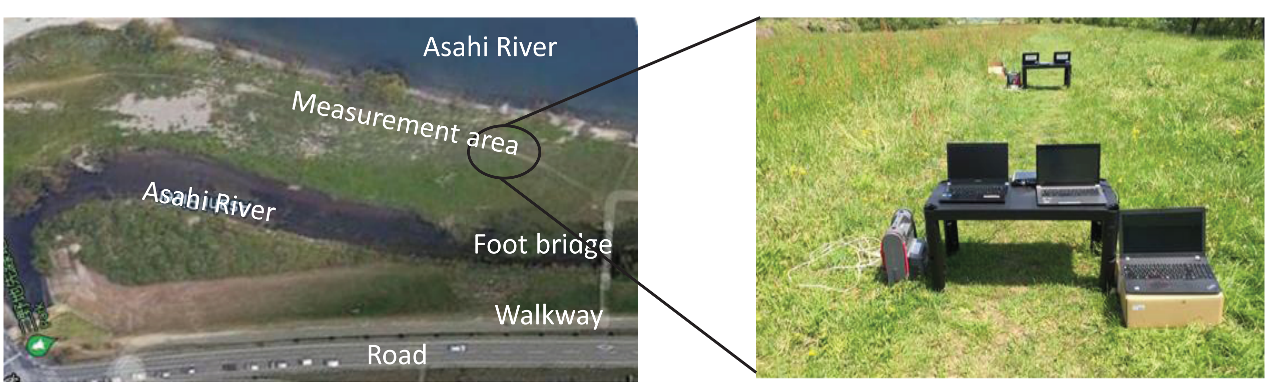

Figure 4.3: Measurement field at outdoor.

4.2.3 Measurement Field in Indoor

The third floor of Engineering Building #2 and the second floor of Graduate School of Natural Science and Technology Building at Okayama University are adopted for indoor fields. Figure 4.4 shows the floor layouts. In either field, several other WLANs can be observed, which may cause the *hidden terminal problem* to the target link in our experiments. Fortunately, the signals from them are weaker than the signals of our devices.

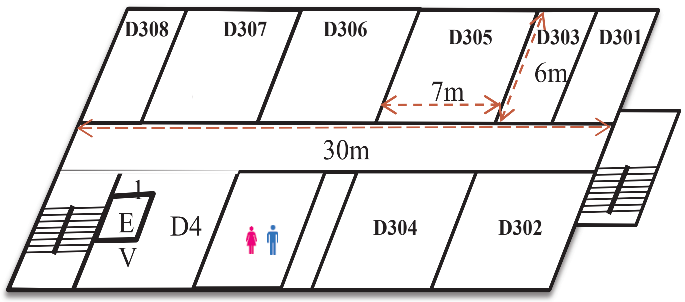

(a) 3rd Floor in Engineering Building #2.

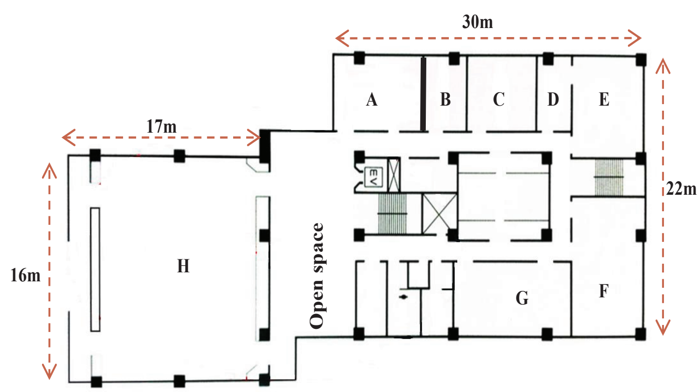

(b) 2nd Floor in Graduate School Building.

Figure 4.4: Measurement fields in indoor.

4.3 TCP Verses UDP Protocols

Currently, the *TCP protocol* has been used in a lot of important network applications such as the Web application system, the file transmission, and the electric mail. In [85], Ryu et al. have demonstrated that the TCP traffics have dominated the current usages of the Internet where more than 90% of the Internet traffics is TCP. In [86], Afanasyev et al. shows that the TCP protocol carries most of the Internet traffics, and the performance of the Internet depends to a great extent on how well TCP traffics work. Thus, the TCP throughput significantly impacts the user experience in the application as well as the network resource utilization.

On the other hand, the *UDP protocol* does not adopt the *flow control* or have the *data reception acknowledgement*. This makes UDP less reliable since the successful packet delivery cannot be guaranteed. Thus, UDP is less adopted for the Internet access due to these limitations, although it is lighter and can be faster than TCP.

Therefore, the *TCP throughput* significantly impacts the user experience in the application as well as the network resource utilization. Thus, we study the throughput drop estimation models for TCP traffics in this thesis.

4.4 Motivation of Empirical Model

In [87], Reis et al. indicate that most of physical protocol explorations with respect to interferences may adopt simple abstract models with multiple assumptions, including that the signal propagation obeys a simple function of the distance, the radio coverage area forms a circle, and the interference range is twice of the transmission range. Unfortunately, experimental data using a real WLAN have shown that all of these models appear to be largely inaccurate [88, 89].

In contrast to a physical model, an empirical model is based on observations on actual network environments. Thus, the empirical model for interference in WLAN is expected to be more descriptive and accurate compared to a physical model. Therefore, the models presented in this thesis are empirically derived based on extensive experiment results.

4.5 Summary

In this chapter, firstly, we define the three distances that describe the proposed models. Secondly, we describe the details of throughput measurement methods. Thirdly, we explain the TCP verses UDP protocols. Finally, we explain the motivation of adopting empirical models. In the next chapter, we will present the throughput drop estimation model under channel bonding.

Chapter 5

Throughput Drop Estimation Model under Channel Bonding

In this chapter, we present the *throughput drop estimation model under channel bonding*. Firstly, we illustrate the preliminary measurement observations. Secondly, we discuss the throughput drop measurements. Thirdly, we present the model under interfered links and its evaluation. Finally, we present the evaluation of the channel assignment by model under channel bonding.

5.1 Introduction

As demonstrated in Section 4.4, an empirical model is based on observations on actual network environments. Therefore, it is expected that the empirical model for interferences in WLAN can be more descriptive and accurate compared to a physical model that may adopt simple abstract approaches with multiple assumptions [87]. In this chapter, the empirical model is derived from extensive measurements of *throughput* and *received signal strength (RSS)* under different conditions of interference in both outdoor and indoor fields.

The model under channel bonding is considered since channel bonding can provide high throughputs due to the wide channel width in general, where two adjacent channels are used together as one channel [7, 8, 24]. It can increase the number of sub-carriers for data transmissions with *Orthogonal Frequency Division Multiplexing (OFDM)* to 108 from 52 in the conventional $20MHz$ *non-channel bonding* [25]. In addition, *channel bonding* increase the number of frames to be transmitted together by the frame aggregation, because of the higher bit-rate with the increased number of data sub-carriers to send data frames as a bundle. With the fixed pulse length for packet transmissions, the CB can send more data bits than the non-CB. The frame aggregation can reduce the overhead induced by the CSMA/CA protocol to send multiple frames in a single bundle and be acknowledged together over a single channel access.

5.2 Preliminary Throughput Measurement Observations

First, we conduct preliminary throughput measurements for concurrently communicating links under various conditions of interferences to understand the effects of *channel distance*, *physical distance* and *link distance* on throughput of a wireless link.

Figure 5.1 shows measured individual and average throughput under concurrently communicating two links. In this measurement, the outdoor field of *Asahi riverbed* in Figure 4.3 was adopted.

Here, we changed the *channel distance (chD)* of the two links, while we fixed the *physical distance (phD)* and *link distance (lkD)*. The chD is varied from 0 to 8, where the channel of AP1 was fixed at the bonded channel 1+5 (center frequency 3) and that of AP2 was changed from bonded channel 1+5 to bonded channel 9+13 (center frequency 11). The phD and lkD was fixed at 5m and 0.5m respectively.

It is noted that the individual throughput fluctuates, because the contention among the links is not well resolved by the carrier sense mechanism [90], which often cause the unfair channel occupation among the interfering links. Thus, in this thesis, we use the average throughput among them to represent the single link throughput under interference.

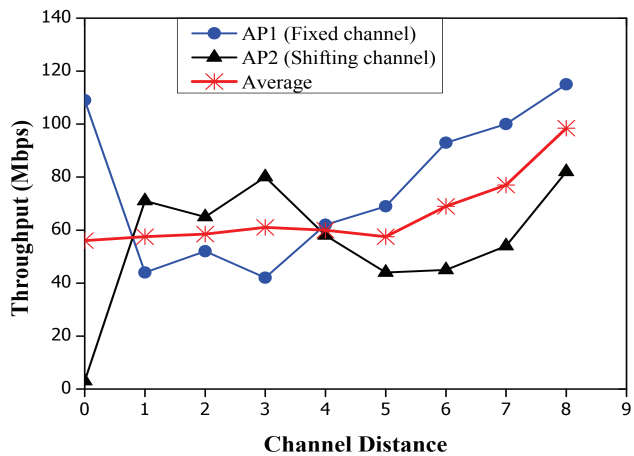

Figure 5.1: Individual throughput fluctuation under two links.

5.2.1 Results under Different Channel Distances

Figure 5.2 shows the average measured throughput of the two links. This measurement is an extension of the measurement for Figure 5.1 at the outdoor field in Figure 4.3, where two more *phD* of 15*m* and 30*m* are included for comparison. Therefore, it shows throughput results where channel distance is increased one by one from chD = 0 to chD = 8 and *phD* was fixed at either 5*m*, 15*m*, or 30*m*. The *link distance (lkD)* was fixed at 0.5*m*. As explained previously, we show only the average due to fluctuations of individual throughputs.

At *phD* = 5*m* or 15*m*, the throughput is not improved for *chD* = 0 to *chD* = 5 due to the strong interference between the two links. However, for *chD* greater than 5 throughput gradually improves due to less interference. Similarly, at *phD* = 30*m* throughput improves due to less interference.

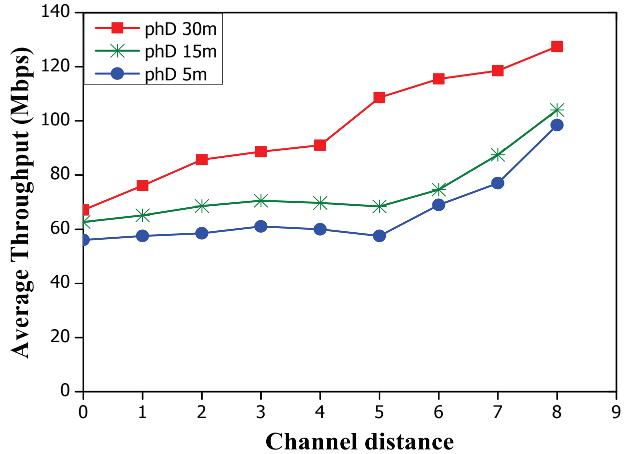

Figure 5.2: Average throughputs under different channel distances.

5.2.2 Results under Different Physical Distances

In this measurements, we changed the physical distance while fixing the both the channel distance and the link distance at the outdoor field in Figure 4.3. The *phD* was varied from 5*m* to 160*m* at the 5*m* interval. The *chD* was fixed at either of 0, 2, 5, or 8. Figure 5.3 (a) and (b) shows the average throughput of the two links and the *received signal strength (RSS)* at AP1 from AP2, respectively. They show that the larger *phD* improves the throughput by reducing the interference signal.

5.2.3 Results under Different Link Distances

In this measurement, we changed the link distance while fixing the others at the outdoor field in Figure 4.3. The *lkD* for both links was changed from 0*m* to 160*m* at the 5*m* interval. The *phD* was fixed at 5*m*. The *chD* was fixed at $chD = 0$, $chD = 7$ or $chD = 8$. Figure 5.4 shows the average throughput of the two links. It is noted that for $chD = 7$, the connection was unstable and frequently disconnected after $lkD = 30m$.

5.3 Throughput Drop Measurements

The throughput drop is calculated by subtracting the measured throughput under two-link interference from the expected throughput for one link under no interference. Figure 5.5 shows the change of the throughput drop of the target link by the *interfering received signal strength* (RSS^i) at the AP for different *chD* in the indoor field of *Engineering Building #2* at Okayama University in Figure 4.4 (a). The interfering RSS^i from the interfered link and the chD between the two links strongly affects the throughput drop of the target AP.

5.4 Throughput Drop Estimation Model under Interfered Links

Based on measurement results in Section 5.3, we propose the *throughput drop estimation model* for concurrently communicating links.

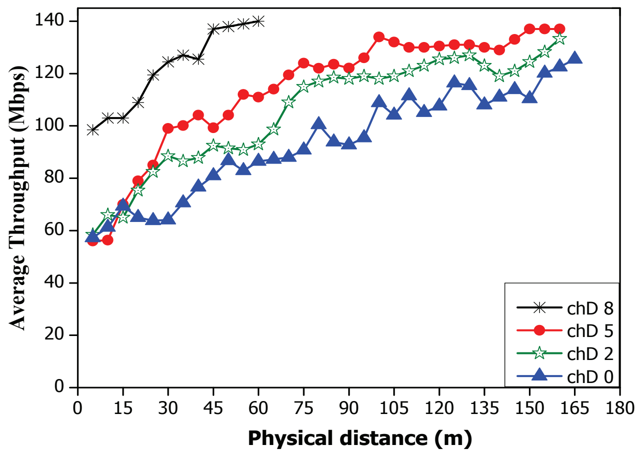

(a) Average throughputs.

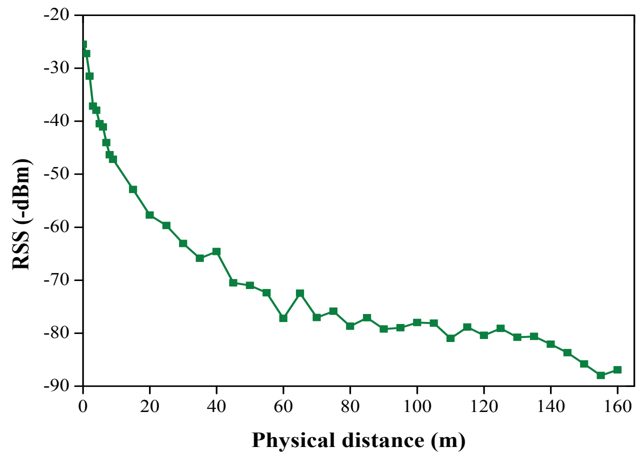

(b) Average received signal strength (RSS).

Figure 5.3: Throughputs and RSS under different physical distances.

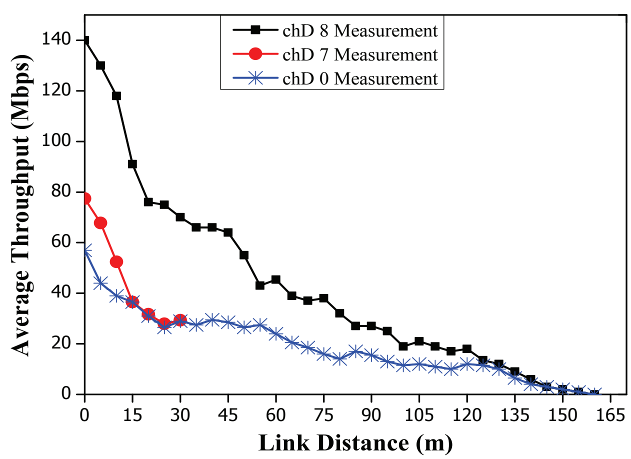

Figure 5.4: Average throughputs under different link distances.

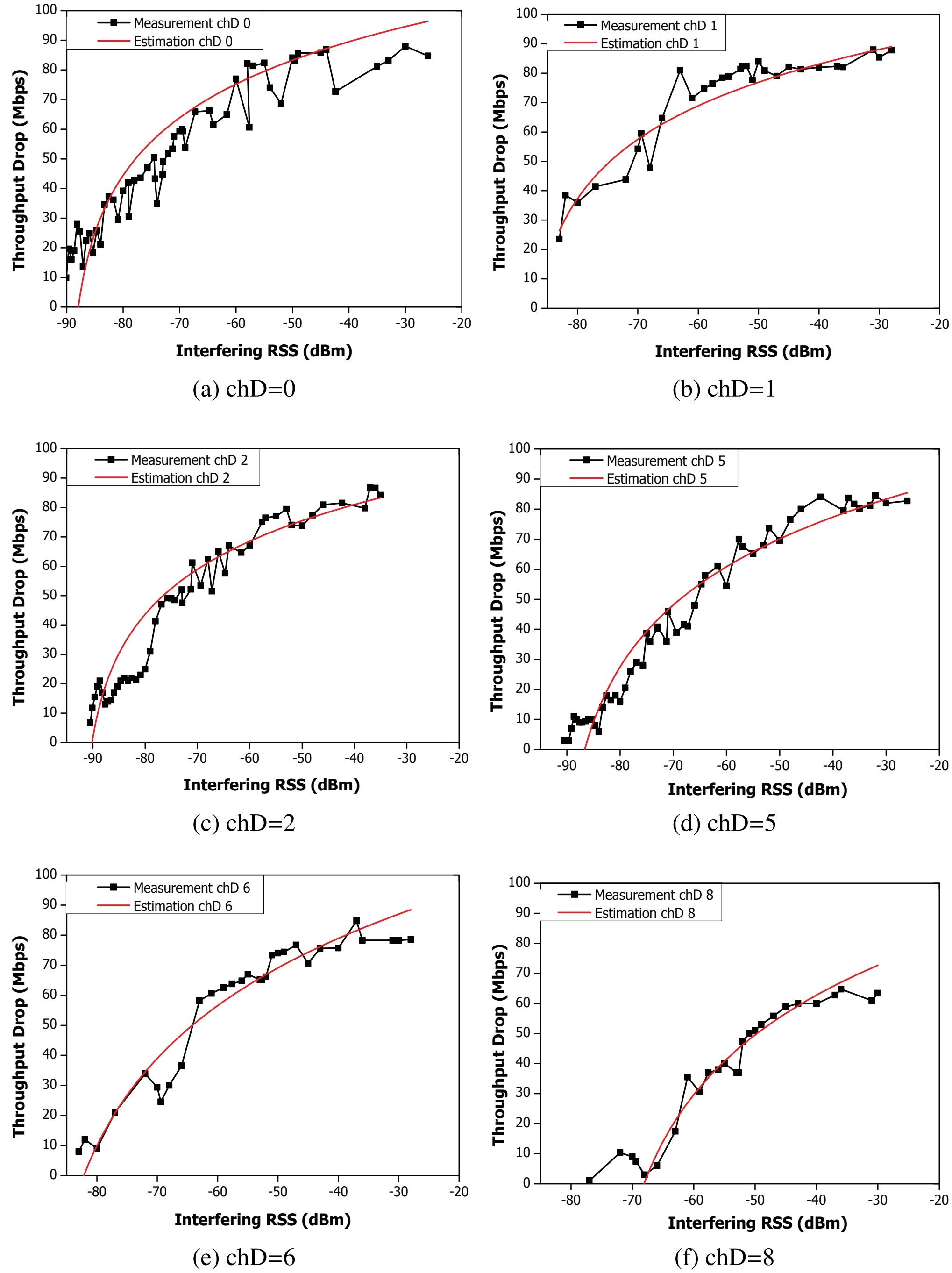

(a) chD=0 (b) chD=1

(c) chD=2 (d) chD=5

(e) chD=6 (f) chD=8

Figure 5.5: Throughput drop results for different interfering RSS at different *chD*.

5.4.1 Two Interfered Links

The throughput drop measurement results indicate that for any channel distance (*chD*), the natural logarithm function can be a good approximation to estimate the throughput drop (tpD) from the interfering RSS (RSS^i) with the particular channel distance *chD* between the two links:

$$tpD(RSS^i, chD) = p(chD) \times \ln(q(chD) + RSS^i) + r(chD). \quad (5.1)$$

where $tpD(RSS^i, chD)$ represents the estimated throughput drop ($Mbps$), and $p(chD)$, $q(chD)$, and $r(chD)$ represent constants determined by the channel distance (chD). The *physical distance* (phD) between the two APs is closely related with the RSS (RSS^i) of the interfering signal at the AP in Eq. (5.1). When phD increases, the corresponding RSS^i decreases, as shown in Eq. (3.2) where RSS_d represents RSS^i and d does phD.

5.4.1.1 Constants for Channel Distance

The values of the three constants p, q, and r in the throughput drop estimation function should be computed from the throughput drop measurement results for each channel distance. In this thesis, their values were obtained using *OriginPro8* [91]. Table 5.1 shows their values for each channel distance. The estimated drop for each channel distance is also illustrated in Figure 5.5. They show that this function can well estimate the throughput drop for any channel distance.

Table 5.1: Constant parameters for each channel distance.

channel distance	p	q	r
0	27	88.17	-20
1	27	87.36	-20
2	27	89.00	-22
3	25	94.50	-22
4	33	92.00	-56
5	34	92.00	-57
6	45	91.00	-98
7	45	88.00	-100
8	40	75.50	-80

Then, the nominal throughput under interference is obtained by subtracting the throughput drop from the throughput under no interference in Section 3.2 by:

$$tp^i_{ij} = tp_{ij} - tpD(RSS^i, chD) \tag{5.2}$$

where tp^i_{ij} represent the throughput from AP i to host j ($link_{ij}$) under POC interferences, tp_{ij} does the throughput estimated by the single link model under no interference in Section 3.2, RSS^i does RSS from the interfered link at AP i, and chD does the channel distance between this link and the interfered link.

5.4.1.2 Model Evaluation for Two Interfered Links

The accuracy of the estimated throughput by the proposed model is evaluated.

- *Evaluation in Different Environment:*
  First, we evaluate the accuracy of the estimated throughput drop by the model in *Graduate School Building* at Okayama University in Figure 4.4 (b) as a different indoor field from Section 5.3. Figure 5.6 shows the estimated and measured throughput drop of the target link against the interfering RSS for $chD = 2$.

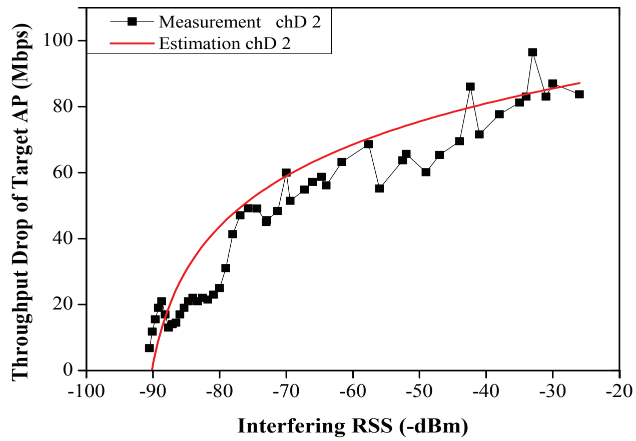

Figure 5.6: Throughput drop results in Graduate School Building.

- *Evaluation under Different Channel Distance:*
  Next, we examine the accuracy of the estimated throughput by using Eq. (5.1) and Eq. (5.2), when the chD is changed in the indoor field of *Engineering Building #2* at Okayama University in Figure 4.4 (a). Figure 5.7 reveals the estimated and measured throughputs of the target link at four interfering RSS values, where the chD is changed from 0 to 8. Generally, they are coincident well. However, being affected by countless of other Wi-Fi signals in this environment, they become different at certain channel distances, although the measurements were conducted in the evening or weekends to minimize their effects.

  Figure 5.8 indicates the measured and the estimated throughputs of the target link at four channel distances in the outdoor field of *Asahi riverbed* in Figure 4.3, where the interfering RSS is changed by increasing the physical distance until $phD = 160m$. In general, they are coincident well, although differences appear at some RSS due to environmental conditions such as grasses.

5.4.2 Model Extension for Multiple Interfered Links

In this Section, we extend the model under two concurrently communicating links to multiple links based on measurement results. The accuracy of this model extension is verified by comparing the estimated results with the measured ones for three links.

5.4.2.1 Throughput Measurements

The devices and software in Table 4.1 were adopted for measurements, where the NEC device was used for the AP. The two links in Figure 4.2 was extended to make three links ($link_1$, $link_2$ and $link_3$) in Figure 5.9, and set up in the indoor field in Figure 4.4 (a) and (b). The server PC is connected to the AP through the Gigabit Ethernet, and the host PC is connected to the AP by the 11n wireless link. The host is 0.5m from its connected AP (lkD), and each AP is $5m$ from the other AP (phD). The maximum transmission power is selected for any AP with the equal antenna gain [17].

Using *iperf 2.05* [65], TCP packets are transmitted from the server to the host. The throughputs are measured while increasing *chD* between the three APs.

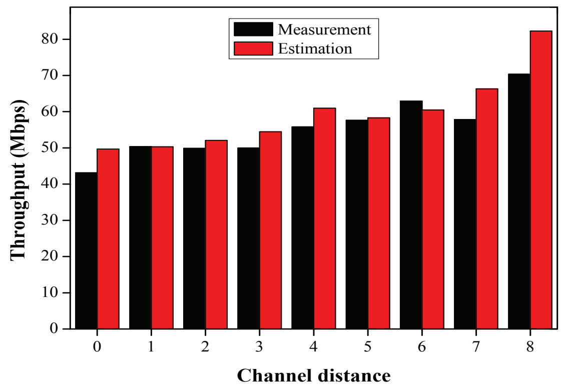

(a) Interfering RSS = -54dBm

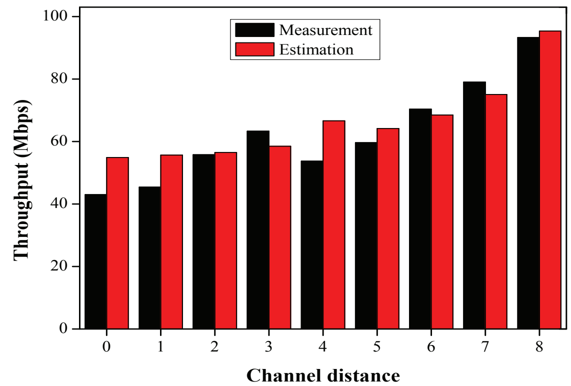

(b) Interfering RSS = -60dBm

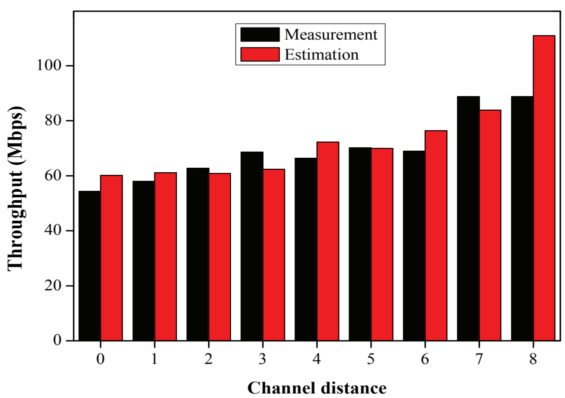

(c) Interfering RSS = -65dBm

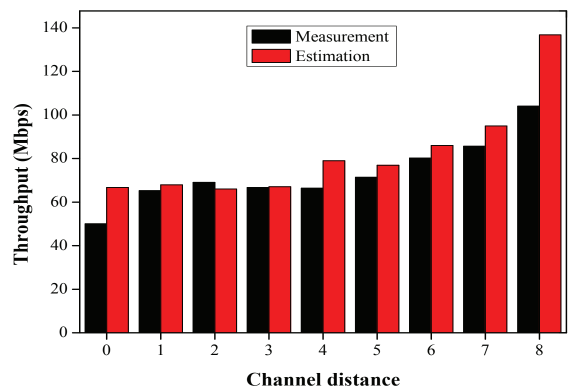

(d) Interfering RSS = -70dBm

Figure 5.7: Throughputs for different RSS^i and channel distances in Engineering Building #2.

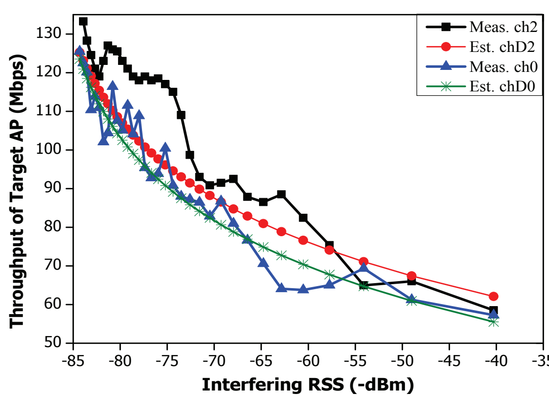

(a) Throughput of target link against interfering RSS, chD 0 and 2.

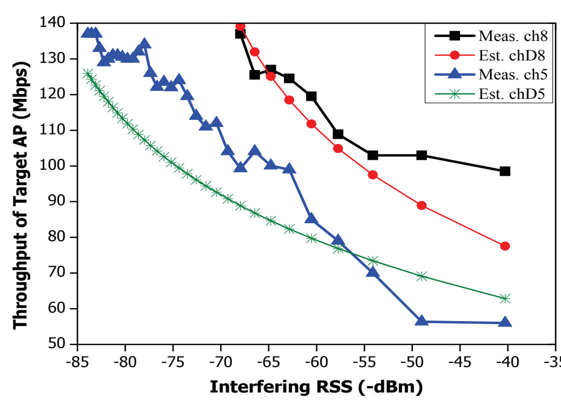

(b) Throughput of target link against interfering RSS, chD 5 and 8.

Figure 5.8: Throughputs for different RSS^i and channel distances in Asahi riverbed.

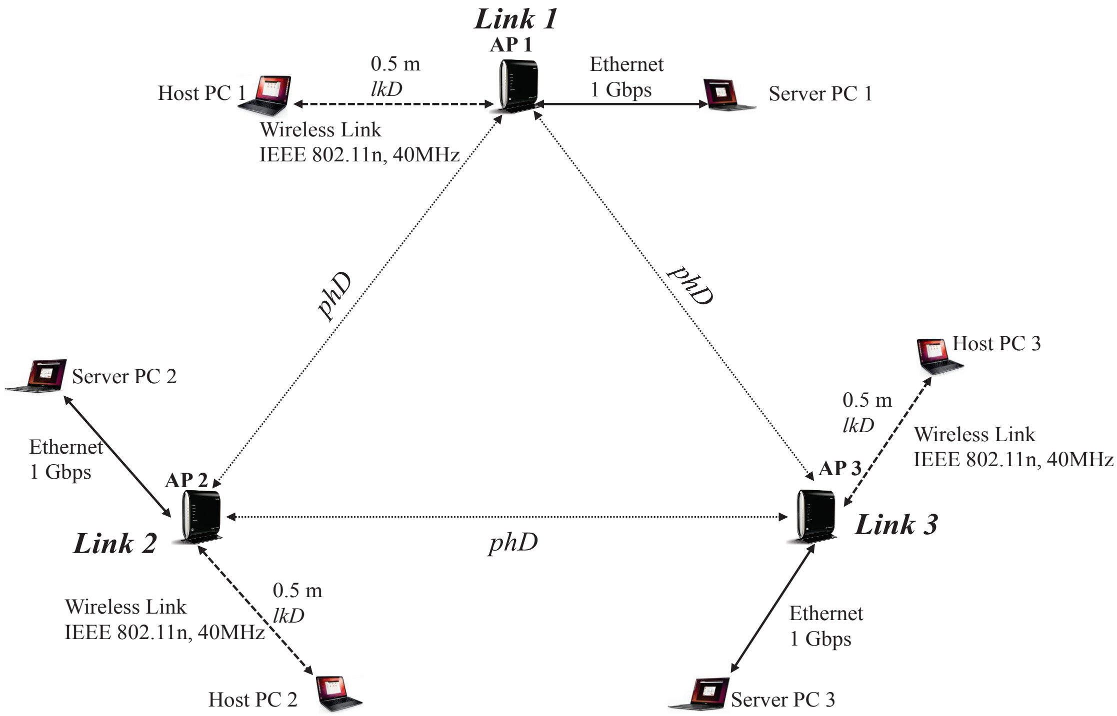

Figure 5.9: Measurement setup for three links.

5.4.2.2 Measurement Results

For AP_1 and AP_2 for three links, the bonded channel 3 is always assigned. For AP_3, the assigned channel is changed from 3 to 11 one by one, so that the channel distance *chD* increases from 0 to 8. The throughput was measured at the same time for all the links. The experiments were conducted on weekends and at night on weekdays to reduce the interference from other Wi-Fi devices.

Figure 5.10 show measured individual and average throughput under concurrently communicating three links. Similar to the observation for two links in Figure 5.1, the individual throughput fluctuates. This is because the contention among the links is not well resolved by the *carrier sense mechanism* [90], which may cause the unfair channel occupation among them. Thus, for three links, again, we use the average throughput among them for the single link throughput.

Figure 5.10 demonstrates that when the three APs are assigned the same channel, one AP can take the entire medium, which makes the others have the lower throughput. As *chD* increases, the throughput of AP_3 will enhance gradually, due to the reduced channel interference.

The measured maximum throughput of one link is about $140Mbps$ under no interference. Then, it drops significantly to about $50Mbps$ under two links in Figure 5.1, when the channel distance is smaller than seven. Furthermore, it drops to about $20Mbps$ under three links in Figure 5.10.

From the throughput analysis for *one link, two links and three links,* it is observed that for the target link, the interference from the first interfering link causes the larger throughput drop (from $140Mbps$ to $50Mbps$). Then, the interference from the second link causes the smaller drop (from $50Mbps$ to $20Mbps$). That is to say, when the target link is interfered by the first link, the rate adaptation mechanism lowers the transmission rate by adopting the robust *modulation and coding scheme (MCS)*. Then, the second interfering link further lowers the rate by adopting the more robust MCS [92][93]. Here, the rate can be lowered exponentially in MCS.

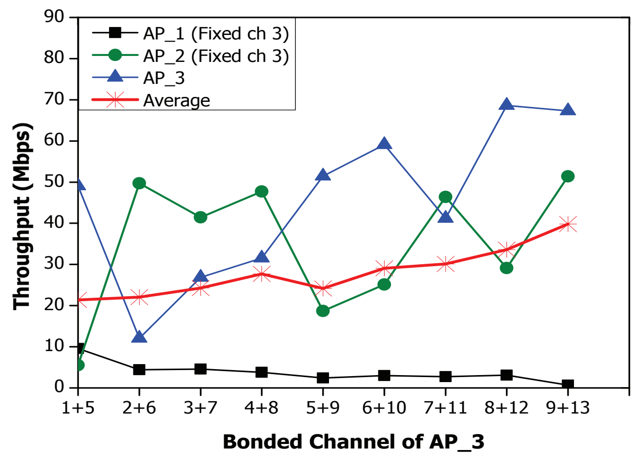

Figure 5.10: Throughput results for three links.

5.4.2.3 Model for Multiple Links

In this section, we present the extension of the throughput drop estimation model for concurrently communicating multiple links based on experimental results.

- *Model Idea:*
  In Section 5.4.1, the throughput drop from several interfering links can be estimated one by one through calculating each drop using the Eq. (5.1) in descending order of the interference. That is, the drop from the link with the largest interference is first estimated, assuming the original maximum throughput. Then, the drop from the link with the second largest interference will be estimated, assuming the maximum throughput has been reduced by the first drop.

- *Model Procedure:*
  The throughput of the target link ($link_{ij}$) under three or more concurrently communicating links is estimated by the following procedure:

  1. Estimate the throughput of the target link using the model for single link in Section 3.2.
  2. Estimate the throughput drop tpD from each of the interfered links using Eq. (5.1) in Section 5.4.1.
  3. Sort them in the descending order of the drop. Here, we consider the two interfered links to the target link, where the drops are given by tpD^{1st} and tpD^{2nd}.
  4. For the largest interfered link, adjust tpD^{1st} by the maximum speed of the AP of the target link, because different APs have different throughput performances:

$$tpD^{1st}_{adj} = tpD^{1st} \times \frac{tpM^{AP}}{140} \tag{5.3}$$

     where tpD^{1st}_{adj} represents the adjusted throughput drop by the largest interfering link, and tpM^{AP} does the maximum throughput for the AP of the target link.
     Then, the throughput tp^{1st}_{ij} of the target link after considering the drop by the first link interference is estimated by:

$$tp^{1st}_{ij} = tp_{ij} - tpD^{1st}_{adj} \tag{5.4}$$

5. For the second largest interfering link, adjust the tpD^{2nd} by;

$$tpD_{adj}^{2nd} = tpD^{2nd} \times \frac{tpM^{AP} - tpD_{adj}^{1st}}{140} \tag{5.5}$$

Then, the throughput tp_{ij}^{2nd} of the target link after considering the drop by the second link interference can be estimated by;

$$tp_{ij}^{2nd} = tp_{ij}^{1st} - tpD_{adj}^{2nd} \tag{5.6}$$

6. If more interfered links exist, repeat the same procedure.

In [93], Su et al. observed that the throughput drop by the accumulated interferences from two interfering links is greater than that from a single interferer, but less than the sum of the drops from the individual interference. The second interfering link will cause a smaller drop than the first one. This observation also supports our throughput drop estimation model for concurrently communicating multiple links.

5.4.2.4 Model Evaluation for Three Links

In this section, we evaluate the throughput drop estimation model for three concurrently communicating links under POCs through experiments and simulations.

- *Experiment Results in One Room:*
  First, the devices in Table 4.1 are set up in room H in Figure 4.4 (b). In experiments, the bonded channel 1+5 is always assigned to AP_1. Then, the either channel of 1+5, 5+9, and 9+13 is assigned to AP_2. To AP_3, the assigned channel is shifted from 1+5 to 9+13 one by one so that the chD is changed. The throughputs are measured at the same time for all the links.

  Throughput Results:
  Figures 5.11, 5.12, and 5.13 show the measured average throughput and estimated ones by the model among the three APs when the channel 1+5, 5+9, and 9+13 is assigned AP_2, respectively.

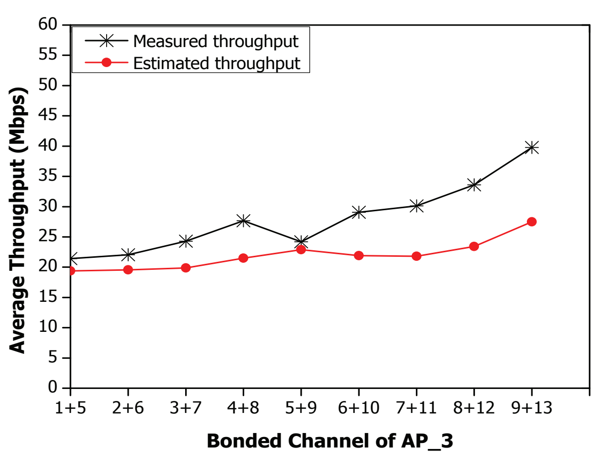

Figure 5.11: Throughput results in one room for AP_1:ch 1+5, AP_2:ch 1+5.

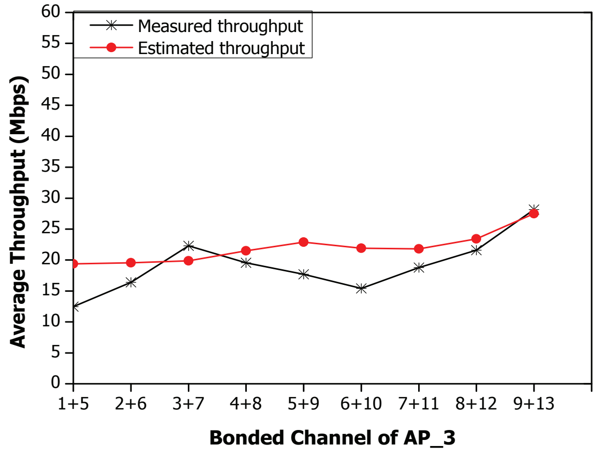

Figure 5.12: Throughput results in one room for AP_1:ch 1+5, AP_2:ch 5+9.

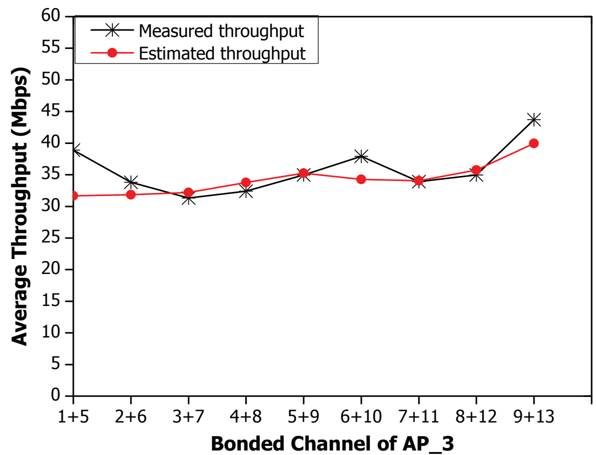

Figure 5.13: Throughput results in one room for AP_1:ch 1+5, AP_2:ch 9+13.

When the three results are compared, Figure 5.12 indicates the lowest throughput among them, because AP_2 is strongly interfered with both AP_1 and AP_3. Figure 5.13 presents the highest throughput in general, because AP_1 and AP_2 are less interfered. On the other hand, Figure 5.11 shows that as the channel distance increases, the throughput will raise as the reduction of the interference between (AP_1 and AP_2) with AP_3.

Then, the estimated throughput is calculated by the proposed throughput drop estimation model, and is compared with the measured throughput. Figures 5.11- 5.13 demonstrate that these throughputs are similar in any case. Thus, the accuracy of the proposed model for three concurrently communicating links is confirmed.

- *Experiment Results in Three Rooms:*
  Next, the model is evaluated through measurements in three rooms in Figure 4.4 (a) where each AP and host pair for the three links are located in rooms *D308, D307, and D306*. The physical distance between the APs is changed by locating each AP/host pair in a different room from the previous experiments in Section 5.4.2.4. By allocating each AP/host pair in a separate room, the overall interference between them is reduced. The link distance between the AP and its associated host is set 0.5*m* or 4*m*. The channel assignments in Section 5.4.2.4 are adopted.

Throughput Results with 0.5*m Link Distance:*

Figures 5.14- 5.16 show the measured and the estimated throughput results when the link distance is 0.5*m*. These throughput turns out to be similar at any channel distance, which confirms the accuracy of the proposed model. At the same time, they are higher than the ones in Figures 5.11- 5.13, since they are less interfered here.

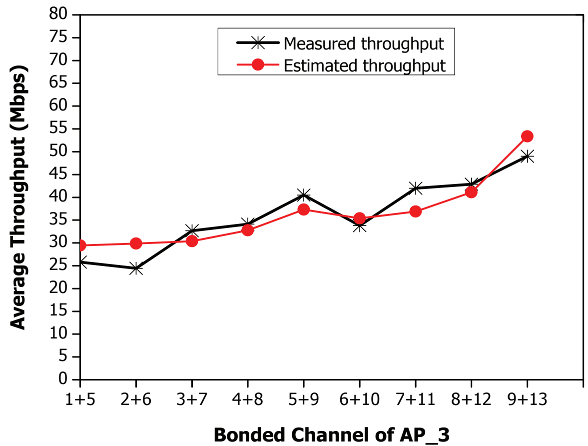

Figure 5.14: Throughput results in three rooms with 0.5m link distance for AP_1:ch 1+5, AP_2:ch 1+5.

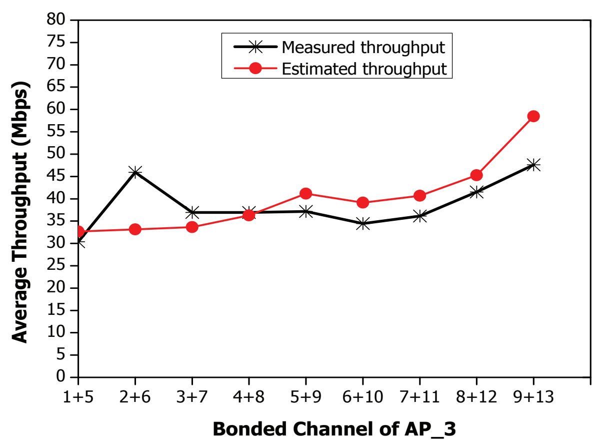

Figure 5.15: Throughput results in three rooms with 0.5m link distance for AP_1:ch 1+5, AP_2:ch 5+9.

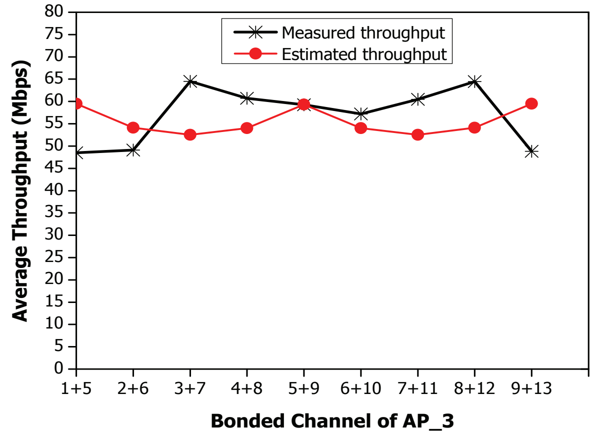

Figure 5.16: Throughput results in three rooms with 0.5m link distance for AP_1:ch 1+5, AP_2:ch 9+13.

Throughput Results with 4m *Link Distance:*
Figures 5.17- 5.19 show the measured and the estimated results when the link distance is 4m. In Figures 5.18 and 5.19, they are similar at any channel distance. Thus, the accuracy of the model is verified in the larger link distance as well. However, in Figure 5.17, the measured throughput is lower than the estimated one at each channel distance. This is due to the strong interference between the three links and from non-target APs in the field which is stronger around channel 1 + 5.

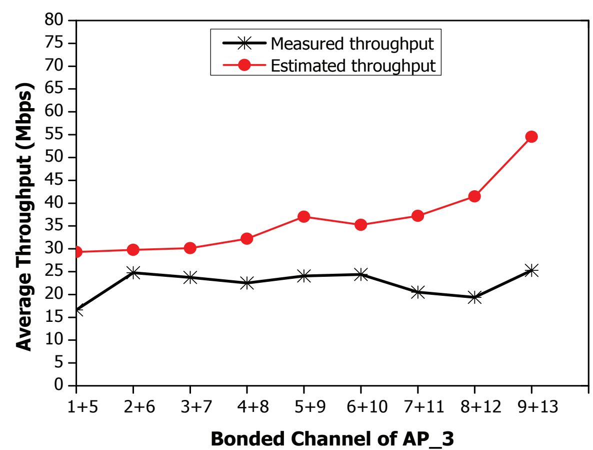

Figure 5.17: Throughput results in three rooms with 4m link distance for AP_1:ch 1+5, AP_2:ch 1+5.

5.5 Evaluation of Channel Assignment by Model under Channel Bonding

In this section, we discuss the application of the proposed throughput drop estimation model to the POC assignment at the APs and its evaluation.

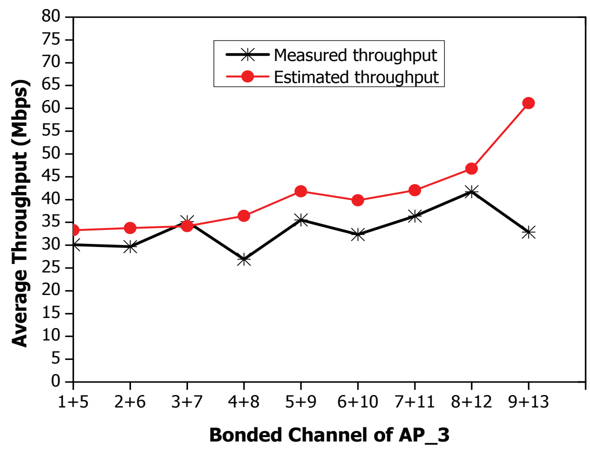

Figure 5.18: Throughput results in three rooms with 4m link distance for AP_1:ch 1+5, AP_2:ch 5+9.

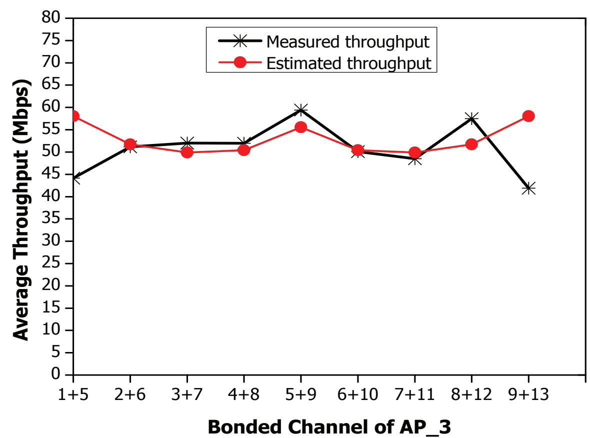

Figure 5.19: Throughput results in three rooms with 4m link distance for AP_1:ch 1+5, AP_2:ch 9+13.

5.5.1 Modifications of Algorithm

The channel assignment phase of the *active AP configuration algorithm* in [12] is modified to assign POC using the proposed model. Specifically, the formulations for this phase are revised from the previous one as follows:

5.5.1.1 Input and Output

The number of *partially overlapping channels (POC)* is adopted in place of the number of *orthogonal channels (OC)* for C as input. Then, the POC assigned to every active AP is adopted rather than the OC assigned to every active AP.

5.5.1.2 Objective

The total interfered communication time E_3 is minimized, where it is modified to consider partially overlapping channels by:

$$E_3 = \sum_{i=1}^{N} [IT_i^i] \tag{5.7}$$

where IT_i^i denotes the interfered communication time under partially overlapping channels for AP_i.

Under POCs, the link speed drop by the interfered links needs to be examined in the throughput estimation model. Therefore, IT_i^i can be simply given by:

$$IT_i^i = \sum_{j \in AH_i} \frac{1}{tp_{ij}^{2nd}} \tag{5.8}$$

where AH_i denotes the set of hosts associated with AP_i.

The throughput estimation model for POCs only examines the interference between three links. In this section, we assume that the target link is interfered by the two strongest interfering links, while the other interfering links may have negligible effects. This can be supported by the results in Section 5.4.2.2, where the highest interfering link causes the large drop and the second link causes the far small drop.

5.5.2 Evaluations by Simulations

First, we evaluate the performance of the POC assignment through simulations.

5.5.2.1 Simulation Platform

The *WIMNET simulator* [26] is adopted for simulations. Table 5.2 sums up the parameters for simulations.

Table 5.2: Simulation Parameters in WIMNET Simulator.

parameter	value
packet size	$1,500$ bytes
max. transmission rate	150 Mbit/s
propagation model	log-distance path loss model
rate adaptation model	sigmoid function
carrier sense threshold	−85 dBm
transmission power	19 dBm
collision threshold	10
RTS/CTS	yes

5.5.2.2 Results for Random Topology

To evaluate the performance in various network topologies for WLAN, first, the *random topology* is considered. As shown in Figure 6.9, in this topology we consider a network field of size $80m \times 20m$, where two rooms are located, each of length $40m$. Eight APs and 25 hosts are allocated randomly.

Then, the minimum host throughput and the overall throughput are compared between the POC assignment and the conventional orthogonal channel (OC) assignment through simulations. The center frequencies of bonded channels in Table 2.4 are used. Two channels (3, 11) are used for the OC assignment all the time. On the other hand, three channels (3, 7, 11), six channels (3, 5, 7, 8, 9, 11), and nine channels (3, 4, 5, 6, 7, 8, 9, 10, 11) are used for the POC assignment. Table 5.3 shows the results.

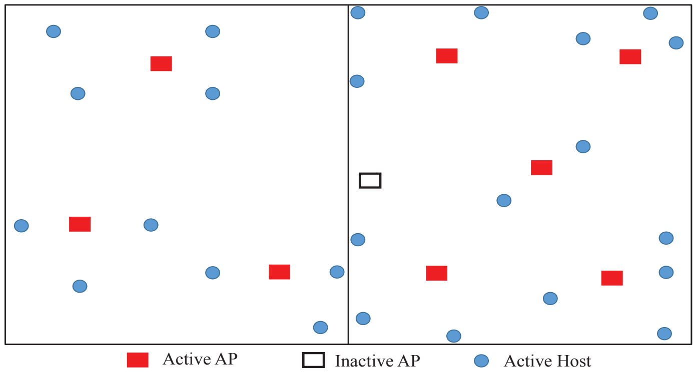

Figure 5.20: Random topology for channel assignment.

.

Table 5.3: Throughput results for *random topology*.

channel assignment	OC	POC		
# of channels	2	3	6	9
min. host throu. (Mbps)	7.12	9.16	8.42	8.63
overall throu. (Mbps)	174.56	196.74	197.04	198.46

5.5.2.3 Results for Regular Topology

Next, the *regular topology* in the third floor of Engineering Building #2 at Okayama University is considered. The room size is either $7m \times 6m$ or $3.5m \times 6m$. Eight APs and 55 hosts are regularly allocated, as signified in Figure 5.21.

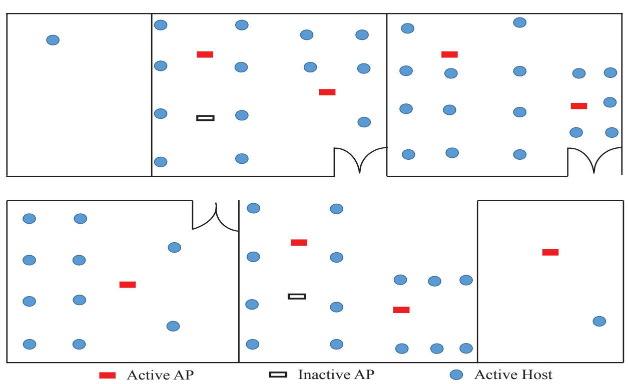

Figure 5.21: Regular topology.

The same two, three, six, and nine channels as for *random topology* are considered. Table 5.4 shows the minimum host throughput and the overall throughput for them.

It is noted that in both topologies, as the number of POCs is increased, the overall throughput will enhance by reducing the interference while maintaining the minimum host throughput.

5.5.3 Evaluations by Experiments

Lastly, the throughput of the POC assignment is evaluated through experiments using the *two-rooms topology* in Figure 5.22. Two channels 3 and 11 are used for the OC assignment, and three

Table 5.4: Throughput results for *regular topology*.

channel assignment	OC	POC		
# of channels	2	3	6	9
min. host throu. (Mbps)	2.68	3.11	3.06	3.15
overall throu. (Mbps)	147.76	170.88	168.76	173.49

channels 3, 7, and 11 are for the POC.

Table 5.5 shows the simulation and measurement results. This table indicates the following: 1) the POC assignment improves the overall throughput, and 2) the estimated throughput is well coincident with the measured one. The accuracy of the throughput estimation model and the effectiveness of the POC assignment are confirmed.

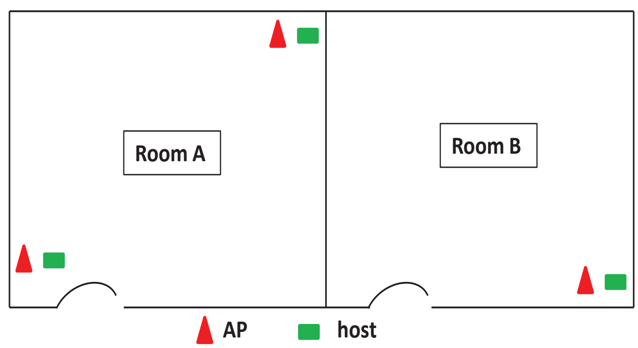

(a) Two-rooms topology

Figure 5.22: Two-rooms topology.

Table 5.5: Throughput results for *Two-room topology*.

channel assignment	OC	POC
# of channels	2	3
measurement (Mbps)	146.36	158.20
simulation (Mbps)	143.50	157.31

5.6 Summary

In this chapter, we presented the throughput drop estimation model under channel bonding. First, we illustrated the preliminary measurement observations. Second, we discussed the throughput drop measurements. Third, we presented the model under interfered links. Finally, we evaluated the channel assignment by using the model under channel bonding. In the next chapter, we will present the throughput drop estimation model under non-channel bonding.

Chapter 6

Throughput Drop Estimation Model under Non-Channel Bonding

In this chapter, we present the *throughput drop estimation model under non-channel bonding*. Firstly, we discuss the throughput measurement results under non-channel bonding. Secondly, we present the model under interfered links. Thirdly, we verify the model estimation accuracy. Finally, we present the evaluation of the channel assignment by the model under non-channel bonding.

6.1 Introduction

In Chapter 5, we presented the *throughput drop estimation model under channel bonding*. It has been demonstrated that the *channel bonding (CB)* is one of the key technologies to enhance the data transmission speed in wireless communications in general. However, CB reduces the number of non-interfered channels. Besides, as shown in [29], the wider bandwidth of the CB link can cause the reduction of *signal to interference plus noise ratio (SINR)* at the distant host from the AP. Then, the lower $SINR$ can cause the adoption of the slower *modulation and coding scheme (MCS)* and the *hidden terminal problem* can arise, which can further lower the throughput.

As a result, the conventional *non-channel bonding (non-CB)* links with $20MHz$ width are still common in a lot of WLANs. Especially, the *non-CB* links should be used in a dense WLAN, since the CB links cannot provide the required capacity due to high interferences from other links. Actually, we have observed that non-CB links provide higher throughputs than CB when several APs are co-located together. Because of this, in this chapter, we extend the throughput drop estimation model under POCs for CB links to the conventional non-CB links.

6.2 Throughput Measurement Results

The hardware and software in Table 4.1 are adopted in our experiments using NEC AP devices. These devices are set up in the indoor field in Figure 4.4 (a). The *Iperf* is adopted as a popular software tool for measuring the TCP throughput by generating TCP packets [65].

First, we examine the largest *channel distance* (*chD*) that can cause the interference between two adjacent links. In the experiments, the *link distance (lkD)* between a host and an AP is fixed at 0.5*m*, and the *physical distance* between the two APs (*phD*) is at 5*m*. The *non-CB* channel of the first link is fixed at *channel 1*, and that of the second link is changed from *channel 1* to *channel 13*.

From the throughput results of the individual links under interferences, it has been known that the individual throughput always fluctuates, as in Chapter 5. Thus, we use the average throughput among them in the evaluations.

Figure 6.1 shows the average throughput of the two links for a different *chD*. For *chD* = 4 or smaller, the average throughput is extremely low due to the high interference [94]. Then, for *chD* = 5 or larger, it is quickly increasing as the less interference. For *chD* = 6 or larger, it becomes maximum due to no interference. Therefore, we will assess the throughput drop for *chD* = 5 or smaller.

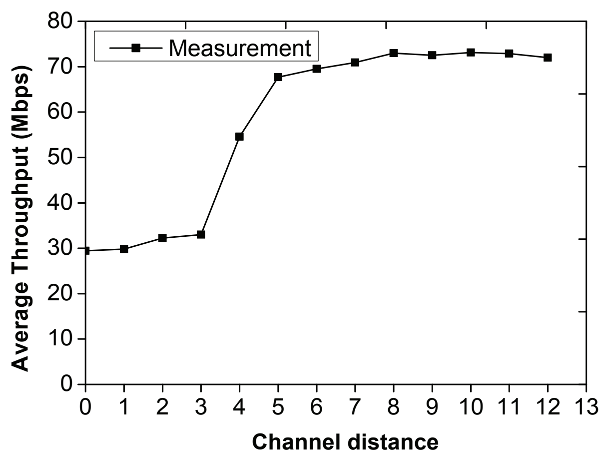

Figure 6.1: Average throughput of two links for different *chD*.

Figure 6.2 shows the changes of the throughput drop of the first link for a different *chD*. Here, *lkD* = 0.5*m* is fixed, and *phD* is changed from 3*m* to larger ones to obtain the different interfering RSS.

6.3 Model under Interfered Links

Based on throughput drop measurement results in Section 6.2, we present the *throughput drop estimation model under non-CB* links.

6.3.1 Two Interfered Links

The results in Figure 6.2 suggest that again, the natural logarithm function in Eq. (5.1) can be used to estimate the *throughput drop* (tpD) for *non-CB* links. Then, the parameter values for Eq. (5.1) in Table 6.1 are derived from measurement results in Figure 6.2.

6.3.2 Multiple Interfered Links

Then, the throughput drop estimation model is presented for three or more interfered links. As for *CB* links in Chapter 5, the interfered links are explored sequentially in descending order of their drops. It is noted that only two interfered links are considered here. If three or more interfered links exist, the same procedure should be repeated as in Section 5.4.2.3.

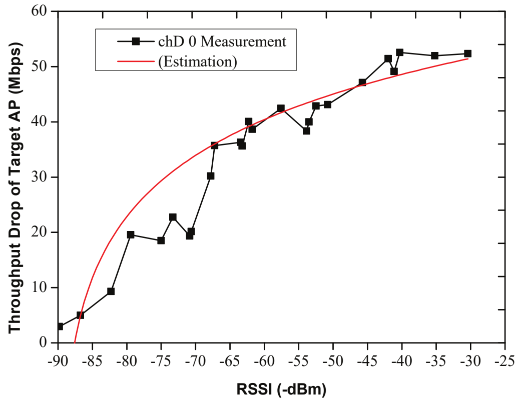

(a) $chD = 0$

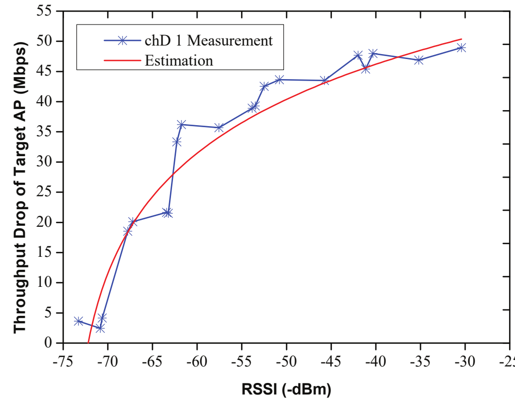

(b) $chD = 1$

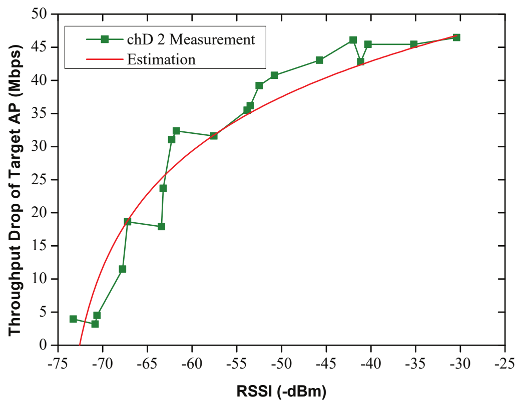

(c) $chD = 2$

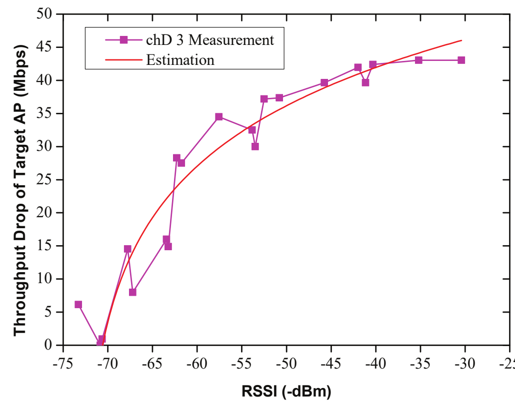

(d) $chD = 3$

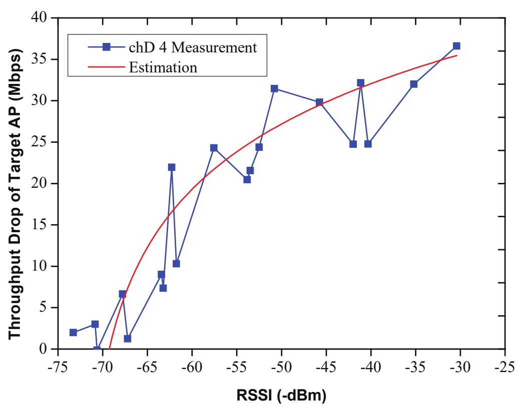

(e) $chD = 4$

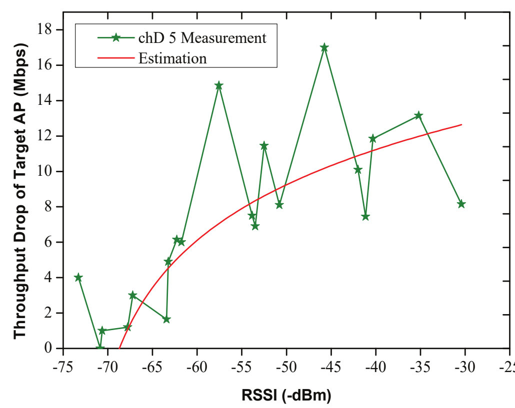

(f) $chD = 5$

Figure 6.2: Throughput drop results for different interfered RSS at different *chD*.

First, the equations for the throughput drop estimation in Eq. (5.3) and Eq. (5.5) should be adjusted to consider the difference of the maximum throughput of the APs for *non-CB* ($75Mbps$) and *CB* ($140Mbps$) as follows:

$$tpD^{1st}_{adj} = tpD^{1st} \times \frac{tpM^{AP}}{75} \tag{6.1}$$

Table 6.1: Parameter values of throughput drop estimation model for *non-CB*.

channel distance	p	q	r
0	16.0	90.0	-14
1	17.0	74.5	-14
2	16.0	75.0	-14
3	16.0	73.0	-14
4	13.0	72.0	-13
5	5.5	73.0	-8

$$tpD_{adj}^{2nd} = tpD^{2nd} \times \frac{tpM^{AP} - tpD_{adj}^{1st}}{75} \tag{6.2}$$

Then, the dropped throughput under the interferences for the target link is obtained by sequentially subtracting the tpD_{adj}^{1st} and tpD_{adj}^{2nd} from tp_{ij}, as in Eq. (5.4) and Eq. (5.6).

6.4 Evaluation of Model Estimation Accuracy

In this section, we evaluate the accuracy of the throughput drop estimation model for *non-CB* links by comparing the estimated throughput results with the measured ones in two network fields. The measurement setup in Figure 5.9 was adopted for 20MHz non-CB. The indoor fields in Figure 4.4 (a) and (b) were used.

Table 6.2 shows the locations of the server, the APs, and the hosts in Figure 4.4 (a) and (b). Both the high and low interference cases are examined. For the *high interference case*, all the devices for the three links are located in the same room. For the *low interference case*, the devices for each link are located in each of three different rooms.

Table 6.2: Device locations.

interference	field	device location		
		AP_1, $Host_1$	AP_2, $Host_2$	AP_3, $Host_3$
high	Eng. Bldg. #2, Figure 4.4 (a)	D306	D306	D306
	Grad. Sch. Bldg., Figure 4.4 (b)	H	H	H
low	Eng. Bldg., #2 Figure 4.4 (a)	D307	corr. near D301	D306
	Grad. Sch. Bldg., Figure 4.4 (b)	A	E	C

6.4.1 Channel Assignment to APs

Channel 1 for *non-CB* is always assigned to AP_1. Either of *channel* 1, 6, or 13 is assigned to AP_2. To AP_3, the assigned channel is moved from *channel 1* to *channel 13* one by one, so that *chD* is gradually increased. The throughputs for all the links are measured at the same time.

6.4.2 Throughput Results

Figures 6.3 and 6.4 illustrate the average throughput measurement and estimation results for the high and low interferences, respectively. In each figure, the left graph reveals the results for *En-*

gineering Building #2 in Figure 4.4 (a), and the right graph does the ones at the *Graduate School Building* in Figure 4.4 (b). In each case, the measurement results and the estimation ones appear to be similar, which confirms the accuracy of the proposed model.

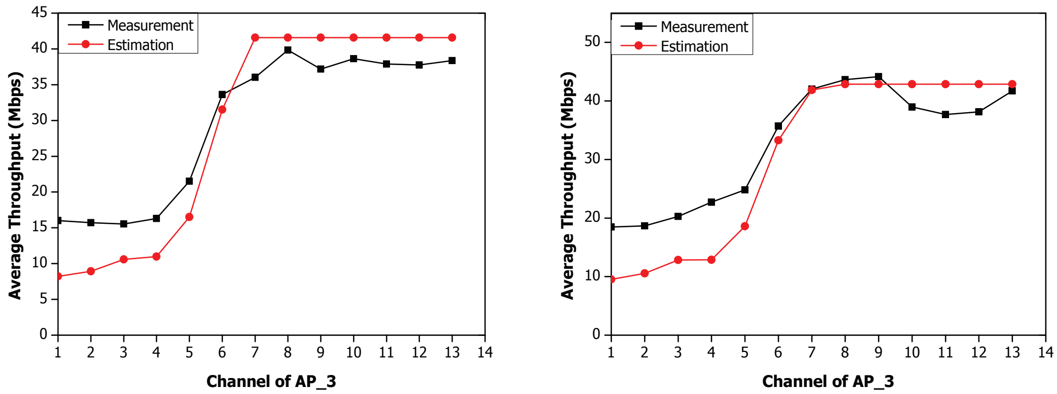

(a) AP_1: $ch1$, AP_2: $ch1$.

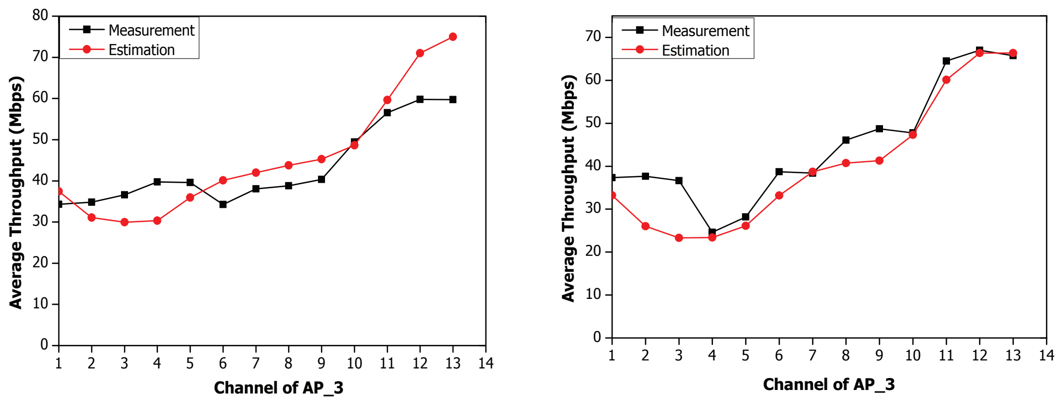

(b) AP_1: $ch1$, AP_2: $ch6$.

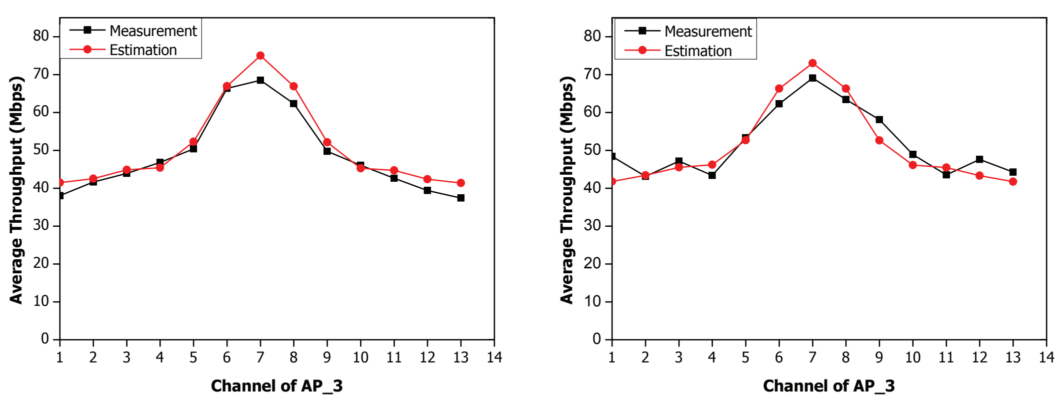

(c) AP_1: $ch1$, AP_2: $ch13$.

Figure 6.3: Throughput results for high interference level.

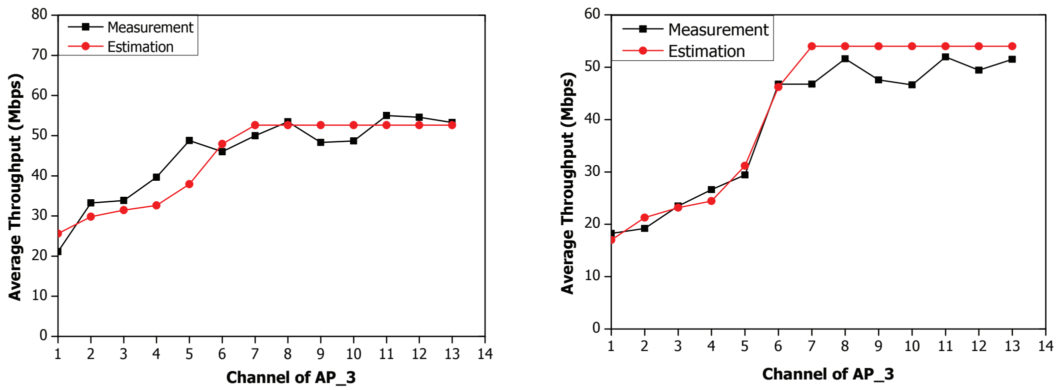

(a) AP_1: $ch1$, AP_2: $ch1$.

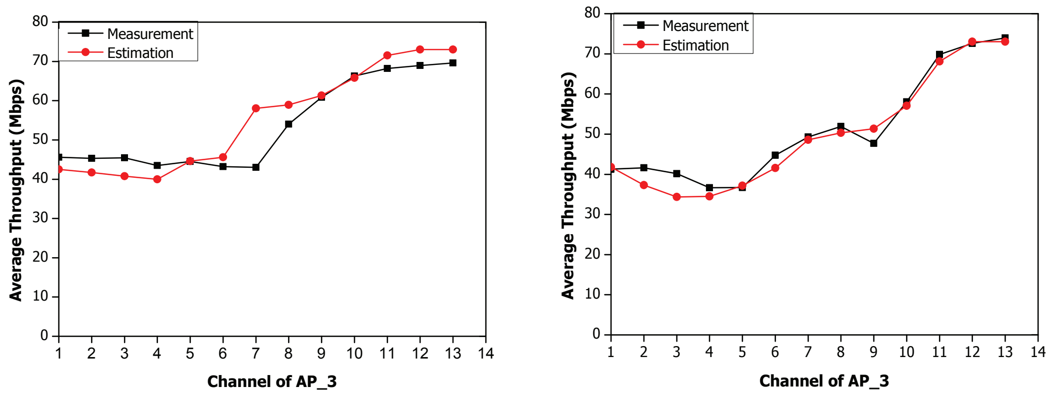

(b) AP_1: $ch1$, AP_2: $ch6$.

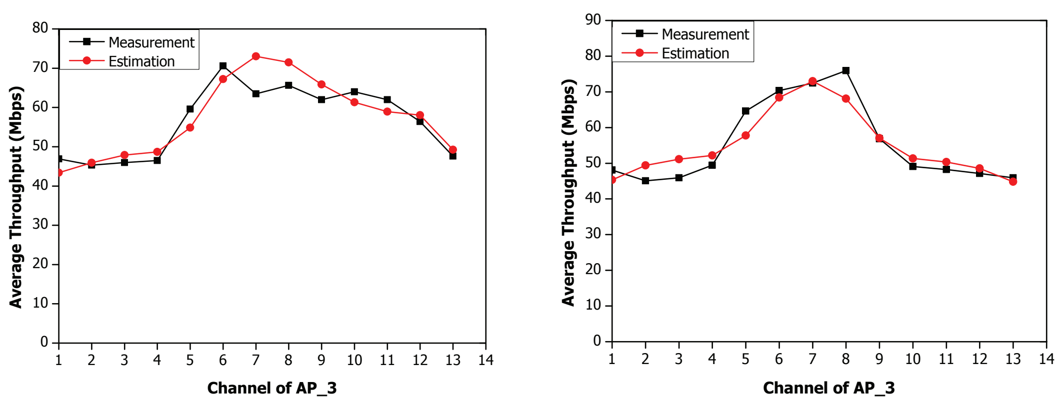

(c) AP_1: $ch1$, AP_2: $ch13$.

Figure 6.4: Throughput results for low interference level.

6.4.3 Discussion

Here, we discuss the details of throughput results for different channel assignments, interference levels and model accuracy.

6.4.3.1 Different Channel Assignments

First, we discuss the results for different channel assignments.

- *Case (a) AP_1: $ch1$, AP_2: $ch1$:*
  The throughput is low when AP_3 is assigned *channel* $1-4$. Here, the three APs are assigned to the same or quite close channels, which causes the high interference. Then, the throughput will turn out to be high when AP_3 is assigned *channel* $8-13$, where the interference becomes low.

- *Case (b) AP_1: $ch1$, AP_2: $ch6$:*
  The throughput is medium when AP_3 is assigned *channel* $1-6$. The three APs are assigned to the similar channels, which causes the medium interference. Then, the throughput becomes highest when AP_3 is assigned *channel* 13, where the three APs are assigned almost non-interfered channels. Thus, the interference becomes exceedingly low.

- *Case (c) AP_1: $ch1$, AP_2: $ch13$:*
  The throughput is highest when AP_3 is assigned *channel* 7, where the three APs are assigned the non-interfered channels. Then, when the channel of AP_3 is close to *channel* 1 or *channel* 13, the throughput is reduced on account of the higher interference.

- *Estimation Curve:*
  The curve of the estimated throughput is not monotonic but has convex or concave, because the throughput drop by the interference is changed non-linearly with the *channel distance* between the assigned channels and on (RSS^i) of the interfering signal at the AP. When the channel distance is small or (RSS^i) is large, the interference is large and the estimated throughput becomes smaller. On the other hand, when the channel distance is large or (RSS^i) is small, the interference is small and the estimated throughput becomes larger.

6.4.3.2 Different Interference Levels

Next, we analyse the results for different interference levels.

The throughput for the high interference level is generally lower than the throughput for the lower one. When the non-interfered channels are assigned to the three APs, the throughput for the high level is similar to the throughput for the lower one. Thus, the non-interfered channels should be assigned to the APs when they are highly interfered.

6.4.3.3 Model Accuracy

Overall, the experiment results confirm the accuracy of the proposed model under various interference conditions among three links. However, the gap between the measured and estimated throughputs is relatively large when AP_3 is assigned *channel* $1-4$ for the high interference level. Here, the collision avoidance mechanism of the CSMA/CA protocol [1] may work more accurately to avoid the further throughput drop.

6.4.4 Evaluation for Different AP Device

To verify the generality of the proposed model, we evaluate the accuracy using different AP devices.

6.4.4.1 Measurement Scenario

Here, we adopt the *Raspberry Pi 3 Model B* for the APs, which uses Raspbian OS, Broadcom BCM2837, 1.2Ghz 64-bit quad-core ARM Cortex-A53 CPU, LPDDR2-900MHz 1GB SDRAM, 10/100Mbps Ethernet, IEEE802.11b/g/n wireless NIC, Blue-tooth 4.1 classics/low energy [82]. The measurement setups and topologies in Sections 6.2 and 6.4 are used.

6.4.4.2 Results and Discussions

Figure 6.5 shows the average throughput of the two links when the channel distance *chD* between them is changed from 0 to 12. Again, the average throughput is small due to the strong interference when the channel distance is smaller than five.

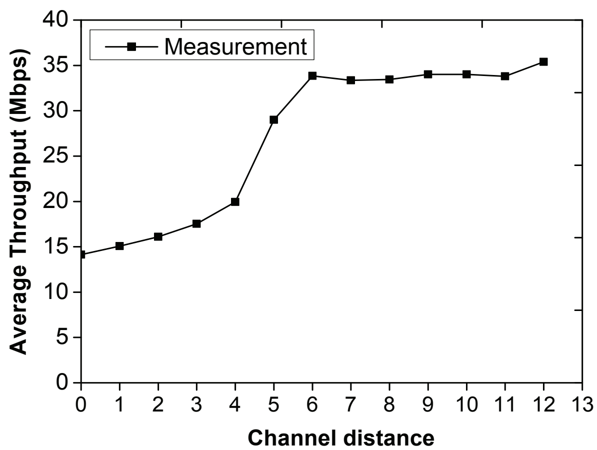

Figure 6.5: Average throughput of two links for different *chD* with Raspberry Pi APs.

Figure 6.6 shows the changes of the measured and estimated throughput drop of the first link using the Raspberry Pi AP when the three parameter values in Table 6.3 are used and the channel distance *chD* is changed. Again, the logarithm function in the model is well matching with the measured throughput.

Table 6.3: Parameter values of throughput drop estimation model for *non-CB* for Raspberry Pi AP.

channel distance	p	q	r
0	6.0	90.0	1.5
1	6.0	85.0	1.0
2	5.5	84.58	1.0
3	5.0	79.5	0.5
4	5.0	62.0	0.5
5	3.2	60.0	-0.25

Figure 6.7 shows the average measured and estimated throughput of the three links with the Raspberry Pi APs. Again, the estimated throughput is well matching with the measured throughput. Therefore, the proposed model can be used for various AP devices.

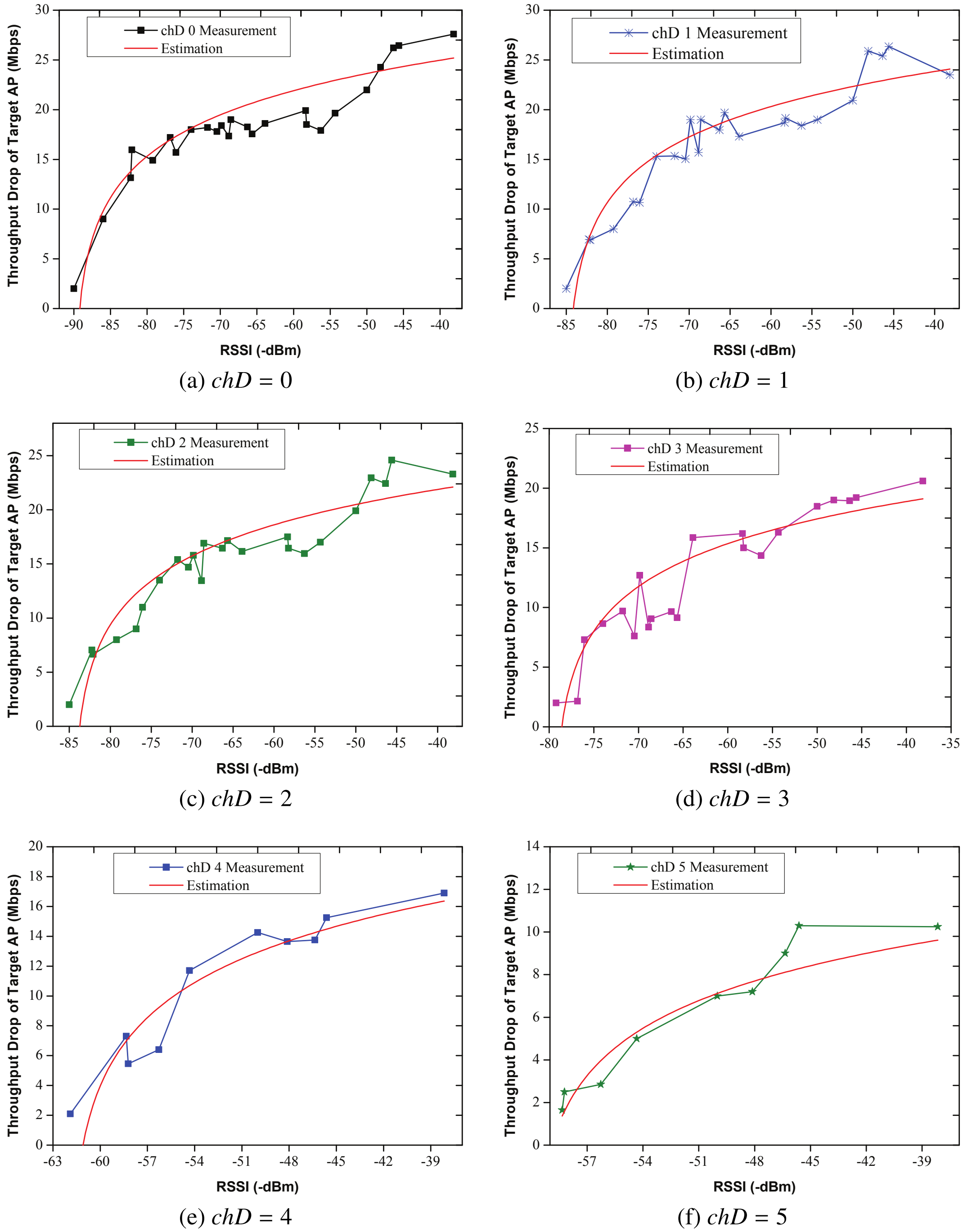

(a) $chD = 0$ (b) $chD = 1$

(c) $chD = 2$ (d) $chD = 3$

(e) $chD = 4$ (f) $chD = 5$

Figure 6.6: Throughput drop results for different interfered RSS at different *chD* for Raspberry Pi AP.

6.5 Channel Assignment Application of Model under Non-Channel Bonding

In this section, we discuss the application of the throughput drop estimation model to the channel assignment to the APs in WLAN.

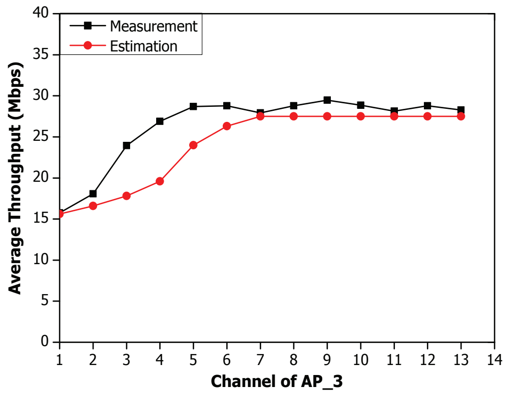

(a) AP_1: $ch1$, AP_2: $ch1$.

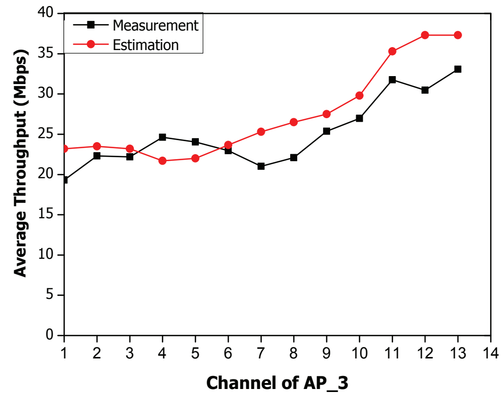

(b) AP_1: $ch1$, AP_2: $ch7$.

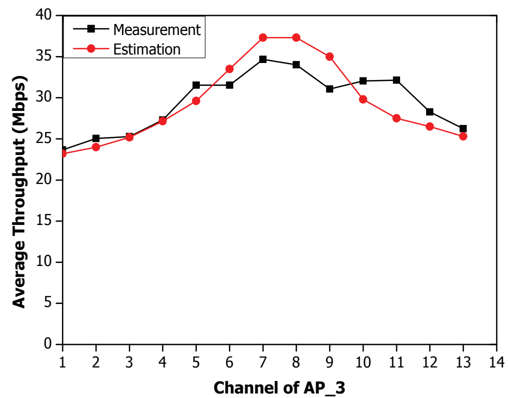

(c) AP_1: $ch1$, AP_2: $ch13$.

Figure 6.7: Throughput results for different channel interferences for Raspberry Pi AP.

6.5.1 Modifications of Algorithm

The channel assignment phase of the *active AP configuration algorithm* in [12] is modified to assign the *non-CB POC* using the proposed model. The modifications of the problem formulation for this phase are described as follows.

6.5.1.1 Input and Output

In the output, *non-CB POC*s are assigned to the active APs, instead of *non-CB orthogonal channels (OCs)*. Then, in the input, the number of channels C represents the number of *non-CB POC*s.

6.5.1.2 Objective

In the objective, the new cost function E_{ch} in Eq. (6.3) is designed to maximize the total throughput of the APs, while it minimizes the difference of the communication time between the fastest AP and the slowest one. The latter part of the function intends averaging the performances of the APs.

$$E_{ch} = \sum_{i=1}^{N} TP_i^{POC} - \alpha(max_i[CT_i^{POC}] - min_i[CT_i^{POC}]) \tag{6.3}$$

where TP_i^{POC} represents the total throughput of the links associated with AP_i under the *POC* assignment, CT_i^{POC} does the required time for every link associated with AP_i to transmit one bit, and α does the coefficient in the function. The function $max_i[x_i]$ ($min_i[x_i]$) returns the maximum (minimum) value of x_i. CT_i^{POC} is particularly small compared to TP_i^{POC}. Thus, a large value of $\alpha = 10,000$ is used in this section.

The *communication time* CT_i^{POC} is defined by the total time required for the AP_i to transmit 1-bit data to all of the hosts associated with the AP. When the communication time for AP_i is small, the throughput is large, since it is given by the inverse of the communication time. Therefore, the communication time should be minimized to maximize the throughput.

TP_i^{POC} is calculated by:

$$TP_i^{POC} = \frac{m}{\sum_{j \in AH_i} \frac{1}{tp_{ij}^{POC}}} \tag{6.4}$$

where AH_i represents the set of the hosts associated with AP_i, m does the number of the hosts in AH_i, and tp_{ij}^{POC} does the estimated throughput of the link between AP_i and $HOST_j$ under the *POC* assignment by the proposed model.

CT_i^{POC} is calculated by:

$$CT_i^{POC} = \sum_{j=1}^{m} \frac{1}{tp_{ij}^{POC}} \tag{6.5}$$

6.5.2 Evaluations by Simulations

First, we evaluate the *POC* assignment using the proposed model through simulations on regular and random topologies. The *WIMNET simulator* [26] is adopted in our simulations. Table 5.2 summarizes the parameters, where the maximum transmission rate is changed to 75 Mbit/s from 150 Mbit/s.

6.5.2.1 Regular Topology

Figure 6.8 shows the network fields and the AP and host locations in simulations as regular topologies. Figure 6.8 (a) models the *third floor in Engineering Building #2*. 9 APs and 31 hosts are located in the nine rooms, where each room size is either $7m \times 6m$ or $3.5m \times 6m$. Figure 6.8 (b) models the *second floor in Graduate School of Natural Science and Technology Building*. 13 APs and 48 hosts are located in the eight rooms and the corridor.

Table 6.4: Simulation results for Engineering Building #2.

channel assig.	*OC*	*POC*									
# of channels	3	4	5	6	7	8	9	10	11	12	13
small. th. (Mbps)	6.134	6.653	6.836	6.977	7.696	7.698	7.836	7.831	7.837	7.918	7.918
total th. (Mbps)	190.151	206.252	211.922	216.289	238.587	238.647	242.911	242.773	242.935	245.463	245.463

Table 6.5: Simulation results for Graduate School Building.

channel assig.	*OC*	*POC*									
# of channels	3	4	5	6	7	8	9	10	11	12	13
small. th. (Mbps)	6.289	7.241	7.243	7.694	7.887	8.008	8.235	8.237	8.334	8.477	8.477
total th. (Mbps)	301.867	347.547	347.653	369.324	378.569	384.390	395.300	395.386	400.022	406.890	406.890

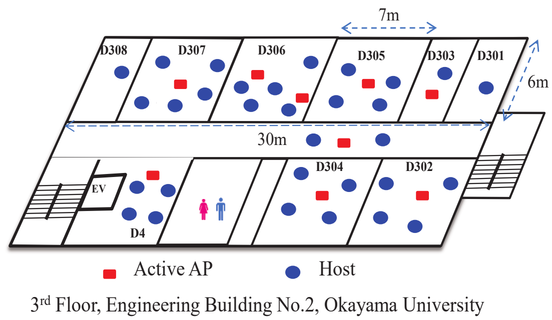

(a) 3rd Floor in Engineering Building #2.

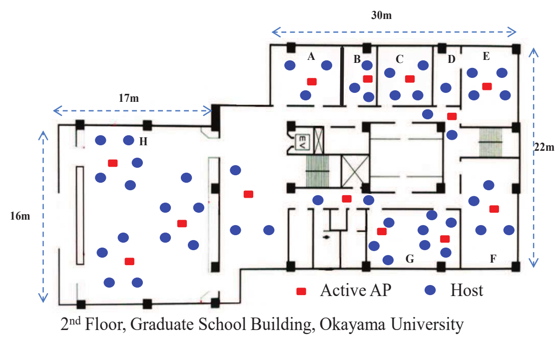

(b) 2nd Floor in Graduate School Building.

Figure 6.8: Regular topology for simulations.

Tables 6.4 and 6.5 show the smallest throughput of one host among the hosts and the total throughput of all the hosts for the two fields respectively, when the number of *POC*s is changed from three to 13. In both topologies, when the number of *POC*s is 12 or 13, both throughputs become highest, where the proper *POC* assignment using the model reduces the interference.

The *POC* assignment improves the smallest throughput by 24.766% and the total throughput by 24.771% on average in the two topologies from the *OC* assignment. Thus, the *POC* assignment using the proposed model outperforms the conventional *OC* assignment.

6.5.2.2 Random Topology

The channel assignment using the proposed model is simulated in a random topology of size $40m \times 30m$ in Figure 6.9. 10 APs and 30 hosts are located in the field. Table 6.6 shows the results where the proposal improves the smallest throughput of one host by 19.624% and the total throughput of all the hosts by 19.620% on average from the *OC* assignment. The effectiveness of *POC* assignment by the proposed model is verified in a different network topology.

Table 6.6: Simulation results for Random Topology.

channel assig.	*OC*	*POC*									
# of channels	3	4	5	6	7	8	9	10	11	12	13
small. th. (Mbps)	7.279	7.576	7.633	8.337	8.906	8.933	8.984	9.088	9.126	9.246	9.246
total th. (Mbps)	218.382	227.284	228.989	250.122	267.176	267.991	269.516	272.648	273.786	277.388	277.388

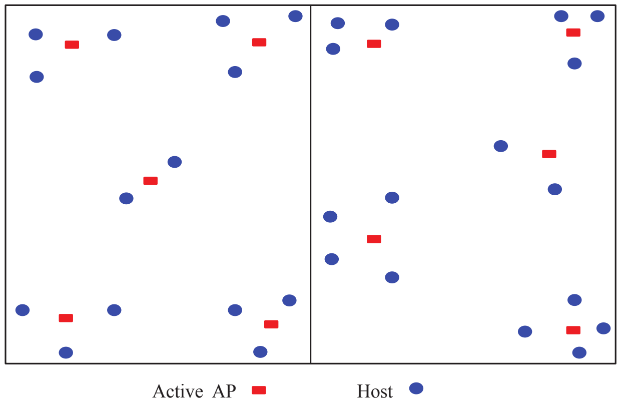

Figure 6.9: Random topology for simulations.

6.5.3 Evaluations by Experiments

Next, we evaluate the *POC* assignment using the proposed model through testbed experiments in two topologies in *Engineering Building* #2. Figure 6.10 illustrates the locations of the four APs and the four hosts in *topology 1*. In *topology 2*, the AP and the host in room *D*4 are moved to *D*307 for higher interferences. In each topology, three channels (1, 7, 13) are used for the *OC* assignment, while four channels (1, 5, 9, 13) are for the *POC* assignment.

Figures 6.11 and 6.12 show the total throughput results for *topology 1* and *topology 2* respectively. In either topology, the channel assignment with four *POC*s by the proposal improves the measured one by 12.89% on average over the assignment with three *OC*s. Besides, the measured throughput and the simulated one are similar to each other. Again, the effectiveness of the proposed *POC* assignment and the accuracy of the proposed throughput drop estimation model are both confirmed.

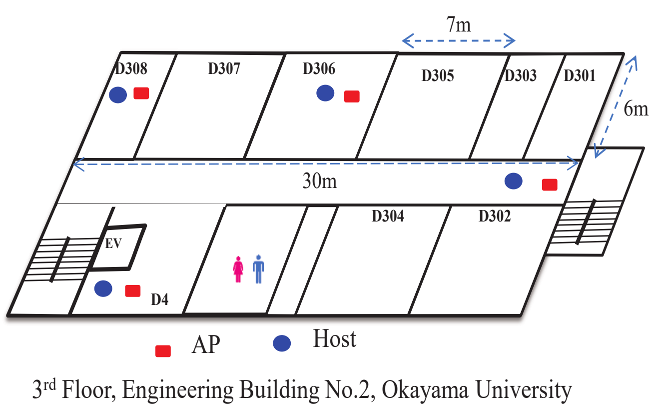

Figure 6.10: AP and host locations for *topology 1*.

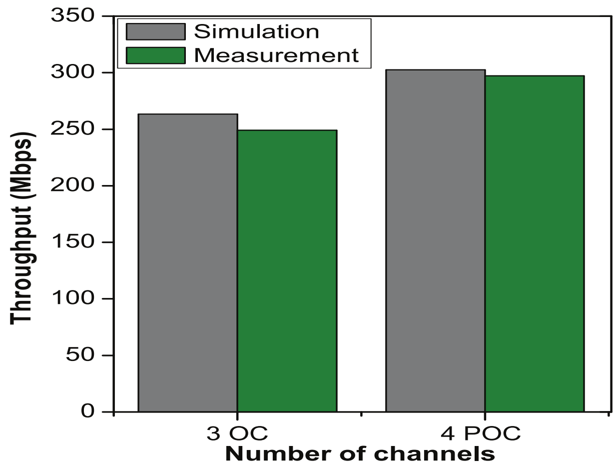

Figure 6.11: Throughput results for *topology 1*.

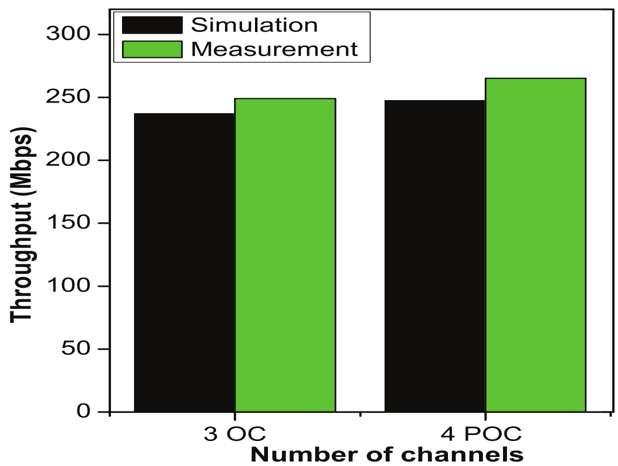

Figure 6.12: Throughput results for *topology 2*.

6.6 Summary

In this chapter, we presented the throughput drop estimation model under non-channel bonding. Firstly, we discussed the throughput measurement results under non-channel bonding. Secondly, we presented the model under interfered links using non-channel bonding. Thirdly, we demonstrated the model estimation accuracy. Finally, we evaluated the channel assignment by using the model under non-channel bonding. In the next chapter, we will present the throughput drop estimation model under coexistence of channel bonding and non-channel bonding.

Chapter 7

Throughput Drop Estimation Model under Coexistence of Channel Bonding and Non-Channel Bonding

In this chapter, we propose the *throughput drop estimation model under coexistence of channel bonding (CB) and non-channel bonding (non-CB)*. Firstly, we describe throughput measurement results under coexistence of CB and non-CB. Secondly, we present the throughput drop estimation model for it. Thirdly, we discuss the application of the model to the transmission power optimization. Finally, we verify the model estimation accuracy.

7.1 Introduction

In Chapters 5 and 6, we presented the throughput drop estimation models with the maximum transmission power at the AP under *channel bonding (CB)* and *non-channel bonding (non-CB)* respectively. The model under CB was considered first because it can provide higher throughputs due to the wide channel width in general. However, CB has a fewer orthogonal channels, and may cause higher interferences and reduce throughputs. Therefore, in Chapter 6, we proposed the model under conventional non-CB at *20MHz* that is still common in WLANs. Non-CB should be used in dense WLANs to reduce interferences.

In WLAN, the higher transmission power of the AP can increase the transmission capacity and range in general, but can also increase the interference to other APs. When a host is located near to the AP, the minimum transmission power can provide the same maximum throughput due to the non-linear relationship between the *received signal strength (RSS)* and the throughput [32]. It can reduce the interference. Thus, it has been observed that either the maximum or minimum transmission power of each AP can offer the highest overall throughput of the WLAN depending on the distance between the host and the AP. Thus, the selection can be determined by the relative distance between them.

In this chapter, we propose the throughput drop estimation model under coexistence of *channel bonding* and *non-channel bonding* links with different transmission powers at the AP, based on our previous studies in Chapters 5 and 6. This model exploits the advantages of both CB and non-CB together with the power tuning to increase the throughput under interferences. The parameters of this model are newly adjusted based on our measurement results under coexistence of CB and non-CB links in two network fields, with various conditions of channel distances.

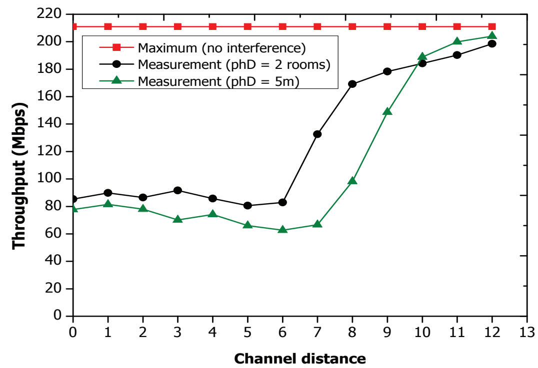

Figure 7.1: Total throughput of two links coexisting under CB and non-CB for different *chD* and *phD*.

7.2 Throughput Drop Measurement under Coexistence of CB and Non-CB Links

Figure 4.2 illustrates the measurement setup using two interfered links. The hardware and software in Table 4.1 are adopted in measurements. These devices are allocated in the indoor field on *third floor of Engineering Building #2* at Okayama University in Figure 4.4 (a). The channel of the first link is fixed at *CB channel 1+5*, and that of the second link is changed from *non-CB channel 1* to *non-CB channel 13*. For the throughput measurements, *Iperf* is adopted as a popular tool for measuring the TCP throughput by generating TCP packets [65].

7.2.1 Measurement Results and Discussion

First, we examine the throughput measurement results under interferences between two adjacent links. From the results of the individual links under interferences, it has been discovered that the individual throughput always fluctuates, like in Chapter 5 and in Chapter 6. Besides, the maximum throughput performance of one link on *CB* is different from that of *non-CB*. Thus, we will use the sum of the throughputs from the two links in our evaluations.

Figure 7.1 shows the total throughput of the two links for no interference case, one wall case between APs *(phD = two rooms)*, and *phD = 5m* case at different *chD*. In the experiments, the link distance (*lkD*) between a host and an AP is fixed at 0.5*m*.

For $chD = 4$ or smaller channel distances, the total throughput for the two links is similar among them, because the *non-CB* interference level from the *CB* link is not changed regardless of the channel distance. By shifting *non-CB* from channel 1 to 5, it is still fully overlapped with *CB* on *1+5*.

Then, from $chD = 5$ to $chD = 7$, the throughput slightly decreases due to increasing interferences from non-target APs in the environment, where most of them use *non-CB* channel 6. For *chD* = 8 or larger channel distances, the throughput increases due to less interferences. It becomes maximum at *chD* = 12 where no interference exists.

Figure 7.2 shows the changes of the total throughput drop of the two links for a different *chD*. Here, *lkD = 0.5m* is fixed, and *phD* is changed from 3*m* to larger ones to obtain the different RSS^i. The total throughput drop for the small *chD* and strong RSS^i is large while that of the large *chD* and weak RSS^i is small for less interference.

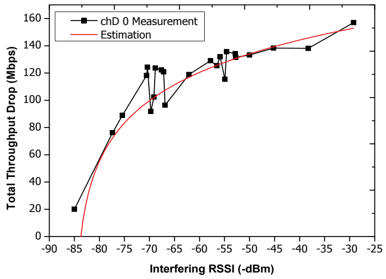

(a) *chD* = 0

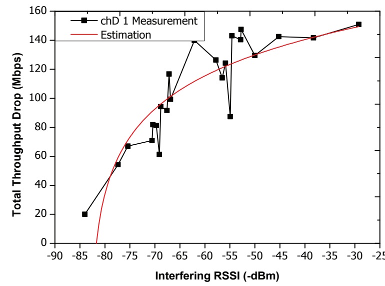

(b) *chD* = 1

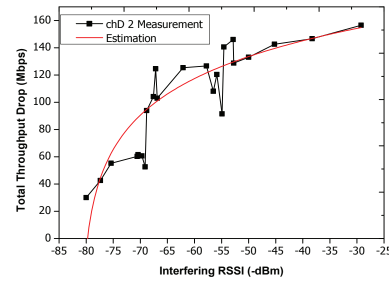

(c) *chD* = 2

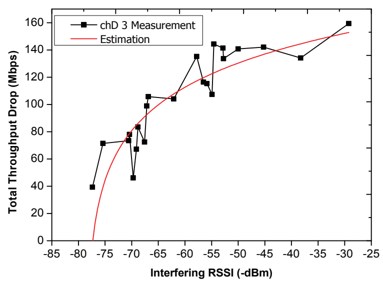

(d) *chD* = 3

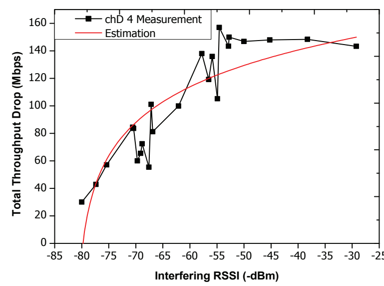

(e) *chD* = 4

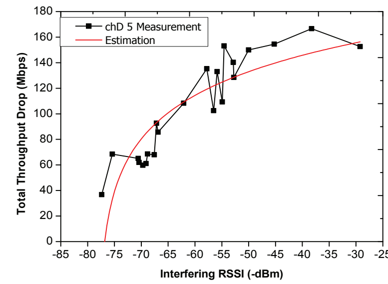

(f) *chD* = 5

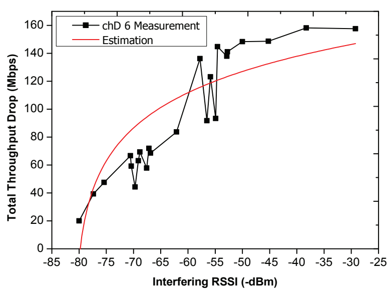

(g) *chD* = 6

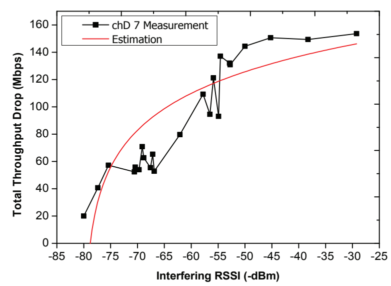

(h) *chD* = 7

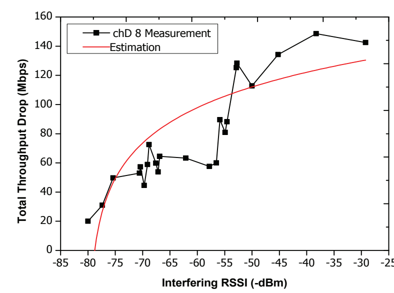

(i) *chD* = 8

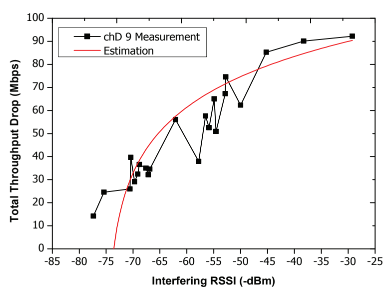

(j) *chD* = 9

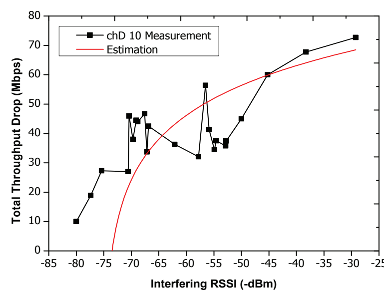

(k) *chD* = 10

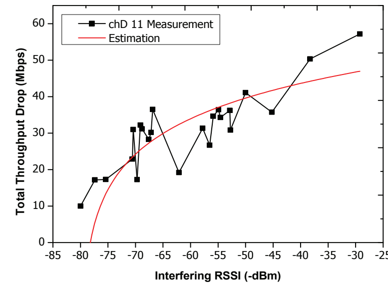

(l) *chD* = 11

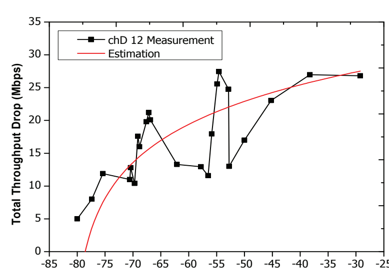

(m) *chD* = 12

Figure 7.2: Total throughput drop results for different interfered RSS at different *chD*.

7.3 Model under Interfered Links

Based on the throughput drop measurement results in Section 7.2, in this section, we present the *throughput drop estimation model under coexistence of channel bonding and non-channel bonding* by extending our works in Chapters 5 and 6.

7.3.1 Two Interfered Links

From the throughput drop measurement results in Figure 7.2, the *natural logarithm function* can be again used to estimate the *throughput drop (tpD)* from the interfering *received signal strength* (RSS^i) and the *channel distance (chD)*, as in Eq. (5.1). The parameters for the throughput drop estimation model are newly tuned under coexistence of *CB* and *non-CB* as in Table 7.1.

Table 7.1: Throughput drop estimation model parameters for coexistence of CB and non-CB.

channel distance	p	q	r
0	40.5	85.0	-10.0
1	40.0	83.0	-10.0
2	41.5	81.0	-9.0
3	41.0	78.5	-7.0
4	40.0	81.0	-8.0
5	42.0	79.0	-7.0
6	41.0	81.0	-7.0
7	39.0	80.0	-7.0
8	35.0	80.0	-7.0
9	26.0	75.0	-9.0
10	20.0	75.0	-8.0
11	14.0	80.0	-8.0
12	9.0	81.0	-8.0

For evaluating this model, the center frequency is used as the channel number for a CB channel. For $1+5$ CB channel, the channel number is 3. The parameters in Table 7.1 are obtained by shifting *non-CB* from channel 1 to channel 13. Hence, the largest is *chD* = 12.

The non-CB channel may take channel 1 to channel 13, while the CB channel may take channel 3 to channel 11. Therefore, for CB channel 3, *chD* = 2 appears when non-CB channel is 1 or 5. This is the least channel distance between the channels of the two links. Similarly, *chD* = 1 appears when non-CB channel is 2 or 4. In Figure 7.1, for *chD* = 4 or smaller channel distances, the total throughput for the two links is almost same since the channel of *non-CB* link fully overlaps with the CB link in Figure 2.7. Similarly, the parameter values for *chD* = 4 or smaller channel distances are similar. Therefore, when the non-CB channel is 5 or smaller, the throughput drop is estimated by taking the estimated average by parameters for *chD* = 0 to *chD* = 4. When the non-CB channel is 6 or larger, the estimation is done using parameters for *chD* = 5 or larger.

7.3.2 Multiple Interfered Links

Then, the throughput drop estimation model for multiple interfered links is considered. Again, the interfered links are explored sequentially in descending order of their throughput drops. It is noted that only two interfered links are described here.

1. When both of the interfering APs adopt *CB*, estimate the throughput drop under *CB* in Chapter 5.

2. When both of the interfering APs adopt *non-CB*, estimate the throughput drop under *non-CB* in Chapter 6.

3. When one AP adopts *CB* and another does *non-CB*, the following procedure is applied:

   (a) Estimate the single link throughput for each host by Eq. (3.2) and Eq. (3.3).

   (b) Estimate the sum of the throughput drops for the two APs by Eq. (5.1) using the parameters in Table 7.1.

   (c) Sort the links in descending order of the throughput drops that are given by tpD^{1st} and tpD^{2nd}.

   (d) For the largest interfered link, adjust tpD^{1st} with the maximum speed of the target AP by Eq. (7.1) and Eq. (7.2).

$$tpD^{1st}_{adj} = tpD^{1st} \times \beta \times \frac{tpM^{AP}}{140}. \tag{7.1}$$

$$tpD^{1st}_{adj} = tpD^{1st} \times \beta \times \frac{tpM^{AP}}{75}. \tag{7.2}$$

   Here, one AP represents the target AP and the other does the interfering AP. Eq. (7.1) is applied if the target AP uses *CB*, and Eq. (7.2) is applied otherwise. β represents the throughput drop normalization factor of *0.635* for *CB* and *0.365* for *non-CB*.

   (e) For the second interfered link, adjust the tpD^{2nd} by Eq. (7.3) and Eq. (7.4) for the target AP with CB channels and the AP with *non-CB* channels respectively.

$$tpD^{2nd}_{adj} = tpD^{2nd} \times \beta \times \frac{tpM^{AP} - tpD^{1st}_{adj}}{140}. \tag{7.3}$$

$$tpD^{2nd}_{adj} = tpD^{2nd} \times \beta \times \frac{tpM^{AP} - tpD^{1st}_{adj}}{75}. \tag{7.4}$$

   The dropped throughput under the interferences for the target link is obtained by sequentially subtracting tpD^{1st}_{adj} and tpD^{2nd}_{adj} from tp_{ij}, as in Eq. (5.4) and Eq. (5.6).

   (f) If more interfered links exist, repeat the same procedure.

7.4 Application of Transmission Power Optimization to Throughput Drop Estimation Model

In WLAN, the maximum transmission power at the APs is basically used to achieve higher throughputs. However, as demonstrated in [32], the minimum transmission power at the AP can provide the throughput similar to that of the maximum transmission power when the host is located near the AP, due to the non-linear relationship between *RSS* and the throughput. At the same time, the minimum transmission power can reduce interferences among the co-located APs. When the host is located far from the AP, the maximum transmission power at the AP is necessary to provide the sufficient RSS for the better throughput. Therefore, in the throughput drop estimation model, either the maximum or minimum transmission power should be selected properly to improve the throughput.

When the transmission power is changed, the P_1 value in Eq. (3.2) is changed while the other parameter values are fixed [95]. In the proposed model, the same Eq. (3.2) is applied to estimate both the *received signal strength (RSS)* at the host of the signal from the AP, and the *interfered received signal strength (RSS^i)* at the target AP from the interfering AP. In [32], either the *maximum* or *minimum* transmission power at the AP was selected since other powers do not cause significant throughput changes. Therefore, the proposed model adopts the P_1 values only for the maximum or minimum transmission power at CB and non-CB in Table 7.2.

Table 7.2: P_1 values for each transmission power.

channel width	transmission power	P_1
CB	maximum	-20.0
	minimum	-33.2
non-CB	maximum	-28.2
	minimum	-33.2

7.5 Evaluation of Model Estimation Accuracy

The accuracy of the proposed model is evaluated for the interfered links by comparing the estimated throughput results with the measured ones, when the AP is assigned either the maximum or minimum transmission power under *CB case*, *non-CB case*, and coexistence case of *CB* and *non-CB*. The same hardware and software in Table 4.1 are adopted with NEC AP device.

7.5.1 Results for Two Interfered Links

The two links in Figure 4.2 are prepared in the indoor field in Figure 4.4 (a). Figures 7.3, 7.4, and 7.5 illustrate the throughput measurement and estimation results for *CB case*, *non-CB case*, and coexistence case of *CB* and *non-CB* respectively, under different transmission power combinations.

For *CB case* in Figure 7.3, the channel of the first link is fixed at *CB channel 1+5*, and that of the second link is changed from *CB channel 1+5* to *CB channel 9+13*. In (a), the APs of the two links are assigned the maximum transmission power while in (b), the minimum power is assigned. In (c), one AP is assigned the maximum power while the other AP is the minimum power.

For *non-CB case* in Figure 7.4, the channel of the first link is fixed at *non-CB channel 1*, and that of the second link is changed from *non-CB channel 1* to *non-CB channel 7* where they do not interfere. Again, in (a), the APs of the two links are assigned the maximum transmission power while in (b), the minimum power is assigned. In (c), one AP is assigned the maximum power while the other AP is the minimum power.

For *coexistence of CB* and *non-CB case* in Figure 7.5, the channel of the first link is fixed at *CB channel 1+5*, and that of the second link is changed from *non-CB channel 1* to *non-CB channel 13*. The APs for both links are assigned the maximum transmission power in (a) while the minimum power is used in (b).

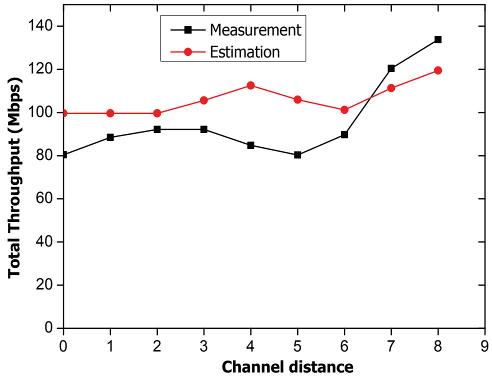

(a) CB links all max. power

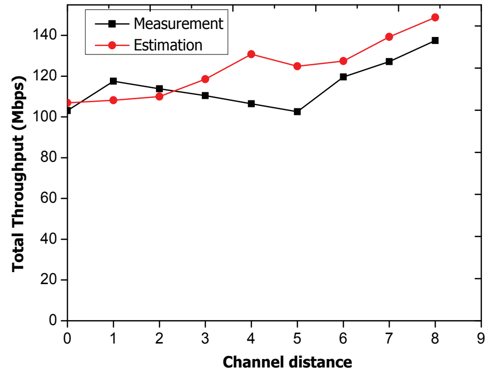

(b) CB links all min. power

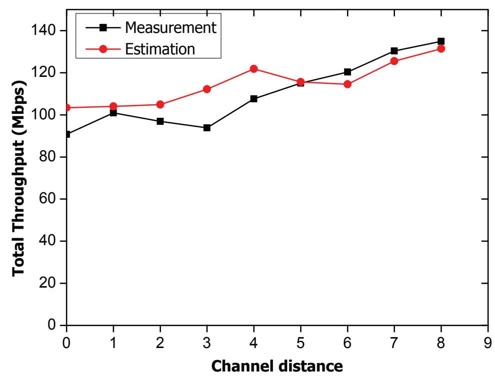

(c) CB links max. and min. power

Figure 7.3: Throughput measurement and estimation results for two links under all CB.

7.5.2 Results for Three Interfered Links

The indoor field in Figure 4.4 (a) is adopted. AP_1, AP_2 and AP_3 are located in rooms *D307*, *D306* and *refresh corner (D4)* respectively. Figure 7.6 illustrate the throughput measurement and estimation results for *CB case* and coexistence of *CB* and *non-CB case*. The *non-CB case* was not evaluated here since the three links would not interfere.

For *CB case* in Figure 7.6 (a), *CB channel 5+9* for AP_1, *CB channel 1+5* for AP_2, and *CB channel 9+13* for AP_3 are assigned. For *coexistence case of CB and non-CB* in Figure 7.6 (b), *CB channel 9+13* for AP_1, *non-CB channel 13* for AP_2, and *CB channel 1+5* for AP_3 are assigned. Then, for each of the two cases, the measured throughputs are compared with estimated ones when the three APs are assigned the maximum power, minimum power and two APs are assigned the minimum transmission power and the other AP is assigned the maximum transmission power.

The comparisons of the measured and estimated throughput results confirm the high accuracy of the proposed model under various channel and transmission power conditions for two or three interfered links. However, small gaps between the measured and estimated throughputs can appear due to interferences from non-target WLANs in the network field.

7.5.3 Evaluation for Different AP Device

To verify the generality of the proposed model, we evaluate the accuracy using different AP devices.

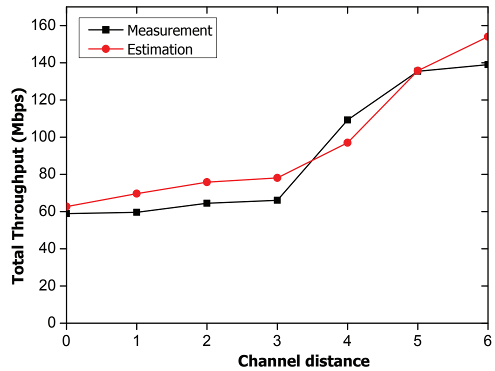

(a) non-CB links with all max. power

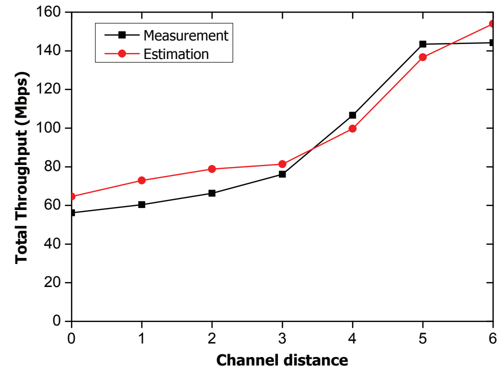

(b) non-CB links with all min. power

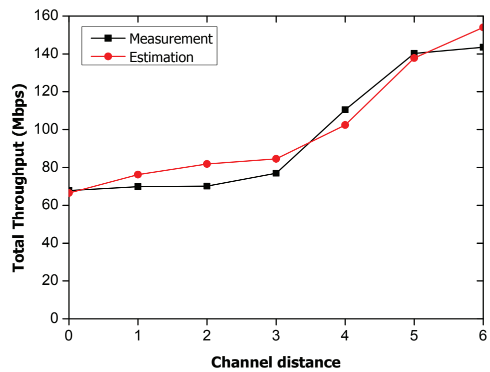

(c) non-CB links with max. and min. power

Figure 7.4: Throughput measurement and estimation results for two links under all non-CB.

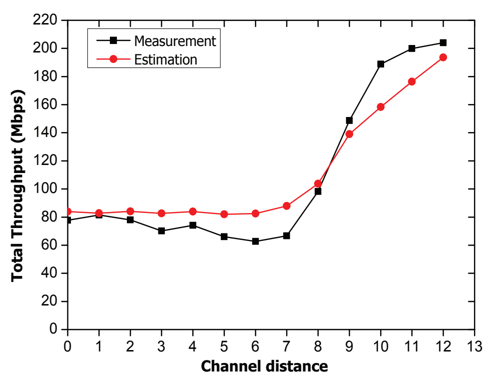

(a) Coexistence of CB and non-CB links with all max. power

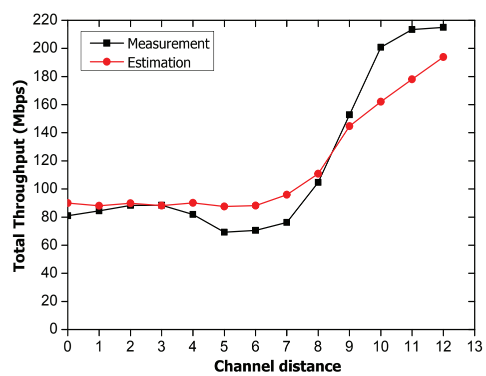

(b) Coexistence of CB and non-CB links with all min. power

Figure 7.5: Throughput measurement and estimation results for two links under coexistence of CB and non-CB.

7.5.3.1 Measurement Scenario

We adopt the *Raspberry Pi 3 Model B* for the APs. It uses Raspbian OS, Broadcom BCM2837, 1.2Ghz 64-bit quad-core ARM Cortex-A53 CPU, LPDDR2-900MHz 1GB SDRAM, 10/100Mbps Ethernet, IEEE802.11b/g/n wireless NIC, Blue-tooth 4.1 classics/low energy [82]. This device

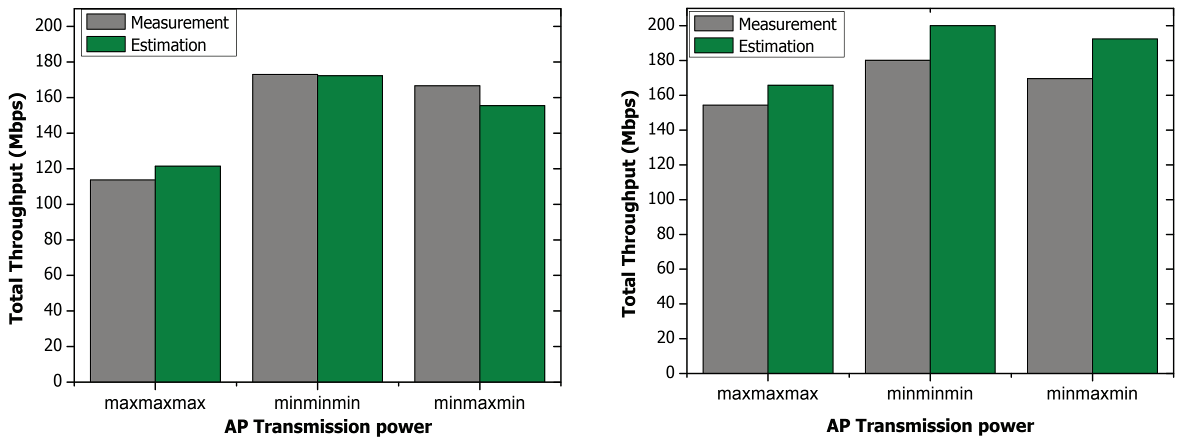

(a) All CB case

(b) Coexistence of CB and nonCB case

Figure 7.6: Throughput measurement and estimation results for three links under only CB and coexistence of CB and non-CB.

does not support *CB*, thus we use *TP-Link TL-WN722N USB NIC* adapter for CB [96].

In [15], it was demonstrated that the *Raspberry Pi 3 Model B* has the similar throughput drop characteristic to the *NEC AP* used in the proposed model. However, the maximum achievable throughput by *Raspberry Pi* AP is smaller than that by *NEC AP*, which is *40 Mbps* and *53 Mbps* for *non-CB* and *CB* respectively. Therefore, in the proposed model, the estimated values by the model are normalized using Eq. (7.5) as follows;

$$tpD_{pi} = tpD_{nec} \times \frac{tpM^{pi}}{tpM^{nec}} \tag{7.5}$$

where tpD_{nec} represent the throughput drop for *NEC AP*, tpM^{pi} and tpM^{nec} does the maximum throughput for *Raspberry Pi* and *NEC* APs respectively.

7.5.3.2 Results and Discussions

Again, the indoor field in Figure 4.4 (a) is used to evaluate the three interfered links under coexistence of CB and non-CB channels for different APs. The channel of each AP is fixed at *non-CB channel 1* for AP_1, *CB channel 9+13* for AP_2, and *CB channel 1+5* for AP_3. Figure 7.7 shows the measured and estimated throughput results for three scenarios.

- *Scenario 1:*
  AP_1 and AP_2 are located in room *D306* and AP_3 in the corridor in front of *D303*. The link distance of each host is *0.5m*. In this scenario, these APs interfere with each other, and the minimum power offers the higher total throughput.

- *Scenario 2:*
  AP_1 is located in room *D307*, AP_2 in *D306* and AP_3 in the corridor in front of *D303*. The link distance of each host is *0.5m*. In this scenario, the APs have less interferences than in *Scenario 1*. Hence, the minimum power offers the higher total throughput.

- *Scenario 3:*
  The locations of the APs is similar to *Scenario 2*. The link distance of the hosts is *0.5m*

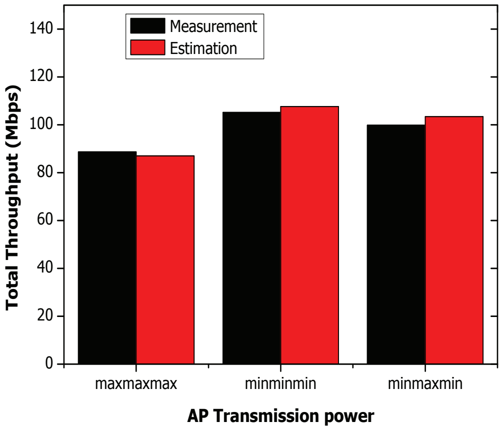

(a) Scenario 1

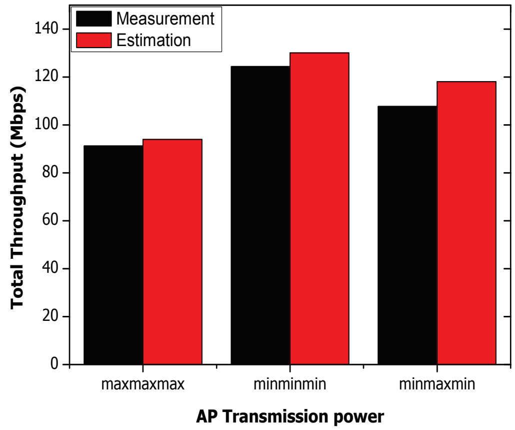

(b) Scenario 2

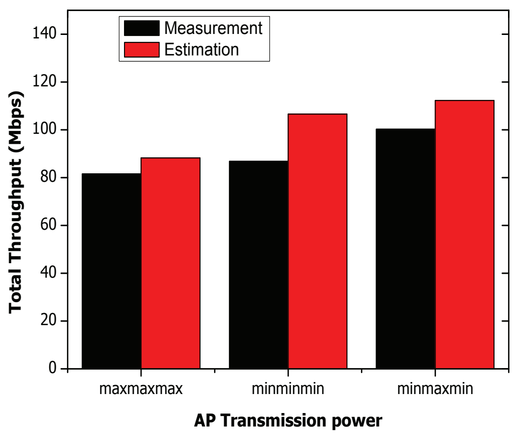

(c) Scenario 3

Figure 7.7: Throughput measurement and estimation results for Raspberry Pi AP.

except for the host connected to AP_2. It is moved to the corridor in front of *D4*. In this scenario, the minimum power to AP_1 and AP_3 and the maximum power to AP_2 offers the higher total throughput since the host connected to AP_2 is located far from it while other hosts are located near to their APs. Again, the estimated throughput is well matched with the measured ones for the three scenarios. Therefore, the proposed model can be used for various AP devices.

7.6 Summary

In this chapter, we proposed the throughput drop estimation model under coexistence of channel bonding and non-channel bonding. Firstly, we described throughput measurement results under coexistence of channel bonding and non-channel bonding. Secondly, we presented the throughput drop estimation model for interfered links. Thirdly, we discussed the application of the model to the transmission power optimization. Finally, we verified the model estimation accuracy. In the next chapter, we will present the model applications to joint optimizations of transmission power, frequency channel, and channel bonding.

Chapter 8

Applications to Joint Optimizations of Transmission Power, Frequency Channel, and Channel Bonding

In this chapter, we present the *application of the throughput drop estimation model to the joint optimization of the transmission power, the frequency channel, and the channel bonding* of each AP in WLAN. Firstly, we present the modification of the *active AP configuration algorithm* in [12]. Secondly, we present the algorithm procedure for the joint optimization using the model. Lastly, we evaluate the results through testbed experiments and simulations.

8.1 Introduction

In Chapter 7, we presented the throughput drop estimation model under coexistence of *CB* and *non-CB* links with different transmission powers at the AP. The accuracy of the model was verified through testbed experiments and simulations. However, it was not applied to joint optimization for WLAN. Therefore, in this chapter, we present the application of the model to the joint optimization of the transmission power, the frequency channel, and the channel bonding of each AP in WLAN.

8.2 Modifications of Active AP Configuration Algorithm

The channel assignment phase of the active AP configuration algorithm in [12] is modified to assign *CB* and *non-CB POCs* together with the proper transmission power to each AP using the proposed model in Chapter 7. Specifically, the modifications of this phase are described as follows.

8.2.1 Input and Output

In the algorithm input, the number of channels C_{CB} for *CB POC*s and C_{non} for *non-CB POC*s, and the center frequency of each channel are given.

In the algorithm output, either the *CB* or *non-CB POC* and either the *maximum* or *minimum* transmission power are assigned to each active AP. Conventionally, the *non-CB orthogonal channel (OC)* and the *maximum* transmission power are assigned to the active AP.

8.2.2 Objective

In the algorithm objective, the new cost function E_{ch} in Eq. (8.1) is designed to maximize the total throughput of the links in WLAN.

$$E_{ch} = \sum_{i=1}^{N} TP_i^{POC} \tag{8.1}$$

where TP_i^{POC} represents the total throughput of the links that are associated with AP_i and N is total number of APs.

TP_i^{POC} is calculated by:

$$TP_i^{poc} = \sum_{j}^{m} \left(tp_{ij}^{poc} \times Srf(m) \right) \tag{8.2}$$

where m represents the number of hosts associated with AP_i, tp_{ij}^{POC} does the estimated throughput of the link between AP_i and $host_j$ under interferences by the proposed model in Chapter 7, and $Srf(m)$ does the empirically derived contention factor at AP_i among the associated hosts to send data by the CSMA/CA protocol.

$Srf(m)$ is calculated by:

$$Srf(m) = \frac{4(11-m)}{41m-1}. \tag{8.3}$$

The constants in Eq. (8.3) are obtained from our extensive measurements by increasing the number of hosts associated to a single AP one by one under no interference. Figure 8.1 demonstrates a simple setup that was adopted. Table 8.1 compares the measured total throughput and the estimated one by Eq. (8.3).

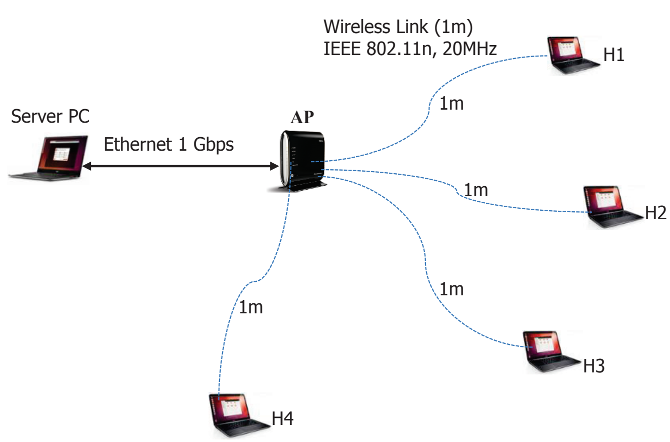

Figure 8.1: Measurement setup to demonstrate host contention at AP.

8.3 Procedure for Joint Optimization

Initially, only *CB* channels with the maximum transmission power are assigned by the greedy procedure, since they can maximize the throughput in general. Then, this assignment is improved

Table 8.1: Total throughput of single AP for increasing number of hosts.

No. of host(s)	Total measured throughput (Mbps)	Total estimated throughput (Mbps)
1	76.38	76.00
2	66.70	67.56
3	56.30	59.80
4	49.61	52.22

through *simulated annealing* by optimizing the selection of *CB* or *non-CB* and the maximum power or the minimum power by the following steps:

1. Randomly select one AP with the maximum transmission power for the change trial.
2. Randomly select a different CB channel from the current one to this selected AP.
3. Run the throughput estimation model. If the estimated throughput improves E_{ch} in Eq. (8.1), this channel change is accepted. To avoid the local optimum, the hill-climbing procedure is applied. If 0-1 random number is smaller than $exp(\Delta E_{ch}/Temp)$, this channel change is accepted. ΔE_{ch} represents the difference between the old E_{ch} and the new E_{ch} and $Temp$ is given as the algorithm parameter of the temperature.
4. Go back to step 1, when the new channel is accepted. Otherwise, go to the next step.
5. Change the transmission power to the minimum and run step 3.
6. Go back to step 1, when the new power is accepted. Otherwise, go to the next step.
7. Change the selected channel to *non-CB* and run step 3.
8. Go back to step 1, when the new non-CB is accepted. Otherwise, go to the next step.
9. Change the transmission power to the maximum and run step 3.
10. Go back to step 1.

8.4 Evaluations

To evaluate the joint optimization algorithm using the throughput drop estimation model, we conduct simulations, and compare the estimated results with test-bed measurement results in several network topologies. In each topology, the total throughput by the proposal is compared with the results by two conventional approaches in literature, *1) CB only*, and *2) non-CB only*. For each of the two conventional approaches, the results for both the *maximum* and *minimum* transmission power are presented.

8.4.1 Evaluation Scenario

The indoor fields in Figure 4.4 are adopted for evaluations. The devices and software in Table 4.1 are used. Table 8.2 shows the locations of the APs and the hosts in the fields for each topology.

Table 8.2: Device Locations

Network field	Topology	Device locations		
		AP1, Host1	AP2, Host2	AP3, Host3
Eng. Bldg. #2 in Figure 4.4 (a)	1	D306	D306	D306
	2	D307	D307	D307, D306
	3	D306	D306	corr. near D303
	4	D308	corr. near D301	refresh corner (D4)
Grad. Sch. Bldg. in Figure 4.4 (b)	1	H	H	H
	2	open space	A	B

8.4.2 Results for Engineering Building

Figures 8.2 to 8.5 show the total throughput results by measurements and simulations. Each figure compares the total throughput by the proposal with the ones by *CB only* and *non-CB only* with the maximum and minimum transmission powers as conventional approaches.

In Figures 8.2 and 8.3, the three APs are located in the same room and are interfered with each other. To reduce the interference, the proposal assigns the three *non-CB channel* 1, 7, and 13, and the minimum transmission power to the APs in Figure 8.2. In Figure 8.3, AP_1 and AP_2 are assigned the minimum power because they are located in the same room, while AP_3 is assigned the maximum power because the associated host exists in the different room.

In Figure 8.4, AP_1 and AP_2 are located in the same room, and AP_3 is located far from them. Due to less interferences, the proposal assigns *joint non-CB channel* 13, and *CB channel* $1 + 5$ and $9 + 13$ to AP_1, AP_2, and AP_3 respectively. The minimum transmission power is assigned to all the APs because they are located in the same room as the associated hosts.

In Figure 8.5, the three APs are located far from each other. Thus, there is few interference between them. The proposal assigns *CB channel* $1 + 5$, $9 + 13$, and $5 + 9$ to AP_1, AP_2, and AP_3 respectively. The transmission power becomes minimum because they are located in the same room as the associated hosts.

The model simulation results and the testbed measurement results are similar to each other. The results by the proposal are better than those by the comparison methods, or at least similar where the proposal assigns the same channel and transmission power as the comparison methods. These results confirm the effectiveness of the proposal.

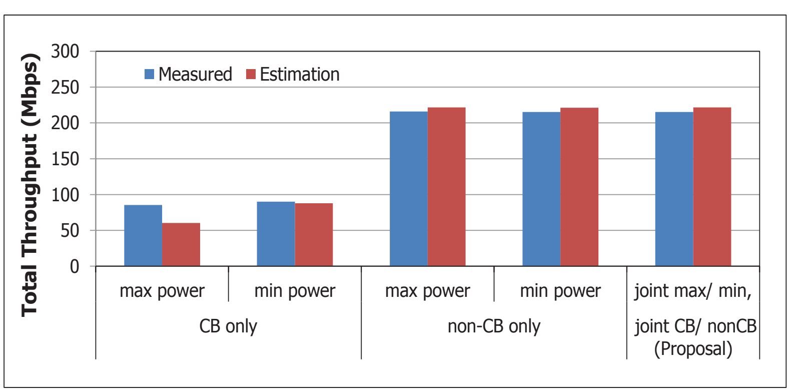

Figure 8.2: Results for topology 1 in Engineering Building.

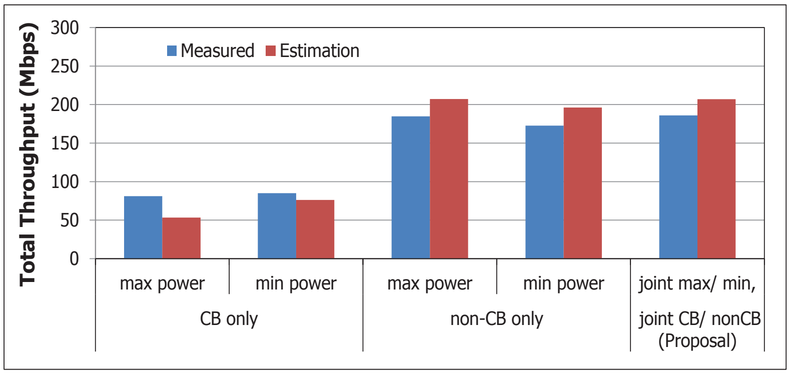

Figure 8.3: Results for topology 2 in Engineering Building.

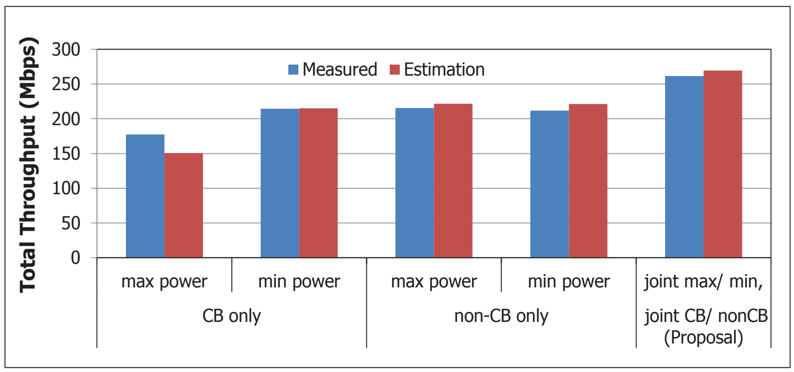

Figure 8.4: Results for topology 3 in Engineering Building.

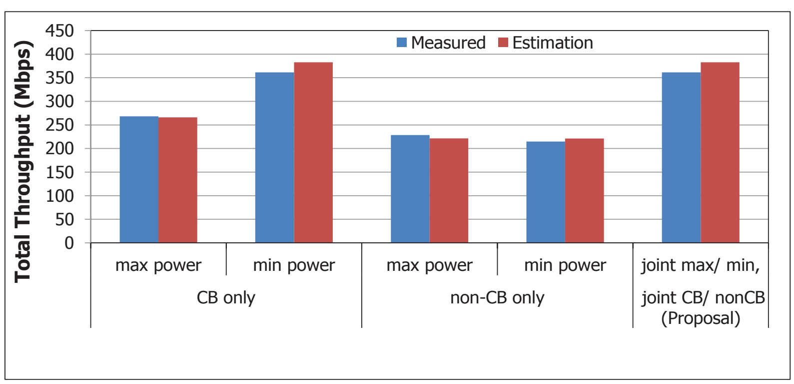

Figure 8.5: Results for topology 4 in Engineering Building.

8.4.3 Results for Graduate School Building

Figures 8.6 and 8.7 show the total throughput results in testbed measurements and model simulations. In Figure 8.6, the three APs are located in the same room. To reduce interferences, the proposal assigns the *non-CB channels* 1, 7, and 13 and the minimum transmission power to AP_1, AP_2, and AP_3 respectively.

In Figure 8.7, the three APs are located relatively far from each other. Due to less interferences, the proposal assigns *CB channel* 9 + 13, 1 + 5, and *non-CB channel* 13 and the minimum transmission power to AP_1, AP_2, and AP_3 respectively. The proposal gives the better performance than the comparison methods.

The model simulation results and the measurement results are similar to each other in them. The results by the proposal are better or at least similar to the results by the comparison methods. These results confirm the effectiveness of the proposal in different network fields.

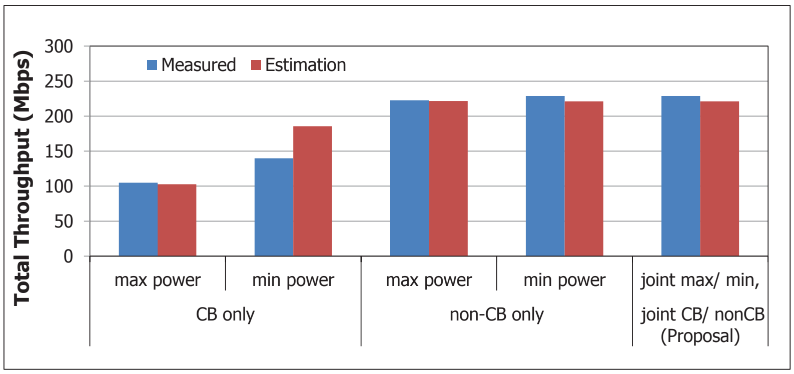

Figure 8.6: Results for topology 1 in Graduate School Building.

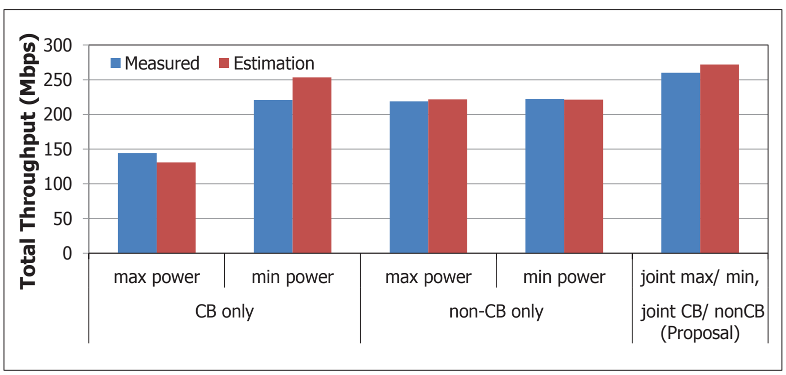

Figure 8.7: Results for topology 2 in Graduate School Building.

8.5 Summary

In this chapter, we presented the application of the throughput drop estimation model to the joint optimization of the transmission power, the frequency channel, and the channel bonding of the AP in the wireless local area network. Firstly, we modified the channel assignment extension of the active AP configuration algorithm in [12]. Secondly, we presented the algorithm procedure. Lastly, we evaluated the optimization results through the testbed experiments and the model simulations. In the next chapter, we will present related works to this thesis in literature.

Chapter 9

Related Works in Literature

In this chapter, we survey works in literature related to this study. A significant amount of research works has addressed the problem of interferences in WLAN to enhance the throughput performance through the channel assignment with and without POCs.

Some works have studied the conventional orthogonal channels with non-channel bonding while others use channel bonding. Besides, most of the works adopt the conventional maximum transmission power, while a few works have tried the power tuning to enhance the throughput. Unfortunately, most of them have several limitations in the adopted interference models. Within our survey, no works have reported the simultaneous optimization of the transmission power, the frequency channel, and the channel bonding of the AP in WLAN.

In [11], Mishra et al. reveals that the *orthogonal channel (OC)* assignment to APs in WLAN is inefficient in a network field, if a substantial number of APs are deployed there. In this case, any AP could exist in the interference ranges of many other APs, because the number of OCs is small compared to the number of APs in the network as suggested in [97]. The advantages of WLAN such as flexibility, low cost and high data transmission capacity has increased not only the number of allocated APs in the network fields, but also the interferences since frequency channels must be shared among multiple APs.

In [10, 18, 19, 98], Zhou et al., Mishra et al., Feng et al., and Zhang et al. demonstrated that the careful design of the POC allocation to APs in WLAN can improve the performance with the efficient spatial reuse. In [99], Zhao et al. observed that as the spatial reuse increases, the capacity of WLAN can be scaled up with additional APs in the network field, where the expected distance from a user to the associated AP becomes shorter. This results in the higher data transmission speed. Using examples, in [20], Mukherjee and Ghosh supports this claim by showing that proper assignment of POCs improves throughput while inappropriate assignment can decrease throughput due to increased interference.

Likewise, in [17], Bokhari and Záruba shows that POCs can make the whole wireless spectrum available to APs for the channel assignment. Thus, using POCs, more APs can be configured to allow multiple concurrent transmissions among adjacent APs. This increases the overall network throughput via the efficient spectrum utilization. Therefore, the proper assignment of POCs to APs in WLAN can maximize the capacity to handle the traffic loads generated by APs and hosts in the network.

In [92], Zhao et al. showed that the effect of interferences on the network performance depends on the channel separation and the degree of the frequency overlapping among the interfered links. In particular, the simultaneous interferences from two links will bring about the higher performance deterioration than the single interference, but the smaller deterioration than the summation of the individual ones. Similarly, in [93], Su et al. observed that for multiple interfering APs, the throughput drop by the accumulated interferences from two interferers is greater than that from a single interferer, but less than the summation of the drops from the individual interferences. When the target AP is interfered by the first interferer, its rate adaptation mechanism lowers the transmission rate by adopting the more robust modulation code. Therefore, the second interferer can cause the smaller drop than the first one.

In [20,99], Mukherjee et al. and Zhao et al. considered the sum of the interfering signal powers at the target node, when more than one APs are interfered. Since the MAC protocol lowers the data transmission rate of the target AP, depending on the level of the individual interference, the simple summation of the individual interferences may fail to identify the real value for the interference. In this thesis, the individual interference was examined sequentially from the highest to the smallest.

In [100], Vanhatupa et al. presented the *graph coloring approach (GCA)* to acquire solutions for the channel assignment. A feasible solution only occurs when available channels can provide a *colored graph*. Where a *colored graph* is not possible, this GCA has no qualitative ordering of possible solutions. On the other hand, our proposed models considers all the *POC*s and evaluates the performance of each channel based on interferences from other channels.

In [11], Mishra et al. presented studies for the weighted GCA under *conventional non-CB 20MHz channels*, where each weight represents the *signal to the noise ratio (SINR)*. Here, the maximization of SINR is the objective function. However in real WLANs, the throughput may not be linearly dependent on SINR. Thus, the throughput should be used as the optimization parameter as in this thesis.

In [101], Elwekeil et al. reported a simulation based study on the channel assignment problem, where the objective is defined to minimize the maximum interference at an AP. The model in [102] was adopted to estimate the interference from the channel overlapping, where it assumes that the interference linearly decreases as the channel separation distance increases. Nevertheless, our experiment results show that the interference does not decrease linearly to the channel separation distance.

In [103], Kandasamy et al. studied the relationship between the interference metric and the throughput to quantify the effect of the interference on the WLAN performance. In their study, the *logarithm function* is adopted to estimate the throughput. They show that the estimated values by the logarithm function fits well with the experiment results.

In [104, 105], Yoon et al. and Kumar et al. investigated the effects of the cross technology interference between IEEE 802.11 for Wi-Fi and IEEE 802.15.4 for ZigBee. The relationship between the Wi-Fi packet error rate and the interfering RSS follows the *logarithmic* curve. They claimed that the *logarithm function* can be applied to model WLAN performance metrics such as the achievable throughput, the SINR, and the bit error rate.

In [106], Nabil et al. presented a mathematical approach to optimally use *CB* to meet the stochastic user demands. In their work, the number of bonded channels can be increased or decreased depending on the throughput demand of each AP. However, it does not present a model to estimate the throughput demands of APs. It is assumed that one *non-CB* channel can satisfy one unit of the AP demand.

In [107], Tewari and Ghosh proposed a joint approach for the power tuning and the POC assignment. In their proposal, the APs in the network field are activated one by one, and transmission power is initially set to maximum. Then, POCs under conventional *20 MHz non-CB* are assigned, and transmission power is reduced considering neighbor interfered APs while ensuring that each AP serves the largest number of hosts and satisfies the minimum host throughput threshold. They also proposed the AP placement through the power control and the POC assignment in [108]. Here, the similar approach in [107] is adopted, where the appropriate location of every AP is also considered to reduce interference while maximizing the number of hosts served. Their works adopt the conventional *non-CB* channels and is evaluated only through simulation.

In [109], Kachroo et al. proposed a joint channel assignment and transmission power control algorithm for a multi-rate WLAN where the conventional 20 MHz *non-CB* POC channels are used. Initially, the algorithm assigns the channels to the APs while keeping the transmission power constant. Then, it optimizes the transmission power such that the *signal to interference plus noise ratio (SINR)* is maximized and the coverage area threshold is maintained for every AP. Their proposal was evaluated only through simulation.

In [87–89], Newport et al., Padhye et al., and Reis et al. suggests that most explorations of protocols with respect to interferences use simple abstract models with multiple assumptions. They indicate that the signal propagation is given by a simple function of the distance, the radio coverage area forms a circle, and the interference range is twice of the transmission range. Unfortunately, experimental data using a real WLAN have shown that all of these models appear to be largely inaccurate. For the proper channel assignment, the precise model to estimate the throughput performance under interferences is essential. Hence, the model should be refined to deal with POCs properly.

Chapter 10

Conclusion

In this thesis, we presented our studies of *throughput drop estimation models* under interfered concurrently communicating links and their applications to joint optimizations of the transmission power, the frequency channel, and the channel bonding of access points (APs) in wireless local-area networks (WLANs).

Firstly, we adopted the *partially overlapping channels (POCs)* instead of the conventional *orthogonal channels (OCs)*. Through experiments, we showed that proper allocation of POCs to *access points (APs)* can improve the throughput performance compared to OCs, by fully utilizing the available spectrum.

Secondly, we proposed the *throughput drop estimation model* for concurrently communicating links under *channel bonding (CB)*. The CB channels can provide high throughputs due to the wide channel width in general, where two adjacent channels are used together as one channel. We verified the accuracy of the model under CB and its effectiveness to the CB assignment to the APs through simulations and experiments where estimated throughputs and measured ones under various conditions match well.

Thirdly, we extended the throughput drop estimation model under CB links to *non-channel bonding (non-CB)* links. Through experiments, we observed that non-CB links provide higher throughputs than CB when several APs are co-located together, because the CB can reduce the transmission capacity due to high interferences. Again, we verified the model accuracy through experiments and simulation where measured throughput and estimated ones match well. The effectiveness of the model to the non-CB assignment was confirmed through simulations and experiments, where the POC assignment outperforms the OC assignment.

Fourthly, by extending the two models under *CB* and *non-CB* links, we proposed the throughput drop estimation model under *coexistences of CB and non-CB* links with different AP transmission powers. This model exploits the advantages of CB, non-CB, and power tuning together to increase the throughput under interferences. In evaluations, the measured throughput and estimated ones by the model match well, and it performs better than *CB only* and *non-CB only*, or at least similar depending on topology.

Lastly, we proposed the *application of the model under coexistences of CB and non-CB* links to the joint assignment optimization of transmission power, frequency channel, and channel bonding. In evaluation, we confirmed that the proposal assigns the proper transmission power and channels for high throughputs.

In future studies, we will study further enhancements of throughput drop estimation models by considering non-controlled APs in the network field, and the joint frequency and channel assignment for 2.4 GHz and 5GHz using the models. Then, we will evaluate them in various network fields and topologies.

Bibliography

[1] M. S. Gast, "802.11 wireless networks - the definitive guide," 2nd ed., O 'Reilly, Sebastopol, Apr. 2005.

[2] B. P. Crow, I. Widjaja, J. G. Kim, and P. T. Sakai, "IEEE 802.11 wireless local area networks," IEEE Commun. Mag., vol. 35, no. 9, pp. 116-126, Sept. 1997.

[3] M. Balazinska and P. Castro, "Characterizing mobility and network usage in a corporate wireless local-area network," in Proc. Int. Conf. Mobile Syst. Appl. Serv. pp. 303-316, 2003.

[4] "Supplement to IEEE standard for information technology telecommunications and information exchange between systems - local and metropolitan area networks - specific requirements. Part 11: wireless LAN medium access control (MAC) and physical layer (PHY) specifications: high-speed physical layer in the 5 GHz band," IEEE STD 802.11a-1999, 1999.

[5] "IEEE Std 802.11-2012, IEEE standard for information technology- telecommunications and information exchange between systems local and metropolitan area network - specific requirements - Part 11: wireless LAN medium access control (MAC) and physical layer (PHY) specifications," IEEE STD 802.11-2007, pp. 1184, 2007.

[6] J. Talvitie, M. Renfors, and E. S. Lohan, "A comparison of received signal strength statistics between 2.4 GHz and 5 GHz bands for WLAN-based indoor positioning," in Proc. IEEE Globecom Work., pp. 1-6, 2015.

[7] L. Deeky, E. Garcia-Villegas, E. Belding, S.-J. Lee, and K. Almeroth, "Intelligent channel bonding in 802.11n WLANs," IEEE Trans. Mob. Comput., vol. 13, no. 6, pp. 1242-1255, 2014.

[8] T.-D. Chiueh, P.-Y. Tsai, and I.-W. Lai, "Baseband receiver design for wireless MIMO-OFDM communications," 2nd ed. Wiley-IEEE Press., 2012.

[9] M. S. Gast, "802.11n: a survival guide," 1st ed., O 'Reilly, 2012.

[10] K. Zhou, X. Jia, Y. Chang, and X. Tang, "Partially overlapping channel assignment for WLANs using SINR interference model," Int. J. Comm. Syst, vol. 27, no. 11, pp. 3082-3095, March 2014.

[11] A. Mishra, E. Rozner, S. Banerjee, and W. Arbaugh, "Exploiting partially overlapping channels in wireless networks: turning a peril into an advantage," in Proc. ACM Conf. Inter. Meas., pp. 311-316, 2005.

[12] M. S. A. Mamun, N. Funabiki, K. S. Lwin, M. E. Islam, and W.-C. Kao, “A channel assignment extension of active access-point configuration algorithm for elastic WLAN system and its implementation using Raspberry Pi,” Int. J. Netw. Comput., vol. 7, no. 2, pp. 248-270, July 2017.

[13] M. S. A. Mamun, M. E. Islam, N. Funabiki, M. Kuribayashi, and I.-W. Lai, “An active access-point configuration algorithm for elastic wireless local-area network system using heterogeneous devices,” Int. J. Netw. Comput., vol. 6, no. 2, pp. 395-419, July 2016.

[14] I. M. Kwenga, N. Funabiki, M. M. Islam, M. Kuribayashi, R. W. Sudibyo, and W. -C. Kao, “A throughput estimation model under two-link concurrent communications with partially overlapping channels and its application to channel assignment in IEEE 802.11n WLAN,” Int. J. Space-Base. Situ. Comp., vol. 8, no. 3, pp. 123-137, 2018.

[15] K. I. Munene, N. Funabiki, H. Briantoro, M. M. Rahman, F. Akhter, M. Kuribayashi, and W. -C. Kao, “A throughput drop estimation model for concurrent communications under partially overlapping channels without channel bonding and its application to channel assignment in IEEE 802.11n WLAN,” IEICE Trans. Inform. Syst., vol. E104-D, no. 5, pp. 585-596, May, 2021.

[16] K. I. Munene, N. Funabiki, H. Briantoro, M. M. Rahman, S. C. Roy, and M. Kuribayashi, “A study of throughput drop estimation model for concurrently communicating links under coexistence of channel bonding and non-bonding in IEEE 802.11n WLAN,” in Proc. Int. Work. Virt. Env. Netw.-Ori. Appl., pp. 700-714, July, 2021.

[17] S. Bokhari and V. Záruba, “i-POCA: interference-aware partially overlapping channel assignment in 802.11-based meshes,” in Proc. IEEE WoWMoM, 2013.

[18] A. Mishra, V. Shrivastava, S. Banerjee, and W. Arbaugh, “Partially overlapped channels not considered harmful,” in Proc. Joint Int. Conf. Meas. Model. Comp. Sys., pp. 63-74, 2006.

[19] Z. Feng and Y. Yang, “How much improvement can we get from partially overlapped channels?,” in Proc. IEEE WCNC, pp. 2957-2962, April 2008.

[20] S. Mukherjee and S. C. Ghosh, “Throughput improvement using partially overlapping channels in WLAN with heterogeneous clients,” Wired/Wireless Inter. Comm., pp. 335-347, 2016.

[21] K. S. Lwin, N. Funabiki, C. Taniguchi, K. K. Zaw, M. S. A. Mamun, M. Kuribayashi, and W.-C. Kao, “A minimax approach for access point setup optimization in IEEE 802.11n wireless networks,” Int. J. Netw. Comput., vol. 7, no. 2, pp. 187-207, July 2017.

[22] K. I. Munene, N. Funabiki, M. M. Islam, M. Kuribayashi, M. S. A. Mamun, R. W. Sudibyo, and W.-C. Kao, “An extension of throughput drop estimation model for three-link concurrent communications under partially overlapping channels and channel bonding in IEEE 802.11n WLAN,” Adv. Sci. Technol. Eng. Syst. J., vol. 4, no. 4, pp. 94-105, 2019.

[23] K. I. Munene, N. Funabiki, R. W. Sudibyo and W. -C. Kao, “A throughput drop estimation model for two-link concurrent communications with partially overlapping channels in IEEE 802.11n WLAN,” in Proc. IEEE GCCE, pp. 809-810, 2018.

[24] “IEEE 802.11n - standard for wireless LAN medium access control (MAC) and physical layer (PHY): enhancements for high throughput,” IEEE, Oct. 2009.

[25] National Instrument: “Introduction to wireless LAN measurements from 802.11a to 802.11ac.,” 2018.

[26] N. Funabiki ed., “Wireless mesh networks,” InTech-Open Access Pub., Jan. 2011, Internet `http://www.intechopen.com/books/wireless-mesh-networks`.

[27] K. I. Munene, N. Funabiki, R. W. Sudibyo, H. Briantoro, M. M. Rahman, and W. -C. Kao, “A study of throughput-drop estimation model for concurrently communicating two links without channel bonding in IEEE 802.11n wireless local-area network,” in Proc. IEEE ICCE-TW, pp. 1-2, Sept. 2020.

[28] K. I. Munene, N. Funabiki, H. Briantoro, M. M. Rahman, F. Akhter, and M. Kuribayashi, “Application of throughput drop estimation model under partially overlapping channels to channel assignment in IEEE 802.11n WLAN,” in Proc. ICETC, B3-2, Dec. 2020.

[29] S. Barrachina-Muñoz, F. Wilhelmi, and B. Bellalta, “To overlap or not to overlap: enabling channel bonding in high-density WLANs,” Comp. Netw., vol. 152, pp. 40-53, 2019.

[30] K. I. Munene, N. Funabiki, M. M. Rahman, H. Briantoro, S. C. Roy, and M. Kuribayashi, “A throughput drop estimation model and its application to joint optimization of transmission power, frequency channel, and channel bonding in IEEE 802.11n WLAN for large-scale IoT environments,” submitted to Internet of Things; Engineering Cyber Physical Human Systems, Elsevier, 2021.

[31] H. Briantoro, N. Funabiki, M. M. Islam, R. W. Sudibyo, K. I. Munene, and M. Kuribayashi, “An investigation of transmission power optimization for performance improvement at concurrent communications of multiple access-points in wireless local-area network,” in Proc. IEICE General Conf., BS-4-30, pp. S66-S67, March 2019.

[32] H. Briantoro, N. Funabiki, M. M. Rahman, K. I. Munene, and M. Kuribayashi, “Joint optimization method of channel assignment and transmission power for concurrently communicating multiple access-points in wireless local-area network,” Int. J. Netw. Comp., vol 11, no. 2, pp. 251-266, July 2021.

[33] S. Banerji and R. S. Chowdhury, “On IEEE 802.11: wireless LAN technology,” Int. J. Mobi. Net. Commun. & Telematics, vol. 3, no. 4, Aug. 2013.

[34] S. Banerji, “Upcoming standards in wireless local area networks,” Wireless & Mobile Technol., vol. 1, no. 1, Sept. 2013.

[35] I. Poole, “IEEE 802.11 Wi-Fi standards,” Internet: `http://www.radio-electronics.com/info/wireless/wi-fi/ieee-802-11-standards-tutorial.php`, Access Jan. 20, 2019.

[36] V. Beal, “What is 802.11 wireless LAN standards?,” Internet: `http://www.webopedia.com/TERM/8/802_11.html`, Access Jan. 20, 2019.

[37] C. C. Choon, "A study of active access-point selection algorithm for wireless mesh network under practical conditions," Ph.D. thesis, Grad. Sch. Natural Sci. Technol., Okayama Univ., Japan, Sept. 2015.

[38] "IEEE 802.11 - Wikipedia," Internet: `http://en.wikipedia.org/wiki/IEEE_802.11`, Access Jan. 20, 2019.

[39] M. E. Islam, "A study of access-point aggregation algorithm for elastic wireless local-area network system and its implementation," Ph.D. thesis, Grad. School of Natural Science and Technology, Okayama Univ., Japan, March 2016.

[40] S. Sendra, M. Garcia, C. Turro, and J. Loret, "WLAN IEEE 802.11 a/b/g/n indoor coverage and interference performance study," Int. J. Adv. Netw. Service., vol. 4, no. 1, pp. 209-222, 2011.

[41] M. M Islam "A study of dynamic access-point configuration and power minimization in elastic wireless local-area network system," Ph.D. thesis, Grad. Sch. Natural Sci. Tech., Okayama Univ., Japan, Sept. 2019.

[42] P. Likhar, R. S. Yadav and K. M. Rao, "Securing IEEE 802.11g WLAN using open VPN and its impact analysis," Int. J. of Netw. Security and Its Applications (IJNSA), Vol. 3, no. 6, pp. 97-113, Nov. 2011

[43] A. S. Tanenbaum, and D. J. Wetherall, "Computer networks," 5th ed., Pearson Prentice Hall, 2011.

[44] J. H. Yeh, J. C. Chen, and C. C. Lee, "WLAN standards," IEEE Potentials, vol. 22, no. 4, 2003.

[45] O. Bejarano, E. W. Knightly, and M. Park, "IEEE 802.11ac: from channelization to multi-user MIMO," IEEE Comm. Mag., vol. 51, no. 10, pp. 84-90, Oct. 2013.

[46] L. Verma, M. Fakharzadeh, and S. Choi, "Wifi on steroids: 802.11ac and 802.11ad," IEEE Trans. Wireless Comm., vol. 20, no. 6, pp. 30-35, Dec. 2013.

[47] M. S. Gast, "802.11ac: a survival guide," O'Reilly Media, Inc., 2013.

[48] B. Bellalta, "IEEE 802.11 ax: High-efficiency WLANs," IEEE Wirel. Commu. vol. 23, no. 1, pp. 38-46, 2016.

[49] E. Khorov, A. Kiryanov, A. Lyakhov and G. Bianchi, "A Tutorial on IEEE 802.11ax High Efficiency WLANs," IEEE Communications Surveys & Tutorials, vol. 21, no. 1, pp. 197-216, 2019.

[50] IEEE, "IEEE SA Standards Board Approvals," Internet: `https://standards.ieee.org/about/sasb/sba/feb2021.html.` Accessed 25 May, 2021.

[51] IEEE, "IEEE 802.11ax-2021 - IEEE Standard for Information Technology," Internet: `https://standards.ieee.org/standard/802_11ax-2021.html.` Accessed 25 May, 2021.

[52] H. Briantoro, "A study of transmission power optimization with channel assignment consideration for access-points in wireless local-area network," Ph.D. thesis, Grad. Sch. Natural Sci. Tech., Okayama Univ., Japan, Sept. 2021.

[53] "WiMAX page, IEEE802.11ac works," Internet: http://123-info.net/wimax-page/archives/918, Access Jan. 20, 2019.

[54] L. Deek, E. Garcia-Villegas, E. Belding, S. J. Lee, and K. Almeroth, "The impact of channel bonding on 802.11n network management," in Proc. Conf. Emer. Netw. Exp. Tech. (CoNEXT), Dec. 2011.

[55] K. I. Munene, "A study of throughput estimation model and channel assignment under partially overlapping channels in IEEE 802.11n wireless local-area network," Master thesis, Grad. Sch. Natural Sci. Tech., Okayama Univ., Japan, March. 2019.

[56] A. Saif, M. Othman, "A reliable A-MSDU frame aggregation scheme in 802.11n wireless networks," in Proc. Comp. Scie., vol. 21, 2013.

[57] "IEEE 802.11n-2009 - Wikipedia," Internet: http://en.wikipedia.org/wiki/IEEE_802.11n-2009, Accessed 12 Nov. 2021.

[58] M. Vipin, and S. Srikanth, "Analysis of open source drivers for IEEE 802.11 WLANs," in Proc. Int. Conf. Wireless Comm. Sens. Comput. (ICWCSC), pp. 1-5, IEEE, Jan. 2010.

[59] J. Malinen, "hostapd: IEEE 802.11 AP, IEEE 802.1 X. WPA/WPA2/EAP/RADIUS authenticator," Internet: https://w1.fi/hostapd/, Access 12 Nov. 2021.

[60] D. J. Barrett, R. E. Silverman, and R. G. Byrnes, "SSH, the secure shell: the definitive guide," O'Reilly Media Inc., 2005.

[61] T. Ylonen and C. Lonvick, "The secure shell (SSH) protocol architecture," 2006.

[62] "OpenSSH," Internet: http://www.openssh.com/, Access Jan. 20, 2019.

[63] O. Terpollari, "How to install and configure OpenSSH server in Linux," Internet: http://www.tecmint.com/install-openssh-server-in-linux/, Access Jan. 20, 2019.

[64] "Running commands on a remote Linux server over SSH," Internet: http://www.shellhacks.com/en/Running-Commands-on-a-Remote-Linux-Server-over-SSH, Access Jan. 20, 2019.

[65] "iPerf - The TCP, UDP and SCTP network bandwidth measurement tool," Internet: https://iperf.fr/, Accessed 20 May 2021.

[66] D. B. Faria, "Modeling signal attenuation in IEEE 802.11 wireless LANs," Tech. Report, TR-KP06-0118, Stanford Univ., July 2005.

[67] N. Funabiki, C. Taniguchi, K. S. Lwin, K. K. Zaw, and W.-C. Kao, "A parameter optimization tool and its application to throughput estimation model for wireless LAN,"in Proc. Int. Work. Virtual Environ. Netw.-Orient. Appli. (VENOA), pp. 701-710, July 2017.

[68] L. A. Wolsey, "An analysis of the greedy algorithm for the submodular set covering problem," Combinatorica, vol.2, no.4, pp. 385-393, Dec. 1982.

[69] D. P. Williamson, and D. B. Shmoys, "The design of approximation algorithms," Cambridge Univ. Press, April 2011.

[70] “Hostapd: the linux way to create virtual Wifi access point,” Internet: nims11.wordpress.com/2012/04/27/hostapd-the-linux-way-to-create-virtual-wifi-access-point/, Access Jan. 20, 2019.

[71] “Setting up a Raspberry Pi as a WiFi access point,” Internet: https://cdn-learn.adafruit.com/downloads/pdf/setting-up-a-raspberry-pi-as-a-wifi-access-point.pdf, Access Jan. 20, 2019.

[72] “Arp Scan,” Internet: http://www.nta-monitor.com/tools-resources/security-tools/arp-scan, Access Jan. 20, 2019.

[73] “nm-tool,” Internet: http://linux.die.net/man/1/nm-tool, Access Jan. 20, 2019.

[74] “View your current network settings with nm-tool,” Internet: https://nfolamp.wordpress.com/2010/05/21/view-your-current-network-settings-with-nm-tool/, Access Jan. 20, 2019.

[75] M. E. Islam, K. S. Lwin, M. S. A. Mamun, N. Funabiki, and I.-W. Lai, “Measurement results of three indices for IEEE802.11n wireless networks in outdoor environments,” in Proc. IEEE Hiroshima Sect. Student Symp. (HISS), pp. 410-414, Nov. 2015.

[76] “nmcli - command-line tool for controlling NetworkManager,” Internet: http://manpages.ubuntu.com/manpages/maverick/man1/nmcli.1.html, Access Jan. 20, 2019.

[77] “Using the NetworkManager command-line tool, nmcli,” Internet: https://access.redhat.com/documentation/en-US/Red_Hat_Enterprise_Linux/7/html/Networking_Guide/sec-Using_the_NetworkManager_Command_Line_Tool_nmcli.html, Access Jan. 20, 2019.

[78] “Learning Linux Commands: sed,” Internet: https://linuxconfig.org/learning-linux-commands-sed, Access Jan. 20, 2019.

[79] Homedale::Wi-Fi / WLAN Monitor., http://www.the-sz.com/products/homedale/ Access Dec., 20, 2017.

[80] C. Pillips, D. Sicker, and D. Grunwald, “A survey of wireless path loss prediction and coverage mapping methods,” IEEE Commun. Survey. Tut., vol.15, no.1, pp.255-270, 2013.

[81] Aterm NEC router [online], https://www.aterm.jp/product/atermstation/trademark.html Access Nov., 24, 2020.

[82] Raspberry Pi. The official website of the Raspberry Pi project, https://www.raspberrypi.org/ Access Sept., 30, 2020.

[83] Toshiba dynabook R731/B [online], https://drp.su/en/laptops/toshiba/dynabook-r731-b/wifi?os=windows-10-x64 Access Oct., 20, 2020.

[84] Fujitsu lifebook S761 [online], https://www.cnet.com/products/fujitsu-s761/, Access Oct., 20, 2020.

[85] S. Ryu, C. Rump, and C. Qiao, “Advances in Internet congestion control,” IEEE Commun. Surv. Tutor. vol. 5, no. 1, pp. 28-39, 2003.

[86] A. Afanasyev, N. Tilley, P. Reiher, and L. Kleinrock, “Host-to-host congestion control for TCP,” IEEE Commun. Surv. Tutor., vol. 12, no. 3, pp. 304-342, 2010.

[87] C. Reis, R. Mahajan, M. Rodrig, D. Wetherall, and J. Zahorjan, “Measurement-based models of delivery and interference in static wireless networks,” in Proc. Conf. Appl., Tech., Arch. Proto. Comput. Comm., pp. 51-62, 2006.

[88] C. Newport, D. Kotz, Y. Yuan, R. S. Gray, J. Liu, and C. Elliott, “Experimental evaluation of wireless simulation assumption,” J. Simu., vol. 83, no. 9, pp. 643-661, Sept. 2007

[89] J. Padhye, S. Agarwal, V. N. Padmanabhan, L. Qiu, A. Rao, and B. Zill, “Estimation of link-interference in static multi-hop wireless networks,” in Proc. ACM IMC, pp. 28, Oct. 2005.

[90] L. B. Jiang and S. C. Liew, “Improving throughput and fairness by reducing exposed and hidden nodes in 802.11 networks,” IEEE Trans. Mob. Comput., vol. 7, no. 1, pp. 34-49, Jan. 2008.

[91] OriginLab, Internet [online], `https://www.originlab.com/`, Access May, 15, 2018.

[92] G. Zhao, Q. Wang, C. Xu, and S. Yu, “Analyzing and modelling the interference impact on energy efficiency of WLANs,” in Proc. IEEE Int. Conf. Comm., May 2018.

[93] Y. Su, Y. Wang, Y. Zhang, Y. Liu, and J. Yuan, “Partially overlapped channel interference measurement implementation and analysis,” in Proc. IEEE Conf. Comp. Comm. Work., pp. 760-765, April 2016.

[94] A. Moriuchi, T. Murase, M. Oguchi, A. Baid, S. Sagari, I. Seskar, and D. Raychaudhuri, “Measurement study of adjacent channel interference in mobile WLANs,” in Proc. IEEE Int. Conf. Commun. Work. Gre. Broad. Access, pp. 566-570, 2013.

[95] M. M. Islam, N. Funabiki, M. Kuribayashi, M. Saha, K. I. Munene, R. W. Sudibyo and W.-C. Kao, “A proposal of transmission power minimization extension in active access-point configuration algorithm for elastic wireless local-area network system,” Int. J. Comp. Soft. Eng. vol. 4, pp. 1-9, 2019.

[96] TP-Link TL-WN722N [online], `https://www.tp-link.com/us/home-networking/usb-adapter/tl-wn722n/` Access Oct., 28, 2019.

[97] M. Elwekeil, M. Alghoniemy, M. El-Khamy, H. Furukawa, and O. Muta, “Optimal channel assignment for IEEE 802.11 multi-cell WLANs,” in Proc. Signal Process. Conf., pp. 694-698, 2012

[98] Z. Zhang, L. Song, Z. Han, and W. Saad, “Coalitional games with overlapping coalitions for interference management in small cell networks,” IEEE Trans. Wirel. Commun., vol. 13, no. 5, pp. 2659-2669, May, 2014.

[99] W. Zhao, H. Nishiyama, Z. Fadlullah, N. Kato, and K. Hamaguchi, “DAPA: capacity optimization in wireless networks through a combined design of density of access points and partially overlapped channel allocation,” IEEE Trans. Vehi. Tech., vol. 65, no. 5, pp. 3715-3722, May, 2016.

[100] T. Vanhatupa, M. Hännikäinen, and T. D. Hämäläinen, "Evaluation of throughput estimation models and algorithms for WLAN frequency planning," Comp. Netw., vol. 51, no. 11, pp. 3110-3124, 2007.

[101] M. Elwekeil, M. Alghoniemy, O. Muta, A. B. Abdel-Rahman, H. Gacanin, and H. Furukawa, "WLAN channel assignment based on minimizing the worst-case interference," Wirel. Pers. Commun., vol. 95, pp. 4867-4881, 2017.

[102] R. Akl, and A. Arepally, "Dynamic channel assignment in IEEE 802.11 networks," in Proc. IEEE Int. Conf. Port. Info. Dev., pp. 1-5, 2007.

[103] S. Kandasamy, R. Morla, P. Ramos, and M. Ricardo, "Predicting throughput in IEEE 802.11 based wireless networks using directional antenna," Wireless Netw., vo. 25, no. 4, pp. 1567-1584, 2019.

[104] D. G. Yoon, S. Y. Shin, W. H. Kwon, and H. S. Park, "Packet error rate analysis of IEEE 802.11b under IEEE 802.15.4 interference," in Proc. IEEE VETECS, pp. 1186-1190, 2006.

[105] S. Kumar, F. Kaltenberger, A. Ramirez, and B. Kloiber, "An SDR implementation of WiFi receiver for mitigating multiple co-channel ZigBee interferers," EURASIP J. Wirel. Commun. Netw., no. 2019:224, 2019.

[106] A. Nabil, M. J. Abdel-Rahman, A. B. MacKenzie, and F. Hassan, "A stochastic optimization framework for channel bonding in wireless LANs under demand uncertainty," IEEE Trans. Wirel. Comm., vol. 19, no. 11, Nov., pp. 7528-7542, 2020.

[107] B. P. Tewari and S. C. Ghosh, "Combined power control and partially overlapping channel assignment for interference mitigation in dense WLAN," in Proc. Int. Conf. Adv. Info. Netw. Appl., pp. 646-653, 2017.

[108] B. P. Tewari and S. C. Ghosh, "Efficient AP placement through power control and partially overlapping channel assignment," Wirel. Person. Commu. vol. 110, pp. 223-244, 2020.

[109] A. Kachroo, J. Park , and H. Kim, "Channel assignment with transmission power optimization method for high throughput in multi-access point WLAN," in Proc. Wire. Commu. Mob. Comp. Conf., pp. 314-319, 2015.